ADVERTIMENT. La consulta d'aquesta tesi queda condicionada a l'acceptació de les següents condicions d'ús: La difusió d'aquesta tesi per mitjà del servei TDX (www.tesisenxarxa.net) ha estat autoritzada pels titulars dels drets de propietat intel·lectual únicament per a usos privats emmarcats en activitats d'investigació i docència. No s'autoritza la seva reproducció amb finalitats de lucre ni la seva difusió i posada a disposició des d'un lloc aliè al servei TDX. No s'autoritza la presentació del seu contingut en una finestra o marc aliè a TDX (framing). Aquesta reserva de drets afecta tant al resum de presentació de la tesi com als seus continguts. En la utilització o cita de parts de la tesi és obligat indicar el nom de la persona autora.

ADVERTENCIA. La consulta de esta tesis queda condicionada a la aceptación de las siguientes condiciones de uso: La difusión de esta tesis por medio del servicio TDR (www.tesisenred.net) ha sido autorizada por los titulares de los derechos de propiedad intelectual únicamente para usos privados enmarcados en actividades de investigación y docencia. No se autoriza su reproducción con finalidades de lucro ni su difusión y puesta a disposición desde un sitio ajeno al servicio TDR. No se autoriza la presentación de su contenido en una ventana o marco ajeno a TDR (framing). Esta reserva de derechos afecta tanto al resumen de presentación de la tesis como a sus contenidos. En la utilización o cita de partes de la tesis es obligado indicar el nombre de la persona autora.

WARNING. On having consulted this thesis you're accepting the following use conditions: Spreading this thesis by the TDX (www.tesisenxarxa.net) service has been authorized by the titular of the intellectual property rights only for private uses placed in investigation and teaching activities. Reproduction with lucrative aims is not authorized neither its spreading and availability from a site foreign to the TDX service. Introducing its content in a window or frame foreign to the TDX service is not authorized (framing). This rights affect to the presentation summary of the thesis as well as to its contents. In the using or citation of parts of the thesis it's obliged to indicate the name of the author

UNIVERSITAT POLITÈCNICA
DE CATALUNYA
BARCELONATECH

Departament de Teoria
del Senyal i Comunicacions

Centre
Tecnològic
de Telecomunicacions
de Catalunya

Exploiting Spatial Modulation and Analog Network Coding for the Design of Energy-Efficient Wireless Networks

PhD Thesis Dissertation

By

Konstantinos Ntontin

Submitted to the Universitat Politècnica de Catalunya (UPC)

in partial fulfillment of the requirements for the degree of

DOCTOR OF PHILOSOPHY

Barcelona, September 2015

Supervised by Dr. Christos Verikoukis and Prof. Ana Pérez-Neira
PhD program on Signal Theory and Communications

Abstract

As the data rate demands of the cellular users increase, together with their number, it is expected that unprecedented capacity demands should be met in wireless networks in the forthcoming years. However, the energy consumption to meet these rates is expected to increase exponentially, according to trends. This can become a serious issue for both the environment, due to CO2 emissions, and the operators, which will have to pay more for electricity. Hence, several energy-efficient solutions have been proposed, such as multiple antenna systems, dynamic spectrum allocation, heterogeneous networks, and Network Coding, to name a few.

Based on the above, the aim of this thesis to propose low-complexity and energy-efficient physical layer-based solutions compared to the already existing approaches, without sacrificing the quality of performance. More specifically, the focus is on the technologies of Spatial Modulation and Analog Network Coding. Both schemes offer the so-called multiplexing gain, which means that multiple streams can be transmitted without sacrificing resources, such as bandwidth.

As far as Spatial Modulation is concerned, Spatial Modulation-based schemes are proposed that are more energy efficient than state-of-the-art technologies. Regarding Analog Network Coding, we study its implementation in relay-based scenarios and how it compares in terms of energy efficiency with conventional protocols, such as the time-division multiple access protocol.

From the obtained results, the conclusion that can be drawn is that depending on the scenario both Spatial Modulation and Analog Network Coding can provide significant energy gains compared to existing technologies without sacrificing performance.

Resumen

A medida que las demandas de velocidad de datos de los usuarios de redes celulares aumentan, así como su número, se espera que las demandas de capacidad sin precedentes se deban cumplir en las redes inalámbricas en los próximos años. Sin embargo, se espera que aumente de forma exponencial el consumo de energía para satisfacer estas tasas, de acuerdo a las tendencias. Esto puede convertirse en un grave problema ambos para el medio ambiente, debido a las emisiones de CO2, y los operadores, que tendrán que pagar más por la electricidad. Por lo tanto, se han propuesto varias soluciones de eficiencia energética, tales como sistemas de múltiples antenas, la asignación de espectro dinámico, redes heterogéneas, y Network Coding, para nombrar unos pocos.

Con base en lo anterior, el objetivo de esta tesis es proponer soluciones de baja complejidad y de eficiencia energética basadas en la capa física, en comparación con los enfoques ya existentes, sin sacrificar la calidad del funcionamiento. Más específicamente, la atención se centra en las tecnologías de Spatial Modulation y Analog Network Coding. Ambos esquemas ofrecen la llamada ganancia de multiplexación, lo que significa que múltiples flujos pueden ser transmitidos sin sacrificar recursos, tales como el ancho de banda.

En lo que se refiere a Spatial Modulation, se proponen esquemas basados en Spatial Modulation que son más eficientes energéticamente que tecnologías ya existentes. En cuanto a Analog Network Coding, se estudia su aplicación en escenarios inalámbricos basados en relays y cómo se compara en términos de eficiencia energética con los protocolos convencionales, tales como el protocolo de acceso mútiple por división de tiempo.

De los resultados obtenidos, la conclusión que se puede extraer es que dependiendo del escenario ambos Spatial Modulation y Analog Network Coding pueden proporcionar

beneficios significativos de energía en comparación con las tecnologías existentes sin sacrificar el rendimiento.

Acknowledgements

First of all, I would like to dedicate this thesis to my parents, whose love and support helped me get through tough times. Secondly, a big thanks to the people that made my stay in Barcelona more pleasant, to Marco Di Renzo who helped me become a better researcher, and to my supervisor Dr. Christos Verikoukis and tutor Prof. Ana Pérez-Neira for their mentoring during the years of the PhD. Finally, I would like to express my gratitude to the FP7-PEOPLE ITN-GREENET (grant 264759), which financed my PhD studies.

List of Publications

Journals

[J1] **Ntontin, K**.; Renzo, M.; Perez-Neira, A.; Verikoukis, C., "Analog Network Coding in the Multiple Access Relay Channel: Error Rate Analysis and Optimal Power Allocation," Wireless Communications, IEEE Transactions on, vol. 14, no. 6, pp.3015,3032, June 2015.

[J2] **Ntontin, K**.; Di Renzo, M.; Perez-Neira, A.I.; Verikoukis, C., "A Low-Complexity Method for Antenna Selection in Spatial Modulation Systems," Communications Letters, IEEE , vol.17, no.12, pp.2312,2315, December 2013.

[J3] **Ntontin, K**.; Di Renzo, M.; Perez-Neira, A.I.; Verikoukis, C., "Adaptive Generalized Space Shift Keying," Journal on Wireless Communications and Networking, EURASIP, 2013.

International Conferences

[C1] **Ntontin, K**.; Di Renzo, M.; Perez-Neira, A.; Verikoukis, C., "Is Analog Network Coding more energy efficient than TDMA?," Computer Aided Modeling and Design of Communication Links and Networks (CAMAD), 2014 IEEE 19th International Workshop on , vol., no., pp.244,248, 1-3 Dec. 2014.

[C2] **Ntontin, K**.; Di Renzo, M.; Perez-Neira, A.; Verikoukis, C., "Error rate analysis and optimal power allocation in multiple access relay channels with Analog Network Coding," Communications (ICC), 2014 IEEE International Conference on , vol., no., pp.3559,3563, 10-14 June 2014.

[C3] **Ntontin, K**.; Di Renzo, M.; Perez-Neira, A.; Verikoukis, C., "Performance analysis of multistream Spatial Modulation with maximum-likelihood detection," Global Communications Conference (GLOBECOM), 2013 IEEE , vol., no., pp.1590,1594, 9-13 Dec. 2013.

[C4] **Ntontin, K**.; Di Renzo, M.; Perez-Neira, A.; Verikoukis, C., "Performance analysis of antenna subset selection in Space Shift Keying systems," Computer Aided Modeling and Design of Communication Links and Networks (CAMAD), 2013 IEEE 18th International Workshop on , vol., no., pp.154,158, 25-27 Sept. 2013.

[C5] **Ntontin, K**.; Di Renzo, M.; Perez-Neira, A.; Verikoukis, C., "Antenna subset selection for spatial modulation: A novel and energy efficient single RF technique," Communications (ICC), 2013 IEEE International Conference on , vol., no., pp.2454,2458, 9-13 June 2013

[C6] **Ntontin, K**.; Di Renzo, M.; Perez-Neira, A.; Verikoukis, C., "Towards the performance and energy efficiency comparison of spatial modulation with conventional single-antenna transmission over generalized fading channels," Computer Aided Modeling and Design of Communication Links and Networks (CAMAD), 2012 IEEE 17th International Workshop on , vol., no., pp.120,124, 17-19 Sept. 2012.

[C7] **Ntontin, K**.; Di Renzo, M.; Perez-Neira, A.; Verikoukis, C., "Adaptive Generalized Space Shift Keying (GSSK) Modulation for MISO Channels: A New Method for High Diversity and Coding Gains," Vehicular Technology Conference (VTC Fall), 2012 IEEE , vol., no., pp.1,5, 3-6 Sept. 2012.

Contents

List of Figures

List of Tables

List of Acronyms

ABEP	Average Bit Error Probability
AGSSK	Adaptive Generalized Space Shift Keying
AGSSK-TOSD	Adaptive Generalized Space Shift Keying-Time Orthogonal Signal Design
ANC	Analog Network Coding
BER	Bit Error Rate
COAS	Capacity-based Optimized Antenna Selection
CSI	Channel State Information
EDAS	Euclidean Distance Antenna Selection
EE	Energy Efficiency
EGC	Equal Gain Combining
EGT	Equal Gain Transmission
EPA	Equal Power Allocation
FDD	Frequency-Division Duplexing
GSM	Generalized Spatial Modulation
GSSK	Generalized Space Shift Keying
HV	Higher Value
LTE	Long Term Evolution
LV	Lower Value
MARC	Multiple Access Relay Channel
MGF	Moment Generating Function
MIMO	Multiple-Input-Multiple-Output
MISO	Multiple-Input-Single-Output

ML	Maximum Likelihood
MMSE	Minimum Mean Square Error
MRC	Maximum Ratio Combining
NC	Digital Network Coding
OPA	Optimal Power Allocation
PEP	Pair-Wise Error Probability
PPP	Poisson Point Process
PSK	Phase Shift keying
QAM	Quadrature Amplitude Modulation
QPSK	Quadrature Phase Shift keying
SC	Selection Combining
SER	Symbol Error Rate
SIMO	Single-Input-Multiple-Output
SINR	Single-to-Interference-plus-Noise Ratio
SM	Spatial Modulation
SNR	Signal-to-Noise Ratio
SOTA	State of the Art
SSK	Space Shift Keying
STSK	Space-Time Shift Keying
TAS	Transmit Antenna Selection
TDMA	Time Division Multiple Access
TOSD	Time Orthogonal Signal Design
VBLAST	Vertical-BLAST
WiMAX	Worldwide Interoperability for Microwave Access
XOR	Exclusive-Or
ZF	Zero Forcing

Chapter 1

Introduction

1.1 Background and Motivation

Due to the explosive growth of high data rate wireless applications, such as the Internet and video streaming applications, and the number of subscribers in a network, future cellular networks will have to meet unprecedented capacity demands. In fact, Fig. 1.1 shows the expected traffic growth by the year 2016. As it can be observed, a tremendous increase in traffic demand is expected, in particular regarding video services.

Furthermore, the total network energy consumption needed to meet those capacity demands is expected to increase as well due to the creation of much denser networks. This energy consumption increase will eventually lead to an increased amount of CO2 emissions. To be more specific, according to [1] in the year 2020 the CO2 emissions from the mobile industry will amount to more than 235 Mton, which is equivalent to more than one third of the total emissions of the United Kingdom. In a global scale, the total emissions expected by the year 2020 of the mobile industry will amount to 0.6 % of the total CO2 emissions globally.

Hence, the mobile industry is expected to significantly contribute to the global carbon footprint, unless some methods are devised to counteract this expected increase in energy consumption that will come with the capacity increase. Over the recent years, there have been several proposals regarding future energy-efficient wireless communications [2], [3], which involve Multiple-Input-Multiple-Output (MIMO) communications, Orthogonal Frequency Division Multiplexing, radio resource management, heterogeneous networks, cognitive radio, network coding, multihop communications, and distributed antennas, to name a few. It is advisable

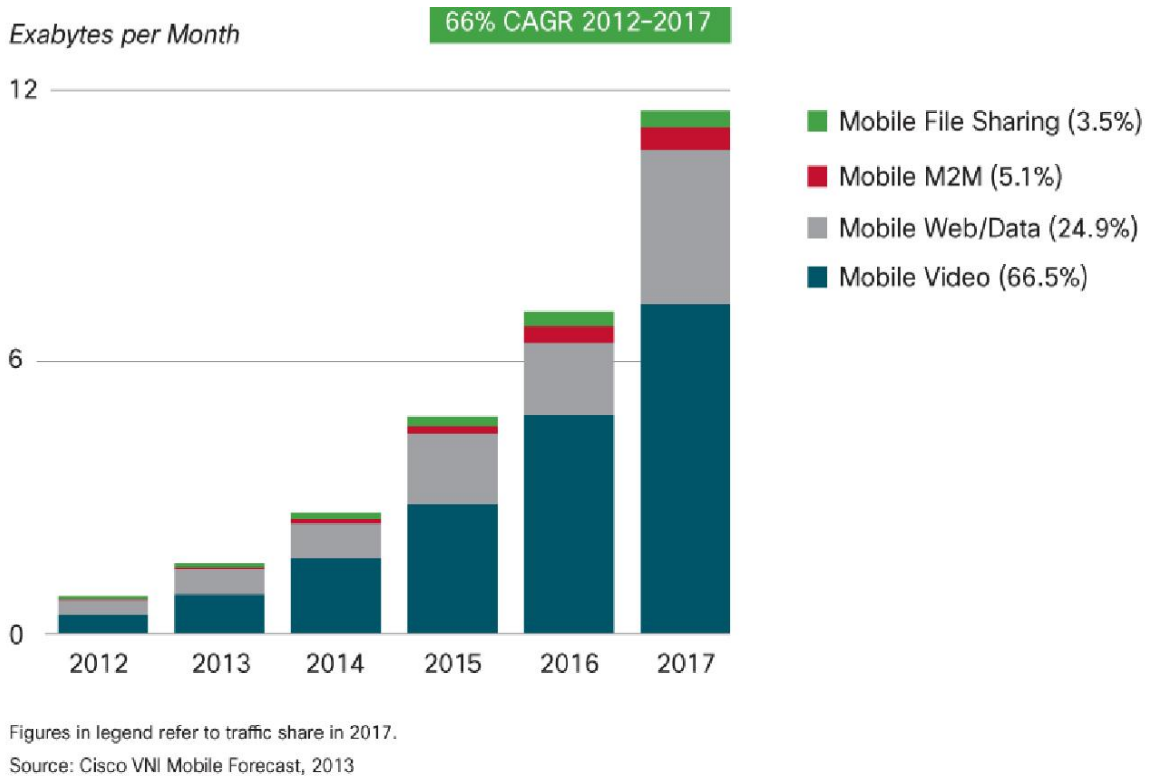

Figure 1.1: Expected traffic load growth by 2016.

that the full energy efficiency maximization potentials will come into effect by implementing as many as possible of the above techniques in a joint approach.

Motivated by the increasing need of designing future energy-efficient networks, this thesis focuses on two different promising approaches for achieving this goal: i) The recently introduced Spatial Modulation (SM) MIMO paradigm [21] is exploited, which has great potentials to be considered as a candidate for future multiple antennas due to its distinct feature of taking into advantage the presence of multiple antennas with a number of RF chains that is smaller than total number of transmit antennas, thus overcoming the main drawback of well-known MIMO systems which require the presence of a number of RF chains equal to the number of transmit antennas. This increases the energy consumption, size, cost, and complexity of the systems transceivers [2]. In particular, methods are proposed for enhancing the energy efficiency potentials of conventional open-loop SM approaches by means of transmit-diversity and higher rates. ii) In the second approach, Analog Network Coding (ANC) is exploited, which is the simplest type of the Network Coding (NC) [5] methods, by employing it as an energy efficient technique to two types of well-known channels, compared to the conventional store-and-forward protocols. These channels are the Multiple Access Relay Channel (MARC)

and the two-way relaying channel. What both approaches have in common is the multiplexing gain that they provide. This means that different data streams can be multiplexed into a single transmitted stream and subsequently at the receiver the streams can be detected and so the information can be recovered. Multiplexing is very important in systems where there is a lack of resources such as bandwidth and time and so an effective way to transmit multiple streams is through multiplexing. Consequently, in this thesis we investigate SM and ANC-based multiplexing enabling schemes as energy-efficient approaches in scenarios of interest.

The rest of this chapter is organized as follows. In Section 1.2, the state-of-the-art literature regarding conventional MIMO is presented together with the SM working principle, the related work on the area, and its advantages and disadvantages. In Section 1.3, the NC operating principle is presented, the state-of-the-art indicative works regarding the two most well-known types of NC, the digital NC and the ANC, and, finally, in Section 1.4 the open areas regarding SM and ANC are presented, which motivated this work.

1.2 Spatial Modulation (SM)

1.2.1 Introduction to MIMO Communications

As it was aforementioned, during the last decade, there has been a tremendous growth in the cellular industry with the number of subscribers and the demands for cellular traffic increasing in a fast pace. A characteristic example of the past few years has been the extension of mobile services even beyond the boundaries of the power grid. In particular, there are already 32 countries where mobile data has broken the electricity barrier: 48 million people in the world have mobile phones, even though they do not have electricity at home. In such a context, mobile data is well on its way to become a necessity. Mobile voice service is already considered a necessity by most, and mobile data, video, and TV services are fast becoming an essential part of lives. However, signal fading, which is caused by the constructive/destructive addition of sinusoidal signals and the limited availability of the frequency spectrum, make it challenging to meet the future demands for wireless data by using single-antenna transmission technology. Fortunately, the introduction of MIMO communication systems offers efficient means to overcome many of these challenges faced by single-antenna systems. Conventional single-antenna transmission techniques aiming at an optimal wireless system performance operate in

the time domain and/or in the frequency domain. In particular, channel coding is typically employed, so as to overcome the detrimental effects of multipath fading. MIMO technology utilizes multiple antennas at both transmitter and/or receiver terminals in order to achieve certain application needs, without having to increase the amount of bandwidth requirement and transmit-energy. In fact, when utilizing multiple antennas, the previously unused spatial domain can be exploited [6]. Having been introduced in the 1990s, multiple-antenna techniques have been shown to offer both higher rates and smaller error rates. In addition, multiple antennas can mitigate co-channel interference, which is a limiting factor regarding the performance of wireless communication systems. In general, MIMO systems can offer spatial multiplexing gains, diversity gains, beamforming gains, or a combinations of the aforementioned features. In the following sections, more details are provided for each one.

1.2.1.1 Spatial Multiplexing for Achieving High Rates

Assuming the presence of multiple antennas at the transmitter, spatial multiplexing means to transmit different data streams from each of the transmit antennas. This way, the total number of bits transmitted is equal to the number of bits transmitted from one of the transmit antennas multiplied by their number. Consequently, there is an increase in the offered rate compared to a single-antenna transmitter, which is denoted as multiplexing gain. This is achieved without sacrificing resources, such as time or bandwidth. At the receiver, the multiple streams can be detected by either the optimal and most complex Maximum-Likelihood (ML) detector, or suboptimal and less complex ones that cancel or mitigate the interference effect of other streams when detecting a particular stream. Such architectures include, for instance, the Zero-Forcing (ZF), Minimum Mean Square Error (MMSE) and the Bell-Labs Layered Space-Time Architecture (BLAST) [8].

1.2.1.2 Spatial Diversity for Smaller Error Rates

Spatial diversity means to take into advantage the presence of multiple antennas at the transmitter or the receiver to transmit or receive, respectively, multiple copies of the same signal. Hence, the bit rate is not increased compared to a single transmission system in contrast to the reliability of the received signal due to the constructive effect of receiving a signal through

different fading channels.Well known schemes that exploit spatial diversity at the transmitter are, for instance, the Alamouti scheme [9] and the space-time codes [10]. If multiple antennas are available only at the receiver, well-known diversity reception techniques are the Maximum Ratio Combining (MRC), the Equal Gain Combining (EGC), and the Selection Combining (SC) [7].

1.2.1.3 Beamforming

Beamforming means steering the transmit and receive beam patterns of a MIMO systems towards favorable directions so that the SNR at the receiver is maximized and the interference is minimized in multi-user systems using the same frequency resources [6]. To achieve this, amplitude and phase coefficients are employed at the transmit and receive antennas that depend on the channel coefficients between them.

1.2.1.4 Disadvantages of MIMO Systems

Clearly, the various benefits offered by multiple-antenna techniques do not come for free. For example, multiple parallel transmitter/receiver chains are required, which are bulky, expensive, and they do not follow Moore's law [2]. In addition, they might lead to increased energy consumption due to the additional circuitry required compared to the single-RF systems. Hence, innovative techniques that exploit the presence of multiple antennas with a smaller or, ideally, a single-RF chain are of great interest. Such techniques are the well-known transmit antenna selection methods in which the 'best' antenna or a subset of antennas based on the channel quality is selected for transmission. The selection of the antenna takes place at the receiver based on the channels estimates before the data transmission and, subsequently, the index of the selected antennas is fed to the transmitter by the receiver. Hence, transmit antenna selection presupposes the existence of a feedback link from the receiver to the transmitter, which might not always be existent.

Over the recent years, another technique has been introduced, the so-called SM method, which exploits the presence of multiple antennas at the transmitter with a smaller number of RF chains and without the need for a feedback channel [21], which is of course a great benefit. In the following, an overview of the work that has been done on SM over the last years is given.

1.2.2 SM Working Principle

The basic idea of conventional single-RF SM is to map a block of information bits into two information carrying units:

• A symbol that is chosen from a complex signal-constellation diagram.

• A unique transmit-antenna index that is chosen from the set of transmit-antenna in the antenna-array (i.e., the so-called spatial constellation diagram).

This creates a hybrid modulation and MIMO technique in which the modulated signals belong to a tri-dimensional constellation diagram, which jointly combines signal and spatial information. An example is shown in Fig. 1.2 (reproduced from [21]) for a linear antenna-array with N_t = 4 antennas at the transmitter and a Quadrature Phase Shift Keying (QPSK) modulation. When the information carrying unit is only the transmit-antenna index, SM reduces to the so called Space Shift Keying (SSK) modulation, which avoids any form of conventional modulation and trades-off receiver complexity for achievable data rates [11]. A simple example of the encoding and decoding processes is shown in Fig. 1.3 (reproduced from [21]) where N_t = 4, N_r = 1 (antennas at the receiver), and M = 4 (modulation order). If multiple antennas are available at the receiver, they are exploited, under the assumption of ML-optimum detection, to achieve receive diversity. This way, the spatial constellation diagram can convey a number of bits that are equal to the logarithm of the number of transmit antennas. To increase the spectral efficiency of the spatial-constellation diagram more than one RF chains can be used at the transmitter and hence more than one antennas can be activated for transmission. In this case, part of the bitstream defines combinations of antennas that are activated for transmission, not only one antenna. This is the concept of Generalized SM (GSM), which increases the spectral efficiency of conventional single-RF SM at the cost of increased complexity [12]. The latter is due to the fact that more than one RF chains need to be employed at the transmitter.

1.2.2.1 Advantages

SM technology offers several advantages. In particular,

• **Spectral Efficiency**: Compared to single-antenna systems, SM offers a multiplexing gain since bits are conveyed by detecting at the receiver which transmit antenna (or antennas) has been activated for transmission. The number of conveyed bits by this spatial constellation

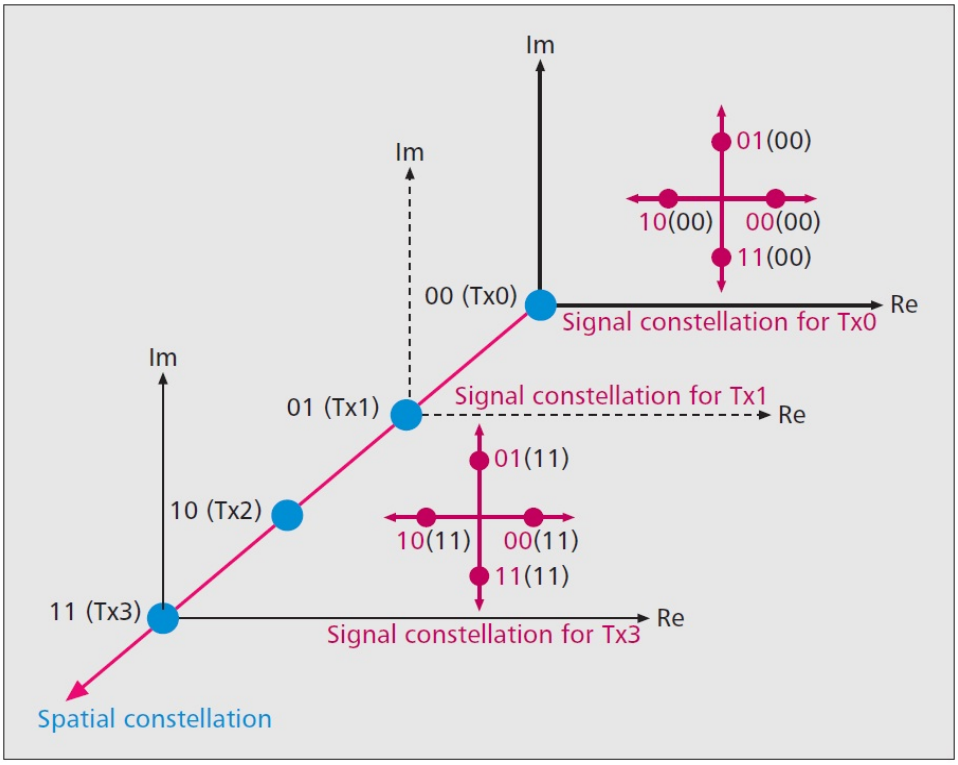

Figure 1.2: Tridimensional constellation diagram of Spatial Modulation: each spatial-constellation point (i.e., the antenna index) defines an independent complex plane of signal-constellation points. For illustration purposes, only two of such planes are shown in the figure for: i) $N_t = 4$, and ii) $M = 4$. Legend: i) Re = real axis of the signal-constellation diagram, and ii) Im = imaginary axis of the signal constellation diagram.

diagram is at least equal to the logarithm of the number of transmit antennas (depending on how many antennas are activated).

• **Energy Efficiency**: The use of a number of RF chains that is smaller than the number of transmit antennas enables energy gains compared to both single-antenna systems (due to multiplexing gain) and multiple-antenna transmission due to the fact that multiple RF chains are a source of increased energy consumption due to the static energy consumption [13].

• **Low Complexity**: Compared to multistream transmission, SM exhibits a lower complexity due to its single-stream nature. This allows the avoidance of complex receive structures for detecting multiple streams such as the Vertical-BLAST (VBLAST), which is based on interference cancellation [14]. In addition, it has been shown that its complexity is similar to known single-stream MIMO schemes, such as the Alamouti scheme [9].

• **Better efficiency of the power amplifiers**: As the linearity requirements of the em-

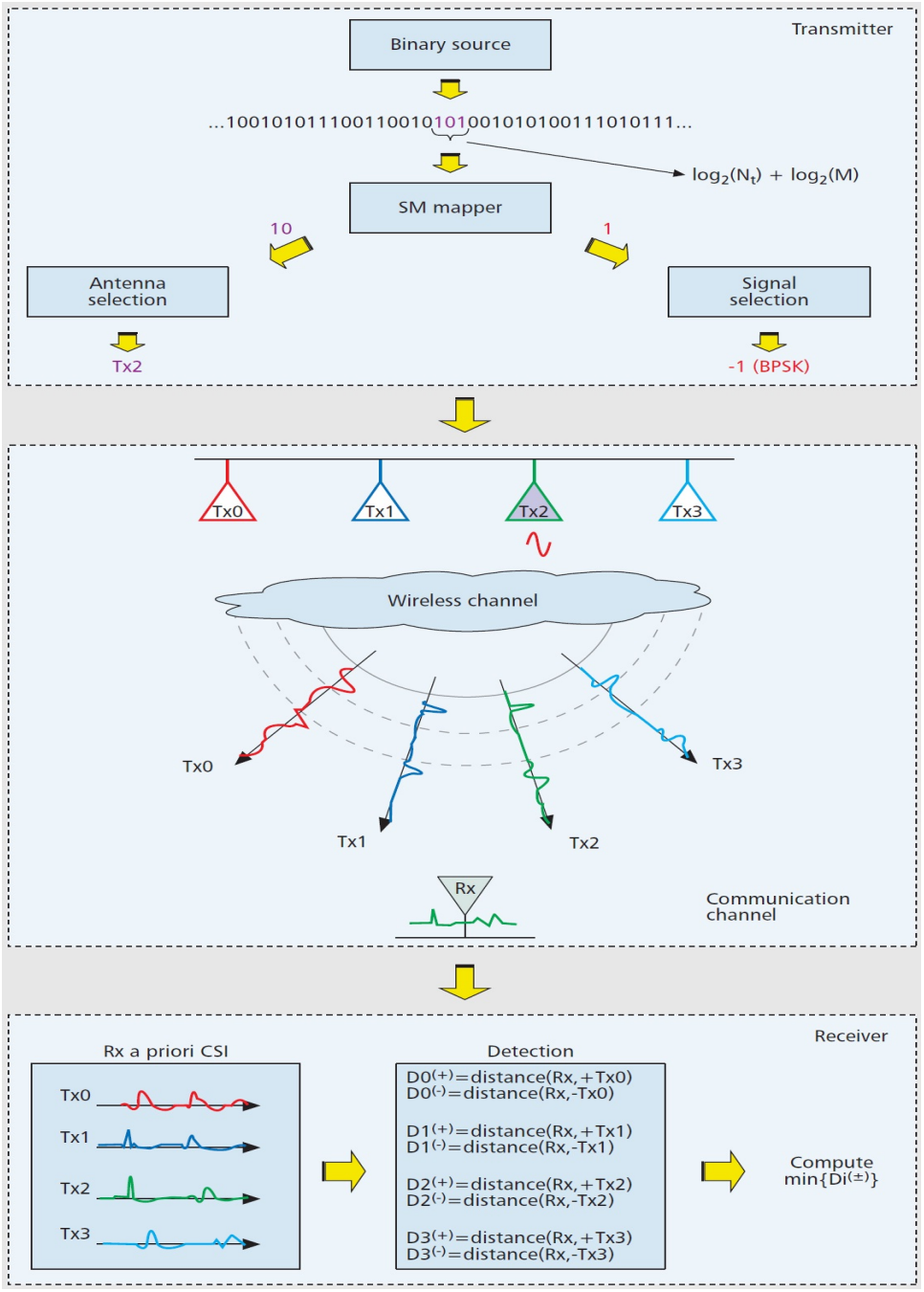

Figure 1.3: SM: Working Principle. Setup: i) $N_t = 4$, ii) $N_r = 1$, and iii) $M = 2$. Legend: i) BPSK = Binary Phase Shift Keying, ii) CSI = Channel State Information, and iii) distance (x, y) = Euclidean distance between signals x and y.

ployed modulation scheme increase (Quadrature Amplitude Modulation (QAM), for instance), the efficiency of the power amplifiers decreases [19]. SM can be beneficial in decreasing the linearity requirements of the modulation scheme since it has been shown that SM with constant-envelope modulation such as PSK can achieve the same or better error rate than SM

with QAM [20]. Consequently, energy gains at the transmitter can be achieved since smaller linearity requirements can lead to smaller power consumption at the amplifier.

1.2.2.2 Disadvantages

However, there are some issues regarding the practical implementation and the exploitation of the full potentials of SM. More specifically,

• **Fast switching**: Different than the conventional antenna selection method [15], in which the transmit antenna that is activated changes at the channel level, SM requires switches that are fast enough to change at the symbol level. In the literature, there are several works regarding fast switches that can perform the switching at nanoseconds or even sub-nanoseconds in various frequency bands with a low insertion loss and good isolation properties [16]- [18].

• **Channel differentiation**: Due to the fact that the successful detection of the bits conveyed from the spatial constellation diagram depends on how much the channel impulse responses differ among the transmit-to-receive links, the performance of SM in terms of error rate becomes better as the differentiation between these channel increases [21]. On the other hand, the error rate of SM increases as the differentiation of these channels decreases.

• **Rate increase compared to single-antenna systems and transmit-diversity**: Conventional single-stream SM architectures can offer a rate increase compared to single antenna systems that can be much less than the one achieved with conventional spatial multiplexing in which the rate increase scales with the number of transmit antennas. Hence, depending on the configuration, SM might be in need of a much larger number of transmit antennas to achieve the same rate with spatial multiplexing. In addition, open-loop SM cannot offer transmit diversity, which is a feature that can boost its energy efficiency potentials with respect to conventional MIMO architectures.

• **Energy consumption for channel estimation**: Due to the fact that the benefits of SM can be obtained by employing many antenna elements at the transmitter, channel estimation at the receiver from many elements and the corresponding energy consumption that it requires can pose an important challenge for its practical implementation. Hence, channel estimation methods need to be devised that are energy efficient and do not sacrifice performance.

1.2.3 Previous Works

All the above describe in brief the SM concept together with its advantages and disadvantages. Since its introduction there have been several works dealing with aspects of SM such as imperfect channel estimation at the receiver, low-complexity detector design, closed-loop design, performance analysis in narrowband fading channels, etc. All these works can be found in [21], which is a comprehensive survey of the SM area.

1.3 Network Coding (NC)

1.3.1 Introduction

Multiple-antenna transmission is an effective method to combat the detrimental effects of fading on the single-link wireless communications by exploiting the spatial diversity of the scattering-rich wireless channel [22]. However, although the cost of employing multiple-antennas is practically negligible, having many collocated antennas inside a terminal device with a relatively low correlation factor among them constitutes a big challenge due to the size limitations of such devices [23]. Hence, relay-aided wireless communications were conceived as technique to achieve the same benefits in the uplink for single-antenna terminals as with the case of multiple-antenna terminals. Nonetheless, a fundamental problem of using relays to assist the communication process of multiple source terminal systems is the need of using orthogonal channels in time or frequency for transmission of the packets of different users since this simplifies the decoding complexity at the receiver and the destination. Consequently, the achieved diversity gains come at a cost of throughput reduction and, hence, the available resources are not used efficiently [24], [25].

Due to this, the NC idea [5], which was originally conceived for wired systems, can be extended to wireless communications systems in which the relays can perform bit-level exclusive-or (XOR) operations on the received packets, a concept which is named as Digital NC [26] or symbol-level linear combining with its simplest form being ANC [27]. Fig. 2.4, illustrates how NC achieves a greater throughput than the conventional store-and-forward protocol. An exchange of data packets (packets c and d) occurs between nodes C and D by exploiting the broadcast channel of node R. Each node has an omni-directional antenna and so the coverage

range of each node is one hop. Based on this assumption, nodes C and D have no direct link between them and need to relay their packets to node R, which is in range of each other. Without NC (store-and-forward approach) in total 4 time slots are needed for the end-to-end packet transfer between the two nodes. On the other hand, in Digital NC first the node C sends packet c to the relay, which detects (the bits), subsequently node D sends packet d to the relay at the second time slot and the relay detects its bits, and finally at the third time slot the relay performs a XOR operation at the detected bits of the nodes and send the resulting packet to both nodes C and D, with which they can detect packets d and c, respectively. This way, 3 slots are needed for the end-to-end transmission and, hence, a better throughput is achieved compared to the store-and-forward approach. Finally, the number of time slots needed for the end-to-end transmission can be reduced even further to 2 slots by considering ANC. More specifically, nodes C and D simultaneously send their packets to the relay at the first time slot and at the second slot the relay sends the mixed signal to nodes C and D, which detect packets d and c, respectively. This shows the importance of ANC since it is the least complex scheme in terms of complexity at the relay (no decoding is required) and, furthermore, it is the scheme that requires the smallest number of time slots for the end-to-end transmission between nodes C and D.

From the above, it is clear that a NC system offers multiplexing gains, as in the case of conventional direct link spatial multiplexing MIMO systems without relays, since source signals are multiplexed at the relays.

1.3.2 Previous Works

In this section, we present some indicative works regarding the two main NC types, Digital NC and ANC. The interested reader can find more in the reference list of these works.

Regarding Digital NC, the seminal work of [5] examines the benefits of NC in routers and presents bounds for the capacity that is achieved when the routers perform NC operations at the incoming packets. After the work of [5], several papers have examined possible applications for digital NC. For instance, in [28] the authors consider a communication network where certain source nodes multicast information to other nodes on the network in the multihop fashion where every node can pass on any of its received data to others and prove that linear network coding achieves the maximum information flow form the source to each receiving node. For

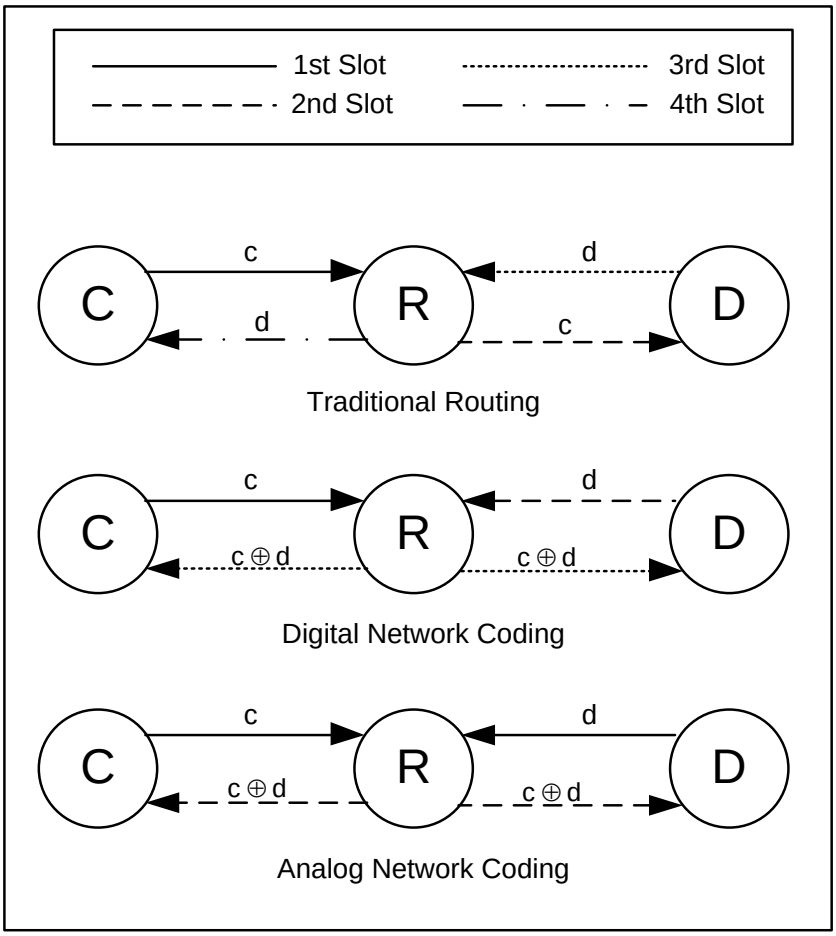

Figure 1.4: Basic NC types.

networks which are restricted to using linear network codes, in [29] the authors find necessary and sufficient conditions for the feasibility of any given set of connections over a given network. In [30], polynomial time algorithms for the design of maximum rate linear multicast network codes are presented that can achieve arbitrarily larger rates than the case without network coding.

Regarding ANC, some related works are information theoretic-based, which show that the throughput is doubled with respect to the store-and-forward approach in the two-way relay channel. Some indicative works, for instance, are the works of [31]- [33]. These works ideally assume that there is a perfect synchronization of the incoming signals from the sources at the relay, which does not hold in practice. However, the authors in [27] present a way of achieving synchronization in practice. In addition, in [34] the authors present a cooperative ANC protocol

in which the transmitted signals of two users are allowed to overlap in a relay and at the destination the recovery of the two signals can be achieved even with significant overlapping. Results show that the proposed protocol can achieve better throughput than an orthogonal amplify-and-forward protocol even with significant overlapping. In [35], the authors consider the two-way relaying channel with two sources and multiple relays in frequency selective fading channels in which the two sources are allowed to simultaneously transmit. Through space-time block coding operations at the relays the authors prove that full diversity can be achieved. In [36], the authors for the first time present the finding that ANC might not always be better than conventional cooperative communications without NC, due to accumulated NC noise at the relay nodes.

1.4 Research Challenges

As aforementioned, in this thesis SM and NC-based schemes are investigated that have the potential to consist energy efficient solutions in future wireless networks without sacrificing performance. This is due to the fact that both schemes provide multiplexing gains, which leads to a throughput enhancement without using additional resources. such as bandwidth and time. In particular,

1) Firstly, the attention is focused on SM which, as aforementioned, is an innovative multiple antenna transmission scheme in the sense that information bits are conveyed by detecting at the receiver which antennas have been activated for transmission (multiplexing gain). This is achieved with low complexity since SM is based on the principle that a smaller number RF chains than the total number of transmit antennas are employed at the transmitter, which reduces both the complexity and the energy consumption at the transmitter [13]. However, although less complex than the conventional MIMO counterparts, the conventional SM approach exhibits two main drawbacks: i) It cannot achieve transmit diversity, which can boost its energy efficiency potentials. ii) Its rate increase with respect to a single-antenna system does not scale linearly with the number of antennas compared with the spatial multiplexing conventional MIMO approach. This can also inhibit its full energy efficiency potentials. Due to this, regarding SM in this thesis SM-based schemes are presented which can achieve either transmit-diversity or higher rates than the conventional approach and compare them in terms of energy efficiency with conventional MIMO counterparts.

2) Secondly, ANC is examined due to the fact that: i) It is the NC scheme with the lowest complexity at the relays since only amplification and forwarding is required instead of decoding, which requires further processing; ii) It provides better throughput than its digital counterpart as we have seen in Section 1.3.1. Hence, it can consist a promising throughput enhancing and, consequently, energy-efficient solution in future relay networks in which the operations at the relays should be kept as low as possible. To the best of the author knowledge, the literature lacks an energy-efficiency evaluation of ANC with respect to conventional relaying methods without NC in known communication channels. This motivates this work regarding NC and in particular the study of the implementation of ANC as an energy-efficient solution in two known communication channels with relays. The first channel is the Multiple Access Relay Channel (MARC) in which a number of sources want to communicate with a common destination through a number of relays and the second channel is the two-way relaying channel in which two sources want to exchange packets through one relay.

The rest of this thesis is organized as follows. In Chapter 2, the SM-based approaches are presented. In particular, two transmit-diversity and one high-rate achieving schemes are introduced. In Chapter 3, the ANC-based study is presented, which is focused on the MARC and the two-way relaying channel. Finally, Chapter 4 concludes the work in this thesis and gives sum ideas for future work.

Bibliography

[1] `https://bscw.ictearth.eu/pub/bscw.cgi/d38532/EARTH_WP2_D2.1_v2.pdf`

[2] Li, G.Y.; Zhikun Xu; Cong Xiong; Chenyang Yang; Shunqing Zhang; Yan Chen; Shugong Xu, "Energy-efficient wireless communications: tutorial, survey, and open issues," Wireless Communications, IEEE , vol.18, no.6, pp.28,35, December 2011.

[3] Joung, J.; Ho, C.K.; Adachi, K.; Sun, S., "A Survey on Power-Amplifier-Centric Techniques for Spectrum and Energy Efficient Wireless Communications," Communications Surveys & Tutorials, IEEE , vol.PP, no.99, pp.1,1.

[4] Di Renzo, M.; Haas, H.; Grant, Peter M., "Spatial modulation for multiple-antenna wireless systems: a survey," Communications Magazine, IEEE , vol.49, no.12, pp.182,191,

December 2011.

[5] Ahlswede, R.; Ning Cai; Li, S.-Y.R.; Yeung, R.W., "Network information flow," Information Theory, IEEE Transactions on , vol.46, no.4, pp.1204,1216, Jul 2000.

[6] Mietzner, J.; Schober, R.; Lampe, L.; Gerstacker, W.H.; Hoeher, P.A., "Multiple-antenna techniques for wireless communications - a comprehensive literature survey," Communications Surveys & Tutorials, IEEE , vol.11, no.2, pp.87,105, Second Quarter 2009.

[7] A. Goldsmith, *Wireless Communications*, Cambridge University Press, Aug. 2005.

[8] S. Verdu, *Multiuser Derection*, Cambridge University Press, Aug. 2005.

[9] Alamouti, S., "A simple transmit diversity technique for wireless communications," Selected Areas in Communications, IEEE Journal on , vol.16, no.8, pp.1451,1458, Oct 1998.

[10] Tarokh, Vahid; Seshadri, N.; Calderbank, A.R., "Space-time codes for high data rate wireless communication: performance criterion and code construction," Information Theory, IEEE Transactions on , vol.44, no.2, pp.744,765, Mar 1998.

[11] Jeganathan, J.; Ghrayeb, A.; Szczecinski, L.; Ceron, A., "Space shift keying modulation for MIMO channels," Wireless Communications, IEEE Transactions on , vol.8, no.7, pp.3692,3703, July 2009.

[12] Younis, A.; Serafimovski, N.; Mesleh, R.; Haas, H., "Generalised spatial modulation," Signals, Systems and Computers (ASILOMAR), 2010 Conference Record of the Forty Fourth Asilomar Conference on , vol., no., pp.1498,1502, 7-10 Nov. 2010.

[13] Stavridis, A.; Sinanovic, S.; Di Renzo, M.; Haas, H., "Energy Evaluation of Spatial Modulation at a Multi-Antenna Base Station," Vehicular Technology Conference (VTC Fall), 2013 IEEE 78th , vol., no., pp.1,5, 2-5 Sept. 2013.

[14] Wolniansky, P.W.; Foschini, G.J.; Golden, G.D.; Valenzuela, R., "V-BLAST: an architecture for realizing very high data rates over the rich-scattering wireless channel," Signals, Systems, and Electronics, 1998. ISSSE 98. 1998 URSI International Symposium on , vol., no., pp.295,300, 29 Sep-2 Oct 1998.

[15] Sanayei, S.; Nosratinia, A., "Antenna selection in MIMO systems," Communications Magazine, IEEE , vol.42, no.10, pp.68,73, Oct. 2004.

[16] Qiang Li; Zhang, Y.P., "CMOS T/R Switch Design: Towards Ultra-Wideband and Higher Frequency," Solid-State Circuits, IEEE Journal of , vol.42, no.3, pp.563,570, March 2007.

[17] Ruei-Bin Lai; Shih-Fong Chao; Zuo-Min Tsai; Lee, J.; Huei Wang, "Topology Analysis and Design of Passive HEMT Millimeter-Wave Multiple-Port Switches," Microwave Theory and Techniques, IEEE Transactions on , vol.56, no.7, pp.1545,1554, July 2008.

[18] Jeong Ho Lee; Seungpyo Hong; Won Ki Kim; Jae We An; Myoung Youl Park, "A Switched Array Antenna Module for Millimeter-Wave Wireless Communications," Millimeter Waves, 2008. GSMM 2008. Global Symposium on , vol., no., pp.161,163, 21-24 April 2008.

[19] Hasan, Z.; Boostanimehr, H.; Bhargava, V.K., "Green Cellular Networks: A Survey, Some Research Issues and Challenges," Communications Surveys & Tutorials, IEEE , vol.13, no.4, pp.524,540, Fourth Quarter 2011.

[20] Di Renzo, M.; Haas, H., "Bit Error Probability of SM-MIMO Over Generalized Fading Channels," Vehicular Technology, IEEE Transactions on , vol.61, no.3, pp.1124,1144, March 2012.

[21] Di Renzo, M.; Haas, H.; Ghrayeb, A.; Sugiura, S.; Hanzo, L., "Spatial Modulation for Generalized MIMO: Challenges, Opportunities, and Implementation," Proceedings of the IEEE , vol.102, no.1, pp.56,103, Jan. 2014.

[22] Foschini G.; Gans, M., "On Limits of Wireless Communications in a Fading Environment when Using Multiple Antennas," Wireless Personal Communications, Springer, vol.6, no.3, pp.311,335, March 1998.

[23] Zhinong Ying, "Antennas in Cellular Phones for Mobile Communications," Proceedings of the IEEE , vol.100, no.7, pp.2286,2296, July 2012.

[24] Pabst, R.; Walke, B.H.; Schultz, D.C.; Herhold, P.; Yanikomeroglu, H.; Mukherjee, S.; Viswanathan, H.; Lott, M.; Zirwas, W.; Dohler, M.; Aghvami, H.; Falconer, D.D.; Fet-

tweis, G.P., "Relay-based deployment concepts for wireless and mobile broadband radio," Communications Magazine, IEEE , vol.42, no.9, pp.80,89, Sept. 2004.

[25] Laneman, J.N.; Tse, D.N.C.; Wornell, Gregory W., "Cooperative diversity in wireless networks: Efficient protocols and outage behavior," Information Theory, IEEE Transactions on , vol.50, no.12, pp.3062,3080, Dec. 2004.

[26] Katti, S.; Rahul, H.; Wenjun Hu; Katabi, D.; Medard, M.; Crowcroft, J., "XORs in the Air: Practical Wireless Network Coding," Networking, IEEE/ACM Transactions on , vol.16, no.3, pp.497,510, June 2008.

[27] Katti, S.; Gollacota, S.; Katabi D., "Embracing Wireless Interference: Analog Network Coding," ACM SIGCOMM, 2007.

[28] Li, S.-Y.R.; Yeung, R.W.; Ning Cai, "Linear network coding," Information Theory, IEEE Transactions on , vol.49, no.2, pp.371,381, Feb. 2003.

[29] Koetter, R.; Medard, M., "An algebraic approach to network coding," Networking, IEEE/ACM Transactions on , vol.11, no.5, pp.782,795, Oct. 2003.

[30] Jaggi, S.; Sanders, P.; Chou, P.A.; Effros, M.; Egner, S.; Jain, K.; Tolhuizen, L.M.G.M., "Polynomial time algorithms for multicast network code construction," Information Theory, IEEE Transactions on , vol.51, no.6, pp.1973,1982, June 2005.

[31] Katti, S.; Marie, I.; Goldsmith, A.; Katabi, D.; Medard, M., "Joint Relaying and Network Coding in Wireless Networks," Information Theory, 2007. ISIT 2007. IEEE International Symposium on , vol., no., pp.1101,1105, 24-29 June 2007.

[32] Rankov, B.; Wittneben, A., "Achievable Rate Regions for the Two-way Relay Channel," Information Theory, 2006 IEEE International Symposium on , vol., no., pp.1668,1672, 9-14 July 2006.

[33] Rankov, B.; Wittneben, A., "Spectral efficient protocols for half-duplex fading relay channels," Selected Areas in Communications, IEEE Journal on , vol.25, no.2, pp.379,389, February 2007.

[34] Argyriou, A.; Pandharipande, A., ”Cooperative Protocol for Analog Network Coding in Distributed Wireless Networks,” Wireless Communications, IEEE Transactions on , vol.9, no.10, pp.3112,3119, October 2010.

[35] Zheng Li; Xia, Xiang-Gen; Bin Li, ”Achieving full diversity and fast ML decoding via simple analog network coding for asynchronous two-way relay networks,” Communications, IEEE Transactions on , vol.57, no.12, pp.3672,3681, December 2009.

[36] Sharma, S.; Yi Shi; Jia Liu; Hou, Y.T.; Kompella, S., ”Is Network Coding Always Good for Cooperative Communications?,” INFOCOM, 2010 Proceedings IEEE , vol., no., pp.1,9, 14-19 March 2010

Chapter 2

Enhancing the Energy-Efficiency Potentials of Conventional SM through Transmit Diversity and High Rates

2.1 Introduction

As it was aforementioned in Chapter 1, SM is a recently introduced innovative single-RF transmission MIMO method, in which information is conveyed in two ways: i) through a conventional signal constellation diagram, such as PSK or QAM, and ii) through the use of a spatial constellation diagram, thus offering a rate gain which scales with the binary logarithm of the number of transmit antennas. Depending on the number of transmit and receive antennas, it has been shown that SM can outperform well-known conventional multiple antenna technologies, such as the VBLAST and SIMO systems [1], [2]. In GSM, the single RF restriction is relaxed by allowing more RF chains and, hence, more than one active antennas to be included in the design [3]. GSM can achieve the same rates as SM with a smaller number of transmit antennas, but at a cost of a lower ABEP.

On the other hand, SSK is a simpler, in terms of complexity, implementation of SM in which only the antenna indices are used as a mean to convey information, thus avoiding the use of signal constellation diagrams [4]. Its simplicity comes at a cost of requiring a higher number of transmit antennas than SM to achieve the same rates. In the same way as with GSM, more than one RF chains and, consequently, more than one active antennas can be used in the

so-called Generalized SSK (GSSK) scheme [5].

However, the conventional open-loop implementations of SM/GSM and SSK/GSSK, have two inherent drawbacks: i) They can only offer receiver-diversity gains. ii) Their rate increase compared to a SIMO system can be significantly lower than the corresponding one of a spatial multiplexing MIMO system. It is intuitive to believe that the energy-efficiency potentials of conventional SM methods can be increased by devising SM-based schemes that can offer transmit-diversity gains and higher rates than conventional SM, similar to the ones offered by spatial multiplexing MIMO. This is based on the fact that: i) additional diversity, besides the receive one, leads to a better reliability of the received signal (smaller error rate), which means that a smaller amount of transmit power (energy) would be needed to achieve the same SNR level at the receiver than the case without transmit diversity and ii) higher offered rates with the same power used in other words means that the same rate with conventional SM can be achieved with a smaller power used. Consequently, energy gains can be achieved. As a result, in this chapter such schemes are presented and their energy efficiency advantage with respect to conventional MIMO approaches. Consequently, the contribution of this chapter is related to SM-based schemes that can provide transmit diversity or higher rates than the conventional open-loop approach. More specifically,

Contribution:

1) Motivated by the small amount of previous works related to feedback-based SM systems that offer transmit-diversity gains, which is a feature expected to significantly enhance its energy-efficiency potentials, the following are proposed:

a) A feedback-based precoding technique, which is shown to enhance significantly the performance of GSSK these systems, both in terms of diversity and coding gain. More specifically, the work is focused on Multiple-Input-Single-Output (MISO) systems in which an effective way to improve the performance of the single-antenna mobile terminals is to exploit methods that achieve transmit-diversity. In particular, inspired by the operating principle of the Equal Gain Transmission (EGT) concept [6], it is assumed that the phases of the channel links can be made available to the transmitter by considering a low-delay feedback link. It is analytically shown that for the perfect feedback case the solution, which is denoted as Adaptive GSSK (AGSSK), offers full transmit-diversity for three and four transmit-antennas without reducing the achievable rate.

In addition, due to the fact that the performance of AGSSK degrades as the rate increases due to the smaller average minimum Euclidean distance, an enhancing method for AGSSK is proposed that relies on the use of time-orthogonal waveforms for the different constellation points, as it was aforementioned in the Introduction chapter. It is analytically proved that the transmit-diversity gain achieved by this enhancement is greater than the number of active antennas without any antenna selection technique. Monte Carlo simulations show that the proposed enhanced scheme, which is denoted as AGSSK-Time Orthogonal Signal Design (AGSSK-TOSD), outperforms for certain MISO configurations, rates, and SNR regions well-known feedback-based multiple-antenna technologies, such as the EGT scheme, the antenna subset selection for spatial multiplexing [7], the antenna subset selection for space-time codes [8], and the adaptive SM scheme of [9], as it will be shown in the numerical results of Section 2.2.2.2.4. Finally, an energy efficiency comparison of AGSSK-TOSD with the aforementioned multiple-antenna schemes for a target (uncoded) ABEP is provided. Depending on the MISO configuration and the achievable rate, AGSSK-TOSD achieves various energy gains over them.

b) A single-RF closed-loop method for SM, which is based on the selection of a subset of antennas to perform SM, is proposed. Two algorithms of selection are studied. The first one is the optimal and leads to the selection of the subset that results in the minimum Symbol Error Rate (SER) for the system, but with relatively high complexity at the receiver. The second algorithm alleviates the complexity of the optimal selection without significant degradation in performance. The energy efficiency comparison of both algorithms with the conventional SNR-based single-RF transmit antenna selection (TAS) method substantiates their practical importance.

2) Motivated by the relatively small rates that the conventional SM approach can offer compared to a spatial multiplexing MIMO system, an open-loop rate enhancing technique of conventional SM, which is based on the conjunction of SM with spatial multiplexing, is proposed. Results show that this method can offer higher energy efficiency at the transmitter than spatial multiplexing depending on the configuration.

2.2 Enhancing the Energy-Efficiency Potentials of Conventional SM/SSK Systems through Transmit-Diversity

As aforementioned in the previous section, a drawback of the conventional open-loop SM/GSM and SSK/GSSK schemes is that they can offer only receive-diversity gains, which is proven in [10] by an eigenvalue analysis. Due to this, there have been several works in the literature that improve the performance in the high-SNR region of those schemes through means of transmit-diversity, which can be achieved either by open or closed-loop design.

2.2.1 Previous Works

In this section, the literature works on transmit diversity for SM/GSM systems are presented. these works are categorized into open and closed-loop approached.

Regarding open-loop schemes that enable transmit-diversity gains for SM/GSM systems, the well-known space-time block coding technology [11] is used in conjunction with SM in [12] and [13], which results in transmit-diversity gains at a cost of requiring at least two active antennas and, consequently, two RF chains in contrast to the single-RF conventional SM. In [14], the authors introduce the Space-Time Shift Keying (STSK) modulation scheme, where SM is included as a special case, which encodes additional information bits onto dispersion matrices and exploits space-time coding. It provides a transmit-diversity gain that scales with the minimum between the number of transmit antennas and the number of time slots. A drawback is the linear decrease of the rate with the number of time-slots that are used in the encoding process. To solve this, the generalized version of STSK is proposed in [15] in which more than one active dispersion matrices are used at each time slot. This way, the rate is increased with respect to STSK at a cost of a higher encoding and decoding complexity. Regarding transmit-diversity achieving open-loop SM schemes that retain the important feature of requiring a single-RF chain, to the best of the authors' knowledge there is only the work in [16] in which the authors exploit the Complex Interleaved Orthogonal Design [17] to propose a SM-based scheme that achieves a transmit-diversity gain equal to two without sacrificing rate.

As far as closed-loop SM schemes are concerned, in [18] the authors propose an adaptive single-RF SM scheme in which the receiver chooses at each time slot the most suitable modu-

lation order for each of the possible transmit antennas based on the channel estimates and feeds the selected transmit mode to the transmitter. The same authors generalize their work in [9] where the possibility of selecting the best subset of antennas to implement SM is included in the design apart from the modulation order. A simpler version of the idea presented in [9], where only the subset of antennas is selected and not the possible transmit mode from each of the antennas of the selected subset, was proposed in [19]. Finally, in [20] the authors introduced the so-called adaptive joint mapping generalized SM in which the incoming data bits are jointly mapped to both the signal and spatial symbols in a dynamic way at each time slot, based on the CSI at the receiver.

Transmit-diversity schemes for SSK/GSSK systems is an area with limited contributions. In particular, for open-loop systems the authors in [21], [22] propose the use of time-orthogonal shaping filters for each of the transmit antennas. This way, the achievable transmit-diversity gain with the proposed design, which is denoted as SSK-time orthogonal signal design (SSK-TOSD), is equal to two. The realization of practical time-orthogonal shaping filters is discussed in [23]. In addition, the same authors apply in [24] their time-orthogonal shaping filter design to GSSK systems and they prove that the achievable transmit-diversity gains are equal to the minimum number of different channel links among all the possible pairs of constellation points. Hence, there is a significant loss of transmit-diversity and consequently of performance if the constellation points include many common channel links.

As far as closed-loop schemes are concerned, to the best of the author knowledge there is only the work of [25] in which the authors introduced a feedback-based method suitable for 2x1 SSK systems where a phase variable is fed to the transmitter. For perfect feedback, it is proven that the transmit-diversity gain achieved is equal to 2.

2.2.2 SM-Based Schemes for Transmit-Diversity Gains

2.2.2.1 Adaptive Generalized Space Shift Keying

In this section, the first proposed SM-based and closed-loop scheme that achieves transmit diversity is going to be presented, which we name as AGSSK, together with its enhanced version that we name as AGSSK-TOSD.

2.2.2.1.1 System Model and Overview of GSSK

2.2.2.1.1.1 System Model

A generic MISO communication system with N_t transmit antennas is considered. The receiver uses a ML detector, and is able to estimate the N_t channel impulse responses perfectly. Consequently, the receiver has perfect CSI. Furthermore, an error-free and zero-delay feedback channel between the receiver and the transmitter is assumed to be available. The N_tx1 MISO channel matrix $\mathbf{H}$ has entries h_i, $i = 1, 2, ...N_t$, which can be modeled as independent and identically distributed complex Gaussian random variables with zero-mean and unit-variance (Rayleigh fading).

Notation: The following notation is used throughout this section: i) N_a is the number of RF chains and, consequently, the number of simultaneously active transmit-antennas, with $1 \leq N_a \leq N_t$; ii) E_m is the average total energy transmitted at each time slot by the N_a active transmit-antennas. An equal distribution among the active transmit-antennas is assumed, *i.e.* each active antenna emits a signal with energy E_m/N_a; iii) η is the Additive White Gaussian Noise (AWGN) at the receiver input, with both real and imaginary parts having a power spectral density (PSD) equal to $N_0/2$; iv) $Q(x) = (1/\sqrt{2\pi}) \int_x^\infty \exp(-u^2/2)du$ denotes the Q-function; v) $\gamma = E_m/N_0$; vi) $\begin{pmatrix} \cdot \\ \cdot \end{pmatrix}$ denotes the binomial coefficient; vii) $\lfloor \cdot \rfloor$ denotes the floor function of a real number; and viii) vectors are denoted in boldface.

2.2.2.1.1.2 GSSK Modulation Overview

In GSSK modulation, the source generates a random sequence of independent bits, which are grouped in sets of $m = \left\lfloor \log_2 \begin{pmatrix} N_t \\ N_a \end{pmatrix} \right\rfloor$ bits and mapped to one of the possible $N_H = 2^m$ points of the spatial-constellation diagram, which can be chosen randomly. If the p_{th} spatial-constellation point is chosen, with $p = 1, 2, ..., N_H$, then the received signal at a given time-slot is given by:

$$y_p(t) = \begin{bmatrix} h_{p(1)}s_{p(1)}(t) & h_{p(2)}s_{p(2)}(t) & \cdots & h_{p(N_a)}s_{p(N_a)}(t) \end{bmatrix} \mathbf{w}_p + \eta(t) \tag{2.1}$$

where $p(l) \in \{1, 2, ..., N_t\}, l = 1, 2, ..., N_a$, denotes the index of the $l-th$ antenna in the $p-th$ spatial-constellation point. $s_{p(l)}(t)$ denotes the transmitted symbol of the $p(l)-th$ antenna. For

GSSK modulation, $s_{p(l)}(t) = \sqrt{E_m}u(t)\ \forall\, p(l) \in \{1, 2, ..., N_t\}$ where $u(t)$ denotes the unit-energy pulse waveform for each transmission, *i.e.*, $\int_{-\infty}^{\infty} |u(t)|^2\, dt = 1$. $\mathbf{w}_p$ is a (complex) $N_a \times 1$ vector containing the transmit weights of the N_a antennas that belong to the $p-th$ spatial-constellation point, under the energy constraint $\|\mathbf{w}_p\|^2 \leq 1$. In GSSK modulation, no CSI at the transmitter (CSIT) is assumed. Thus, the transmit weights are real numbers, which are designed to provide equal energy allocation, *i.e.*, $w_{pi} = 1/\sqrt{N_a}$, for $p = 1, 2, \ldots, N_H$ and $i = 1, 2, \ldots, N_a$. During the detection process, the ML-optimum receiver solves a N_H-hypothesis testing problem for the estimation of the index of the N_a active antennas. This way, the unique message emitted by the encoder is detected. The achievable rate of GSSK modulation is equal to $R_{GSSK} = m$.

By using the tight Codeword-Union based Bound of [26, Eq. (35)], the ABEP of GSSK is bounded as:

$$\mathrm{ABEP}_{GSSK} \leq A \sum_{p}^{N_H} \sum_{k,k\neq p}^{N_H} N_{b_{p,k}} Q\left(\sqrt{\frac{\gamma}{2N_a}\left|\sum_{l=1}^{N_a}\left[h_{p(l)} - h_{k(l)}\right]\right|^2}\right) \tag{2.2}$$

where $A = 1/\left[N_H \log_2(N_H)\right]$ and $N_{b_{p,k}}$ denotes the number of bits in error between the $p-th$ and $k-th$ spatial-constellation points, which depends on the GSSK mapper rule. These symbols will also be used in the rest of this paper. From (2.2), it is evident that no transmit-diversity can be achieved due to the coherent summation of complex Gaussian channel gains. Furthermore, energy is wasted due to the subtraction of the channel gains of common antennas in different spatial-constellation points.

2.2.2.1.2 Proposed Schemes

2.2.2.1.2.1 AGSSK

In AGSSK, we exploit the knowledge of the channel phases to achieve transmit-diversity gains in contrast to GSSK, which are assumed to be available at the transmitter through a feedback channel in the case of Frequency-Division Duplexing (FDD) systems. Its principle is illustrated in Fig. 2.1. By setting the phase of one of the N_t wireless links as a reference, denoted as ϕ_{ref}, the receiver needs to feedback to the transmitter $N_t - 1$ phase differences. The phases of the N_t channel links are denoted as $\phi_i,\ i = 1, 2, ..., N_t$. If, for instance, $\phi_{ref} = \phi_1$, the feedback vector $\boldsymbol{\phi}_{feedback}$ of the phase differences is given by: $\boldsymbol{\phi}_{feedback} = \begin{pmatrix} \phi_1 - \varphi_2 & \cdots & \phi_1 - \varphi_{N_t} \end{pmatrix}$.

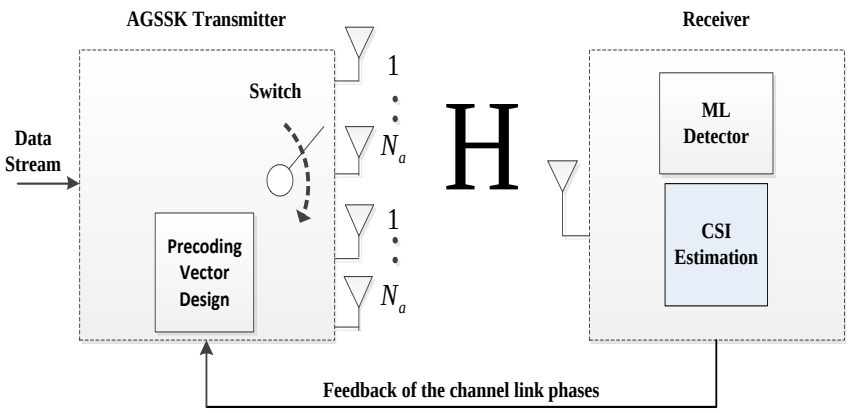

Figure 2.1: AGSSK principle.

Similar to GSSK modulation, the same pulse waveform $u(t)$ is used for all the constellation points.

Design of the Precoding Vectors

The design of the precoding vectors $\mathbf{w}_p, \quad p = 1, 2, ..., N_H$ is based on the following observation. From (2.2), it follows that the main reason why GSSK modulation cannot achieve transmit-diversity gains is the coherent summation of the channel gains, which is caused by the presence of random channel phases in the spatial-constellation points. Consequently, the goal with the proposed precoding design is to avoid random channel phases. Specifically: i) for any spatial-constellation point, the channel phases of the N_a active antennas are aligned to ϕ_{ref}, *i.e.*, they are *co-phased*. This step is equivalent to conventional Equal Gain Combining (EGC) [27] scheme at the receiver, but it is performed at the transmitter by exploiting the knowledge of $\boldsymbol{\phi}_{feedback}$; and ii) the resulting *co-phased* N_H spatial-constellation points are adequately *phase-rotated* in order to maximize the minimum Euclidean distance among them, and, consequently, maximize the coding gain of the system. Based on geometrical considerations, this step is equivalent to uniformly distributing the *co-phased* spatial-constellation points over a circle, similar to PSK modulation. Hence, the spatial-constellation diagram resulting after applying the precoding vector geometrically resembles a PSK modulation scheme, whose N_H points are random variables given by the summation of N_a independent Rayleigh channel gains. Accordingly, the $p-th$ spatial-constellation point, after being phase-aligned, is *phase-rotated*

by $(p-1)(2\pi/N_H)$ for $p = 1, 2, ...N_H$ each time that $\boldsymbol{\phi}_{feedback}$ is updated.

Why the maximization of the minimum Euclidean distance of the constellation diagram leads to maximization of the coding gain can be understood by considering the well-known nearest neighbor approximation in the high-SNR region to the symbol error probability of a system that employs ML detection [27, Eq. (5.45)]. Specifically, the symbol error probability conditioned on the channel matrix $\mathbf{H}$, which we denote as $P_e(\mathbf{H})$, can be approximated as $P_e(\mathbf{H}) \approx N_e Q\left(\sqrt{\frac{\gamma}{2N_a} d^2_{\min}(\mathbf{H})}\right)$, where $d_{\min}(\mathbf{H})$ is the minimum Euclidean distance for a particular realization of the channel matrix $\mathbf{H}$ and N_e is the average number of neighbors at this distance. Consequently, maximizing $d_{\min}(\mathbf{H})$ leads to the minimization of $P_e(\mathbf{H})$ and, hence, to the maximization of the coding gain of the system.

In summary, the $p-th$ spatial-constellation point after applying precoding at the transmitter is:

$$x_p(t) = \sqrt{E_m}\left(\left|h_{p(1)}\right| e^{j\phi_{p(1)}} \quad \cdots \quad \left|h_{p(N_a)}\right| e^{j\phi_{p(N_a)}} \right) \mathbf{w}_p u(t) \tag{2.3}$$

where $h_{p(l)} = \left|h_{p(l)}\right| e^{j\phi_{p(l)}}$ for $l = 1, 2, \ldots, N_a$, and the precoding vector $\mathbf{w}_p$, which takes into account *co-phasing* and *rotation*, is:

$$\mathbf{w}_p = \frac{1}{\sqrt{N_a}} \begin{pmatrix} e^{j\left(\varphi_{ref} + (p-1)\frac{2\pi}{N_H} - \varphi_{p(1)}\right)} \\ \vdots \\ e^{j\left(\varphi_{ref} + (p-1)\frac{2\pi}{N_H} - \varphi_{p(N_a)}\right)} \end{pmatrix} \tag{2.4}$$

Consequently, (2.3) simplifies as follows (dropping the time variable for convenience):

$$x_p = \sqrt{\frac{E_m}{N_a}} \left(\sum_{l=1}^{N_a} \left|h_{p(l)}\right| \right) e^{j\left(\varphi_{ref} + (p-1)\frac{2\pi}{N_H}\right)} \tag{2.5}$$

for $p = 1, 2, ...N_H$, which resembles a N_H-PSK constellation diagram with points being random variables that depend on the channel gains.

At this point, it is important to comment on how the precoding vector design of (2.4) compares with the precoding vector design of the EGT method, which also uses the channel phases to align the channel links that correspond to the active antennas in order to achieve transmit diversity gains. By observing (2.4), it is observed that the channel links that correspond to each constellation point are aligned at a different angle, which is determined by the factor $(p-1)(2\pi/N_H)$ for $p = 1, 2, ...N_H$, so as to obtain a PSK-like spatial constellation diagram and maximize the coding gain. On the other hand, the corresponding precoding vector for EGT MISO systems, which is given by [6, Eq. (11)] for $N_r = 1$, is the same for all the constellation

points since a conventional signal constellation diagram is used to convey information, in contrast to AGSSK. Hence, the precoding design of (2.4) for AGSSK includes the additional factor that rotates each constellation point in a way that the coding gain is maximized, compared to the precoding design of EGT, that includes only the phase alignment feature.

Performance Analysis

By using again [26, Eq. (35)], the union bound of the ABEP of AGSSK can be computed as follows:

$$\mathrm{ABEP}_{Adaptive-GSSK} \leq A \sum_{p}^{N_H} \sum_{k,k\neq p}^{N_H} N_{b_{p,k}} PEP_{x_p \to x_k|h} \tag{2.6}$$

where $PEP_{x_p \to x_k|h}$ is the Pairwise Error Probability (PEP) between the spatial-constellation points x_p and x_k, conditioned on the fading paths. This PEP can be computed as follows:

$$\begin{aligned} PEP_{x_p \to x_k|h} &= Q\left(\sqrt{\frac{1}{2N_0}\left|x_p - x_k\right|^2}\right) \\ &= Q\left(\sqrt{\frac{1}{2N_0}\left[|x_p|^2 + |x_k|^2 - 2\left|x_p\right|\left|x_k\right|\cos\left(\phi_{p,k}\right)\right]}\right) \end{aligned} \tag{2.7}$$

where $\phi_{p,k} = |p-k|\,(2\pi/N_H) \in (0,\pi]$ is the phase difference between x_p and x_k, which, unlike (2), is no longer a random variable.

By comparing (2.7) with (2.2), it can be noticed that the common fading gains between pairs of spatial-constellation points do not cancel out and, furthermore, no random phases are present in the expression of the PEP. This results in transmit-diversity gains and higher coding gains than GSSK, as it will be shown in the numerical results of Section 2.2.2.1.3.

Analysis of the Diversity Order for $N_t = 3$ and $N_t = 4$

Three Transmit-Antennas: Let us consider a setup with $N_t = 3$ and $N_a = 2$, where $N_H = 2$ and R = 1 bpcu. Without loss of generality, it is assumed that the spatial-constellation diagram is composed by the pairs of antenna indexes given by $(1,2)$ and $(1,3)$, which correspond to the

transmission of bits '0' and '1', respectively, and $\phi_{ref} = \phi_1$. By using (2.3) and (2.4), we have:

$$x_1 = \sqrt{E_m}\left(|h_1|\, e^{j\phi_1} \;\; |h_2|\, e^{j\phi_2}\right)\begin{pmatrix} 1/\sqrt{2} \\ \\ e^{j(\phi_1 - \phi_2)}/\sqrt{2}\end{pmatrix}$$

$$= \sqrt{\frac{E_m}{2}}\left(|h_1| + |h_2|\right) e^{j\phi_1} \tag{2.8}$$

and

$$x_2 = \sqrt{E_m}\left(|h_1|\, e^{j\phi_1} \;\; |h_3|\, e^{j\phi_3}\right)\begin{pmatrix} e^{j\pi}/\sqrt{2} \\ \\ e^{j(\phi_1 - \phi_3 + \pi)}/\sqrt{2}\end{pmatrix}$$

$$= \sqrt{\frac{E_m}{2}}\left(|h_1| + |h_3|\right) e^{j(\phi_1 + \pi)} \tag{2.9}$$

By substituting (2.8) and (2.9) in (2.7), we obtain:

$$\begin{aligned} PEP_{'0' \to '1'|h} &= PEP_{'1' \to '0'|h} \\ &= Q\left(\sqrt{\frac{\gamma}{2}}\left[2\,|h_1| + |h_2| + |h_3|\right]\right) \end{aligned} \tag{2.10}$$

By carefully analyzing (2.10), it can be noticed that it resembles, except for a scaling factor, the PEP of an EGC system with three receive-antennas. Thus, we can conclude that a diversity order equal to $L = N_t = 3$ is obtained.

Four Transmit-Antennas: If $N_t = 4$, the angle $\phi_{p,k}$ between a pair $(x_p,\, x_k)$ of spatial-constellation points can take two different values: i) $\phi_{p,k} = \pi$; and ii) $\phi_{p,k} = \pi/2$.

Case $\phi_{p,k} = \pi$: Using (2.5) and (2.7), we obtain:

$$\begin{aligned} PEP_{x_p \to x_k|h} &= Q\left(\sqrt{\frac{\gamma}{N_a}}\left[\sum_{l=1}^{N_a}\left[\left|h_{p(l)}\right| + \left|h_{k(l)}\right|\right]\right]\right) \\ &= Q\left(\sqrt{\frac{\gamma}{N_a}}\left[\sum_{i}^{2d_{p,k}}|h_i| + \sum_{q,q\neq i}^{N_a - d_{p,k}} 2|h_q|\right]\right) \end{aligned} \tag{2.11}$$

where $2d_{p,k}$ is the number of distinct antenna-indexes between the spatial-constellation points x_p and x_k. Once again, (2.11) resembles an EGC diversity scheme with $L_{p,k} = 2d_{p,k} + N_a - d_{p,k} = N_a + d_{p,k}$ antennas at the receiver. Thus, the diversity gain of (2.11) is $L_{p,k}$.

Case $\phi_{p,k} = \pi/2$: By still using (2.5) and (2.7), we obtain:

$$PEP_{x_p \to x_k|h} = Q\left(\sqrt{\frac{\gamma}{N_a}\left[\sum_{i}^{2d_{p,k}}|h_i|^2 + \sum_{q,q\neq i}^{N_a - d_{p,k}} 2\,|h_q|^2 + f\,(h)\right]}\right) \tag{2.12}$$

where $f(h) = 2\sum_{l=1}^{N_a} |h_p(l)| \sum_{m=1}^{N_a} |h_k(m)|$. Consequently, $f(h) \geq 0$ for every channel realization. The diversity order $L_{p,k}$ of (2.12) can be obtained by using the following upper-bound:

$$PEP_{x_p \to x_k|h} \leq Q\left(\sqrt{\frac{\gamma}{N_a}\left[\sum_{i}^{2d_{p,k}} |h_i|^2 + \sum_{q,q\neq i}^{N_a - d_{p,k}} 2|h_q|^2\right]}\right) \tag{2.13}$$

which stems from the fact that $f(h) \geq 0$ and that the Q-function is monotonically decreasing for increasing values of its argument. From the right-side term of (2.13), we notice that the PEP resembles a MRC diversity scheme with $L_{p,k} = 2d_{p,k} + N_a - d_{p,k} = N_a + d_{p,k}$ antennas at the receiver. Thus, the diversity order of (2.12) is $L_{p,k} \geq N_a + d_{p,k}$. If $N_t = 4$, we conclude that different PEPs might have different diversity gains. Overall, the diversity order L of the system is equal to the minimum of the diversity orders of the PEPs, *i.e.*, $L = \min\{L_{p,k}\}$ for $p, k = 1, 2, \ldots, N_H$.

Now, let us consider the setup with N_a=3. In total, there are four combinations of three simultaneously active antennas, *i.e.*, $(1,2,3)$, $(1,2,4)$, $(2,3,4)$, and $(1,3,4)$. Thus, $N_H = 4$. By direct inspection, we have $2d_{p,k} = 2$ for $p, k = 1, 2, \ldots, N_H$. So, $L\big|_{\phi_{p,k}=\pi} = N_a + d_{p,k} = 4$ and $L\Big|_{\phi_{p,k}=\pi/2} \geq N_a + d_{p,k} = 4$. Consequently, $L = N_t = 4$ and so a full diversity order is achieved. In addition, due to the existence of four constellation points the achievable rate is equal to $R = \log_2(4)$ = 2 bpcu, which is the maximum achievable rate for $N_t = 4$.

2.2.2.1.2.2 AGSSK-TOSD

The motivation for introducing AGSSK-TOSD arises by observing (2.7). The negative term inside the argument of the Q-function, which comes as a result of the cross-product between two constellation points, reduces the overall coding and diversity gain. In particular, the higher N_H and, consequently, the data rate is, the smaller the angle $\phi_{p,k}$ between two adjacent constellation points is, which increases the value of the cosine inside the argument of the Q-function. Hence, the average value of the whole expression inside the argument of the Q-function becomes smaller. Consequently, the question that comes into our mind is: Could we somehow enhance the AGSSK method by avoiding the negative term inside the argument of the Q-function? The answer is affirmative by considering the properties of time-orthogonal waveforms [23]. Specifically, assuming two time-orthogonal waveforms $u_i(t)$ and $u_p(t)$, then:

$$\int_{-\infty}^{\infty} u_i(t)u_p(t)dt = \begin{cases} 1 & if \quad i = p \\ 0 & otherwise \end{cases} \tag{2.14}$$

Based on these properties of time-orthogonal waveforms, our proposal is to apply time-orthogonal pulses to the design of (2.3). Specifically, the constellation symbols in the time domain are:

$$x_p(t) = \sqrt{\frac{E_m}{N_a}} \left(\sum_{l=1}^{N_a} \left| h_{p(l)} \right| \right) e^{j\left(\varphi_{ref} + (p-1)\frac{2\pi}{N_H}\right)} u_p(t) \tag{2.15}$$

for $p = 1, 2, ...N_H$. Furthermore:

$$\begin{cases} u_p(t) = u_k(t) \quad if \quad k = p + \dfrac{N_H}{2} \\ \qquad\qquad\qquad\qquad\qquad\qquad p, k = 1, 2, ...N_H \\ \displaystyle\int_{-\infty}^{\infty} u_p(t)\, u_k(t)\, dt = 0 \quad otherwise \end{cases} \tag{2.16}$$

It can be observed from (2.16) that the proposed design is a bi-time-orthogonal design that requires a number of time-orthogonal pulses equal to $N_H/2$. This is analogous to the bi-orthogonal signal design [28, p.178], which requires half the number of orthogonal signals and has a better ABEP than the full-orthogonal design. In other words, the constellation diagram consists of constellation points with the same pulse and phase difference equal to π and points with different pulses that are time-orthogonal with each other.

Example 1: Let us assume that $N_t = 4$ and $N_a = 3$. Consequently, there are 4 possible combinations of three active antennas out of four and so a rate of 2 bpcu is supported. By indexing the four transmit antennas as 1, 2, 3, and 4, the four possible combinations of three active antennas are: (1,2,3), (1,2,4), (1,3,4), and (2,3,4). So, the four possible waveforms to be transmitted based on (2.15) and (2.16) are:

$$\begin{aligned} x_1(t) &= \sqrt{\frac{E_m}{N_a}} \left(|h_1| + |h_2| + |h_3| \right) e^{j\varphi_{ref}} u_1(t) \\ x_2(t) &= \sqrt{\frac{E_m}{N_a}} \left(|h_1| + |h_2| + |h_4| \right) e^{j(\varphi_{ref} + \frac{\pi}{2})} u_2(t) \\ x_3(t) &= \sqrt{\frac{E_m}{N_a}} \left(|h_1| + |h_3| + |h_4| \right)) e^{j(\varphi_{ref} + \pi)} u_1(t) \\ x_4(t) &= \sqrt{\frac{E_m}{N_a}} \left(|h_2| + |h_3| + |h_4| \right) e^{j(\varphi_{ref} + \frac{3\pi}{2})} u_2(t) \end{aligned} \tag{2.17}$$

where $u_1(t)$ and $u_2(t)$ are time-orthogonal with each other.

Example 2: Now, let us assume that $N_t = 5$ and $N_a = 2$. There are ten possible combinations of two antennas out of five and so we randomly choose eight of them in order to have number of combinations that is a power of two. Hence, a rate of 3 bpcu is supported. By indexing the five transmit antennas as 1, 2, 3, 4, and 5, let us assume that the chosen combinations of two active antenna are: (1,2), (1,3), (1,4), (1,5), (2,3), (2,4), (2,5), and (3,4). Based on (2.15) and (2.16), the eight possible waveforms to be transmitted are:

$$\begin{aligned}
x_1(t) &= \sqrt{\frac{E_m}{N_a}}\left(|h_1| + |h_2|\right) e^{j\varphi_{ref}} u_1(t) \\
x_2(t) &= \sqrt{\frac{E_m}{N_a}}\left(|h_1| + |h_3|\right) e^{j(\varphi_{ref}+\frac{\pi}{4})} u_2(t) \\
x_3(t) &= \sqrt{\frac{E_m}{N_a}}\left(|h_1| + |h_4|\right) e^{j(\varphi_{ref}+\frac{\pi}{2})} u_3(t) \\
x_4(t) &= \sqrt{\frac{E_m}{N_a}}\left(|h_1| + |h_5|\right) e^{j(\varphi_{ref}+\frac{3\pi}{4})} u_4(t) \\
x_5(t) &= \sqrt{\frac{E_m}{N_a}}\left(|h_2| + |h_3|\right) e^{j(\varphi_{ref}+\pi)} u_1(t) \\
x_6(t) &= \sqrt{\frac{E_m}{N_a}}\left(|h_2| + |h_4|\right) e^{j(\varphi_{ref}+\frac{5\pi}{4})} u_2(t) \\
x_7(t) &= \sqrt{\frac{E_m}{N_a}}\left(|h_2| + |h_5|\right) e^{j(\varphi_{ref}+\frac{3\pi}{2})} u_3(t) \\
x_8(t) &= \sqrt{\frac{E_m}{N_a}}\left(|h_3| + |h_4|\right) e^{j(\varphi_{ref}+\frac{7\pi}{4})} u_4(t)
\end{aligned} \tag{2.18}$$

where $u_1(t)$, $u_2(t)$, $u_3(t)$, and $u_4(t)$ are pair-wise time-orthogonal.

Let us now provide a discussion regarding the difference between the implementation of time-orthogonal shaping filters in [23] and [24] and in our AGSSK-TOSD proposal. In the aforementioned works, the time-orthogonal shaping filters are used on an antenna-basis, which means that each transmit antenna use a different shaping filter and all of them are time-orthogonal with respect to each other. On the other hand, in AGSSK-TOSD the time-orthogonal shaping filters are used on a constellation point-basis and not on an antenna basis, according to the bi-time-orthogonal design of (2.16). As it is proven in the Appendix, this design leads to the elimination of the cross-product between constellation points during the ML detection process and later in this section we prove that a transmit-diversity order that is greater than the number of active transmit antennas is achieved.

At this point, it is also important to provide a discussion regarding the bandwidth requirements of using time-orthogonal shaping filters. Such a discussion has been provided

in [23, Section V], where it is shown that depending on the technology used to design them, time-orthogonal shaping filters can be designed for narrowband systems with the desired bandwidth spectrum. As it is stated, the method that is proposed in [29] for the design of the time-orthogonal shaping filters guarantees that all of them have the same time-duration and (practical) bandwidth. Although the time-orthogonal filter design in [29] was proposed for Ultra Wide Band systems, the authors show in [23] that the time-duration and bandwidth of the filters can be adequately scaled for narrowband systems, and so the same design can be used. Hence, the time-orthogonal shaping filters can be designed to have the same bandwidth requirements as a single filter narrowband system.

Performance Analysis

Let us assume that x_p and x_k (dropping the time variable for convenience), $p, k = 1, 2, ...N_H$, are two possible constellation symbols to be transmitted, which are given by (2.15). By using again [26, Eq. (35)], the ABEP of AGSSK-TOSD is computed as

$$\text{ABEP}_{AGSSK-TOSD} \leq A \sum_{p}^{N_H} \sum_{k,k\neq p}^{N_H} N_{b_{p,k}} PEP_{x_p \to x_k|h} \tag{2.19}$$

Considering the design of (2.16), the PEP conditioned on the instantaneous channel realization is given by (see the Appendix for the proof):

$$PEP_{x_p \to x_k|h} = \begin{cases} Q\left(\sqrt{\frac{\gamma}{2N_a}}\left[\sum_{l=1}^{N_a}\left(\left|h_{p(l)}\right| + \left|h_{k(l)}\right|\right)\right]\right) & if \quad k = p + \frac{N_H}{2} \\ Q\left(\sqrt{\frac{\gamma}{2N_a}\left[\left(\sum_{l=1}^{N_a}\left|h_{p(l)}\right|\right)^2 + \left(\sum_{l=1}^{N_a}\left|h_{k(l)}\right|\right)^2\right]}\right) & otherwise \end{cases} \tag{2.20}$$

(2.20) can be also written as:

$$PEP_{x_p \to x_k|h} = \begin{cases} Q\left(\sqrt{\frac{\gamma}{2N_a}\left[\sum_{i}^{2d_{p,k}} |h_i| + \sum_{q,q\neq i}^{N_a - d_{p,k}} 2\,|h_q|\right]}\right) & if \quad k = p + \frac{N_H}{2} \\ Q\left(\sqrt{\frac{\gamma}{2N_a}\left[\sum_{i}^{2d_{p,k}} |h_i|^2 + \sum_{q,q\neq i}^{N_a - d_{p,k}} 2\,|h_q|^2 + f(h)\right]}\right) & otherwise \end{cases} \tag{2.21}$$

where again $2d_{p,k}$ is the number of distinct antenna indices between the constellation points x_p and x_k, and $f(h) = 2\sum_{l=1}^{N_a} |h_p(l)| \sum_{m=1}^{N_a} |h_k(m)|$. Hence, $f(h) \geqslant 0$ for every channel realization. From (2.20), we clearly see the advantage of applying time-orthogonal pulses in the AGSSK design: The cross product between the constellation points is eliminated and what remains is the summation of the squared amplitudes of the points.

Analysis of the Diversity Order

Case $k = p + \frac{N_H}{2}$:

By direct inspection of (2.21), we observe that the argument inside the Q-function of the PEP is a summation of independent Rayleigh variables. This is similar to the EGC scheme, and so we conclude that the diversity order is equal to $2d_{p,k} + N_a - d_{p,k} = N_a + d_{p,k}$.

Case $k \neq p + \frac{N_H}{2}$:

By observing (2.21), the argument inside the Q-function consists of the summation of independent chi-squared distributed variables, plus a positive term. Consequently,

$$Q\left(\sqrt{\frac{\gamma}{2N_a}\left[\sum_{i}^{2d_{k,p}} |h_i|^2 + \sum_{q,q\neq i}^{N_a - d_{k,p}} 2\,|h_q|^2 + f(h)\right]}\right) \leqslant Q\left(\sqrt{\frac{\gamma}{2N_a}\left[\sum_{i}^{2d_{k,p}} |h_i|^2 + \sum_{q,q\neq i}^{N_a - d_{k,p}} 2\,|h_q|^2\right]}\right) \tag{2.22}$$

.

The diversity order of the right-hand term in (2.22) is equal to $N_a + d_{p,k}$, due to its MRC nature. Hence, the diversity order of the left-hand term of (2.22) is larger or equal than $N_a + d_{p,k}$. As a result, the total diversity of the system is equal to $N_a + \min\{d_{p,k}\}$, which is greater than the number of active transmit antennas N_a.

2.2.2.1.3 Numerical Results

The aim of this section is twofold: i) To provide a performance comparison (in terms of ABEP) by means of Monte Carlo simulations of our proposed AGSSK and AGSSK-TOSD schemes with the open-loop GSSK modulation [5] and also with the well-known closed-loop and transmit diversity achieving multiple antenna schemes of the EGT [6], the antenna subset selection for spatial multiplexing [7], the antenna subset selection for space-time codes [8], and the adaptive SM scheme of [9] for various MISO setups and achievable rates. For EGT, we consider the selection of the best subset of N_a antennas (that results in the highest SNR) at the receiver [30], which exploits all the available transmit antennas and offers full transmit-diversity gains, and the random selection, which offers transmit-diversity gains equal to the number of active transmit antennas. The random selection can be applicable to low-complexity terminals where the selection of the best subset would pose significant hardware challenges. Moreover, for the antenna subset selection for spatial multiplexing and space-time codes methods we consider the minimum number of RF chains that are needed for these schemes to work, i.e. number of RF chains equal to two. In order to substantiate our diversity analysis, in the figures we also show the union bound analytical models in (2.6) and (2.19) for AGSSK and AGSSK-TOSD, respectively. More specifically, the curves have been obtained by calculating (2.6) and (2.19) for many channel realizations and numerically computing the average. Regarding the generation of time-orthogonal shaping filters for AGSSK-TOSD with the same time duration and bandwidth, we consider the method described in [23]. ii) To provide an energy efficiency comparison for a target (uncoded) ABEP, regarding the required energy at the transmitter, of AGSSK-TOSD with the aforementioned closed-loop multiple-antenna transmission methods.

2.2.2.1.3.1 Performance Comparison

Fig. 2.2 illustrates the performance comparison of AGSSK and AGSSK-TOSD with closed-loop schemes and the open-loop GSSK and GSSK for $N_t = 3$, $N_a = 2$, and a rate of 1 bpcu. Among the possible $\binom{3}{2} = 3$ subsets of 2 antennas, we randomly select 2 of them for the AGSSK proposals and so a rate of 1 bpcu can be supported. As we observe, AGSSK and AGSSK-TOSD significantly outperform GSSK, as expected, and also EGT with random subset selection and closed-loop Alamouti. However, they are outperformed by EGT with

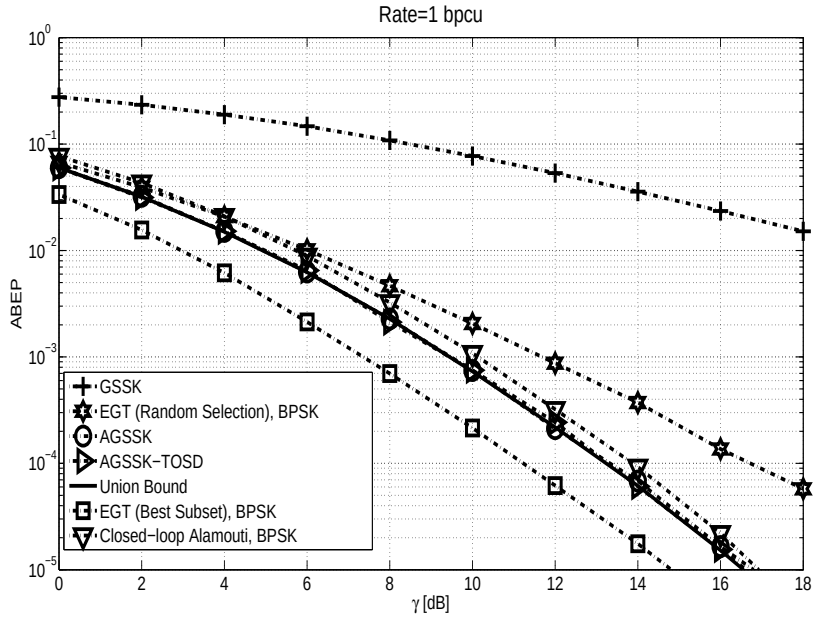

Figure 2.2: Performance comparison of AGSSK and AGSSK-TOSD with closed-loop schemes and the open-loop GSSK for $N_t = 3$, $N_a = 2$, and a rate of 1 bpcu.

selection of the best subset of antennas (the one that results in the minimum ABEP) for all the SNR range. This is because the latter scheme offers a higher coding gain than the the proposals. Moreover, the union bound model of (2.6) and (2.19) for AGSSK and AGSSK-TOSD, respectively, perfectly matches the Monte Carlo simulations in the high-SNR region, as expected.

Fig. 2.3 illustrates the performance comparison of AGSSK and AGSSK-TOSD with closed-loop schemes and the open-loop GSSK for $N_t = 4$, $N_a = 2$, and a rate of 2 bpcu. Among the possible $\binom{4}{2} = 6$ subset of 2 antennas, we randomly select 4 of them for the AGSSK proposals and so a rate of 2 bpcu can be supported. As we observe, the trends are the same as in the case of 1 bpcu rate, i.e. AGSSK and AGSSK-TOSD outperform all schemes except for EGT with selection of the best subset of antennas. Again the reason for this is the higher coding gain that the latter scheme exhibits. Furthermore, again the union bound model of (2.6) and (2.19) perfectly matches the Monte Carlo simulations in the high-SNR region. Finally, we note that in EGT data is conventionally conveyed from a signal constellation, in contrast to AGSSK and AGSSK-TOSD, which means that for a required rate R bpcu, a modulation order of 2^R needs to be employed.

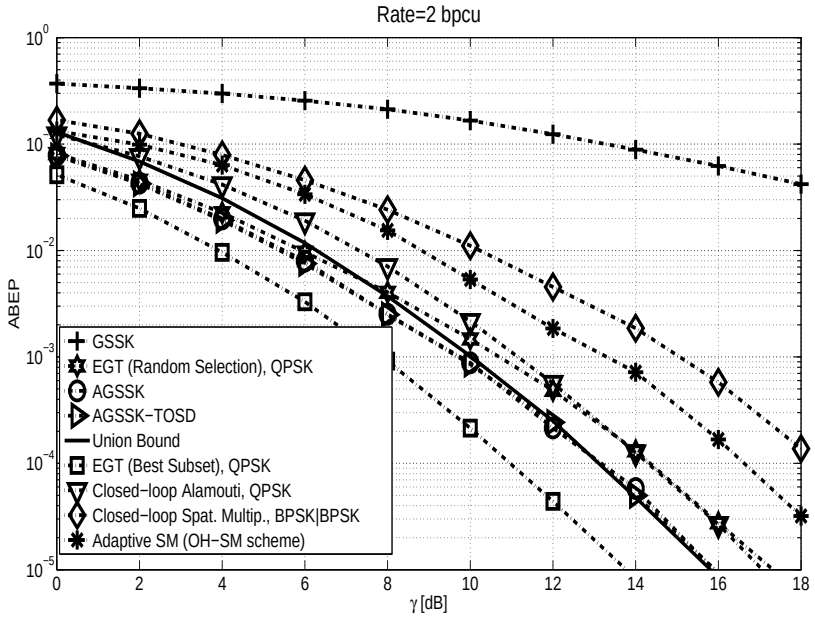

Figure 2.3: Performance comparison of AGSSK and AGSSK-TOSD with closed-loop schemes and the open-loop GSSK for $N_t = 4$, $N_a = 2$, and a rate of 2 bpcu.

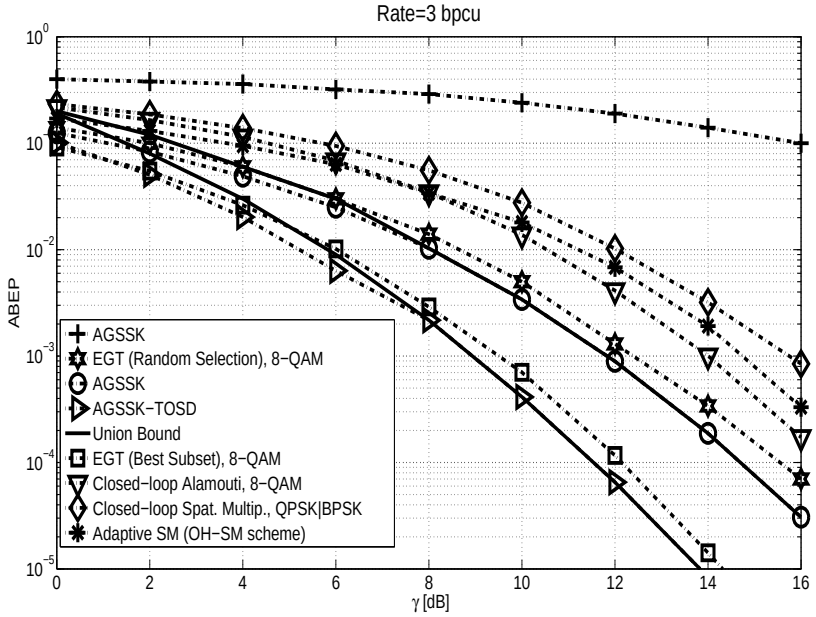

Figure 2.4: Performance comparison of AGSSK and AGSSK-TOSD with closed-loop schemes and the open-loop GSSK for $N_t = 6$, $N_a = 4$, and a rate of 3 bpcu.

Fig. 2.4 shows the performance comparison of AGSSK and AGSSK-TOSD with closed-loop schemes and the open-loop GSSK for a rate of 3 bpcu, where the $N_t = 6$, $N_a = 4$

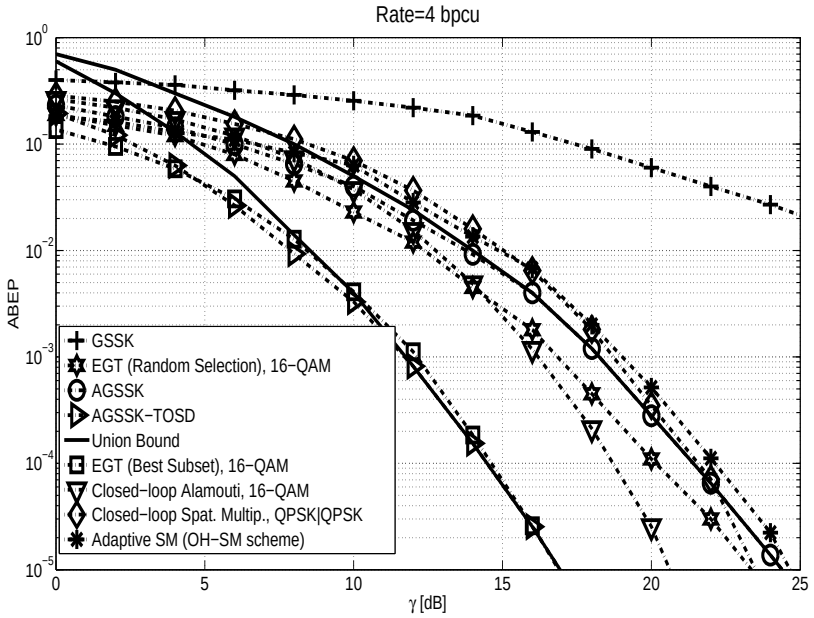

Figure 2.5: Performance comparison of AGSSK and AGSSK-TOSD with closed-loop schemes and the open-loop GSSK for $N_t = 6$, $N_a = 3$, and a rate of 4 bpcu.

configuration was chosen. Consequently, among the possible $\binom{6}{4} = 15$ subsets, 8 are chosen randomly to support a rate of 3 bpcu. As we see in this case, AGSSK-TOSD outperforms EGT with selection of the best subset of antennas and significantly the other closed-loop schemes for the examined SNR range and up to an ABEP value of 10^{-5}. This is due to the fact that as the modulation order of EGT increases its coding gain decreases more than the coding gain decrease of AGSSK-TOSD due to the increase in the number of constellation points. However, due to its full transmit diversity, EGT with selection of the best subset of antennas and closed-loop Alamouti will start outperforming AGSSK-TOSD at some ABEP point, but as we see this crossing point occurs for an ABEP value smaller than 10^{-5}, which is much lower than the uncoded ABEP requirements of many practical systems.

Now, Fig. 2.5 illustrates the comparison of AGSSK and AGSSK-TOSD with closed-loop schemes and the open-loop GSSK for a rate of 4 bpcu. We chose the configuration $N_t = 6$, $N_a = 3$ to achieve such a rate for the AGSSK proposals. As we observe, up to an ABEP of 10^{-5}, AGSSK-TOSD and EGT with selection of the best subset of antennas have almost the same performance. However, AGSSK-TOSD would be the preferable choice because it avoids any kind of conventional modulation order in contrast to EGT and so the RF amplifier

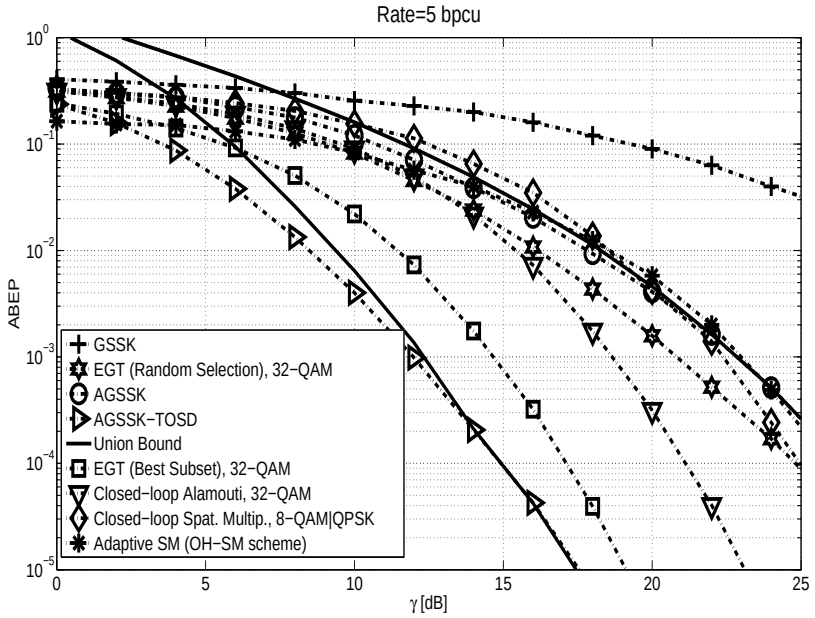

Figure 2.6: Performance comparison of AGSSK and AGSSK-TOSD with closed-loop schemes and the open-loop GSSK for $N_t = 7$, $N_a = 3$, and a rate of 5 bpcu.

avoids the stringent linearity requirements of the RF amplifiers designed for QAM, especially for high-order modulations. In addition, it significantly outperforms the other schemes for the examined SNR range.

Fig. 2.6 shows how the methods compare in terms of performance for a rate of 5 bpcu. The configuration $N_t = 7$, $N_a = 3$ is used for achieving such a rate for the AGSSK proposals. As we observe, AGSSK-TOSD significantly outperform all the other schemes in this case. An intuitive reason for this is that the minimum Euclidean distance of QAM gets smaller as the rate and, consequently, the size of the constellation diagram increases. This is a clear indication that the proposed scheme is useful for medium to high rates.

Finally, Fig. 2.7 shows how the methods compare in terms of performance for a rate of 6 bpcu. The configuration $N_t = 8$, $N_a = 4$ achieves such a rate for the AGSSK proposals. As in the case of a rate of 5 bpcu, AGSSK-TOSD significantly outperforms all the examined schemes.

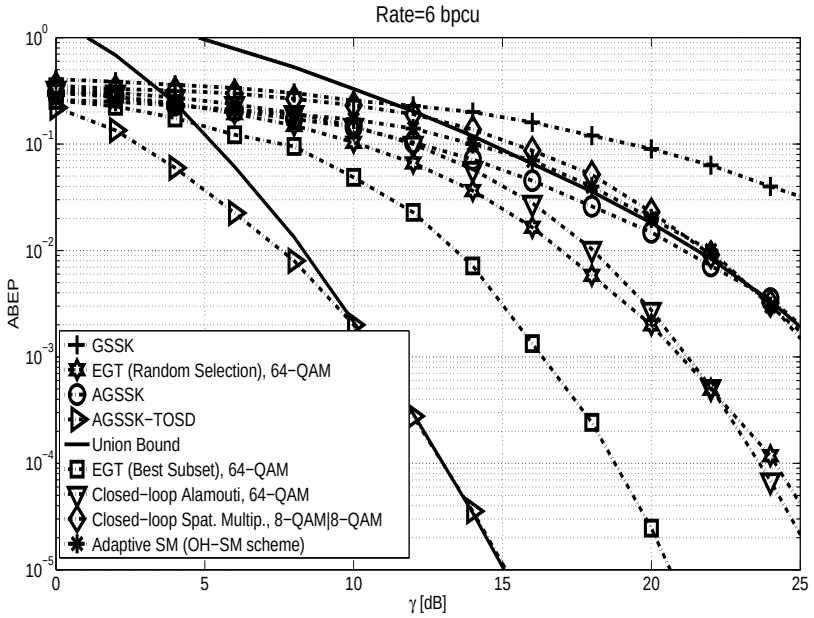

Figure 2.7: Performance comparison of AGSSK and AGSSK-TOSD with closed-loop schemes and the open-loop GSSK for $N_t = 8$, $N_a = 4$, and a rate of 6 bpcu.

2.2.2.1.3.2 Energy Gain Comparison

Now, an energy gain comparison will be provided regarding the energy spent for transmission between AGSSK-TOSD, which is the best scheme in terms of performance with respect to AGSSK and the examined closed-loop multiple-antenna schemes for the MISO configurations of Section 2.2.2.1.3.1 and for a target ABEP of 10^{-3}. In particular, we are interested in the relative energy efficiency (EE) gain, which is calculated as

$$relative\ EE = \frac{\gamma_{conventional\ \ scheme} - \gamma_{AGSSK-TOSD}}{\gamma_{conventional\ \ scheme}} \times 100\% \tag{2.23}$$

The respective values are given in Table 2.1.

As it an be seen from Table 2.1, AGSSK-TOSD can be significantly more energy efficient than the conventional schemes as the rate increases. This is due to the fact that the minimum Euclidean distance for the conventional schemes gets smaller as the rate and, consequently, the QAM order increases, something which is avoided in the AGSSK-TOSD scheme due to the elimination of the cross product between constellation points in the detection process. This is why EGT with selection of the best subset of antennas can outperform the proposed method for rates of 1 and 2 bpcu. Consequently, although some of the baseline closed-loop schemes, such as EGT and space-time codes with selection of the best subset of antennas, achieve higher

Table 2.1: Relative EE gain of AGSSK-TOSD over other closed-loop schemes for a target (uncoded) ABEP of 10^{-3}.

Rate=1 bpcu	Rate=2 bpcu	Rate=3 bpcu	Rate=4 bpcu	Rate=5 bpcu	Rate=6 bpcu
over EGT (Best Subset)					
-55 %	-66 %	10 %	0 %	44%	72%
over EGT (Random Selection)					
41%	15%	53%	68 %	85%	91%
over Closed-loop Alamouti					
11%	24%	68%	65%	79%	91%
over Closed-loop Spatial Multiplexing					
–	70%	80 %	80%	90%	97%
over Adaptive SM [9] (OH-SM scheme)					
–	53%	74 %	80 %	92 %	97 %

transmit-diversity gains than AGSSK-TOSD, there are SNR regions where the latter proposed scheme outperforms them due to its higher coding gain.

2.2.2.2 Antenna Subset Selection for SM in MIMO systems

In this section, the second proposed SM-based and closed-loop scheme that achieves transmit diversity is going to be presented.

2.2.2.2.1 System Model

The system model is illustrated in Fig. 2.8. A generic point-to-point MIMO communication system is considered with the transmitter and receiver equipped with N_t and N_r antennas, respectively. In addition, the existence of a single-RF chain at the transmitter is assumed whereas the receiver has a number of RF chains equal to the number of receive antennas. Such a setup is likely to occur in the uplink since complexity issues and size constraints make it easier for terminals to be equipped with multiple antennas, but only one RF chain. A slow-fading channel and a ML receiver are further assumed. The ML receiver is capable of estimating the channel

impulse responses perfectly during a pilot-based training estimation period, which occurs prior to data transmission. Furthermore, an error-free and zero-delay feedback channel between the receiver and the transmitter is assumed to be available. The channel matrix $\mathbf{H} \in \mathbb{C}^{N_r \times N_t}$ has entries which can be modeled as independent and identically distributed (iid) complex Gaussian random variables with zero-mean and unit-variance (Rayleigh fading).

The receiver uses the channel estimates to select a subset ℓ, $\ell = 1, 2, ..., N_s$, of M transmit antennas out of the possible $N_s = \binom{N_t}{M}$ subsets to implement the SM principle. With $\widehat{\ell}_{selected}$, let us denote the index of the selected subset, which is fed to the transmitter by the receiver through the feedback channel. By assuming that the m_{th} symbol s_m, $m = 1, 2, ..., Q$, is selected to be transmitted from the k_{th} transmit antenna, $k = 1, 2, ..., M$, of the selected subset, the received signal vector $\mathbf{y}$ is given by $\mathbf{y} = \sqrt{E_s}\mathbf{h}_k^{\left(\widehat{\ell}_{selected}\right)} s_m + \mathbf{n}$. Q is the modulation order, E_s is the energy per transmitted symbol, $\mathbf{h}_k^{\left(\widehat{\ell}_{selected}\right)} \in \mathbb{C}^{N_r \times 1}$ is the channel vector that corresponds to the k_{th} antenna of the selected subset, and $\mathbf{n} \in \mathbb{C}^{N_r \times 1}$ is the Additive White Gaussian Noise vector with entries that have a power spectral density equal to N_0.

2.2.2.2.2 Proposed Schemes

2.2.2.2.2.1 Optimal Selection

As aforementioned, one subset of M antennas is selected from the N_s candidate subsets to implement SM. Consequently, the total number of bits that are conveyed is equal to $\log_2(M) + \log_2(Q)$. For calculating the union bound of the instantaneous SER conditioned on the channel realization for each of the N_s subsets, the receiver needs to compute the PEPs of their constellation points according to the ML criterion. For a particular subset ℓ, if the symbol s_m is transmitted from the k^{th} antenna, $k = 1, 2, ..., M$, the received signal vector is given by

$$\mathbf{y} = \sqrt{E_s}\mathbf{h}_k^{(\ell)} s_m + \mathbf{n} \tag{2.24}$$

where $\mathbf{h}_k^{(\ell)} \in \mathbb{C}^{N_R \times 1}$ is the channel vector with elements that correspond to the channel paths from the k^{th} antenna of the ℓ^{th} subset to all the receive antennas.

According to [18] and based on the ML detection principle, the instantaneous PEP for the ℓ^{th} subset conditioned on the channel realization of deciding on the constellation vector $\mathbf{h}_{\widehat{k}}^{(\ell)} s_{\widehat{m}}$ given that the vector $\mathbf{h}_k^{(\ell)} s_m$ is conveyed, which we denote as $P_r\left(\mathbf{h}_k^{(\ell)} s_m \rightarrow \mathbf{h}_{\widehat{k}}^{(\ell)} s_{\widehat{m}} \,|\mathbf{H}\right)$, is

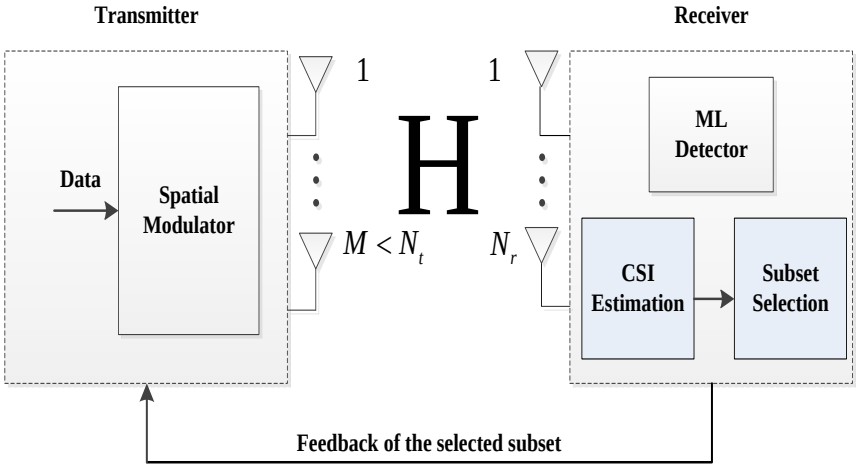

Figure 2.8: Antenna subset selection for SM.

given by

$$P_r\left(\mathbf{h}_k^{(\ell)} s_m \to \mathbf{h}_{\widehat{k}}^{(\ell)} s_{\widehat{m}} \,|\mathbf{H}\right) = Q\left(\sqrt{\frac{\gamma}{2}\left\|\mathbf{h}_k^{(\ell)} - \mathbf{h}_{\widehat{k}}^{(\ell)} s_{\widehat{m}}\right\|_F^2}\right), \tag{2.25}$$

where $\gamma = E_S/N_0$. Hence, the union bound of the instantaneous SER of the ℓ^{th} subset, which we denote as $P_E^{(\ell)}(\mathbf{H})$, is given by

$$P_E^{(\ell)}(\mathbf{H}) \leqslant \frac{1}{MQ}\sum_{k=1}^{M}\sum_{m=1}^{Q}\sum_{\widehat{k}=1}^{M}\sum_{\widehat{m}=1}^{Q} Q\left(\sqrt{\frac{\gamma}{2}\left\|\mathbf{h}_k^{(\ell)} s_m - \mathbf{h}_{\widehat{k}}^{(\ell)} s_{\widehat{m}}\right\|_F^2}\right) \tag{2.26}$$

Consequently, for the selected subset, which we denote as $\widehat{\ell}_{selected}$, it holds that

$$\widehat{\ell}_{selected} = \underset{\ell=1,2,\ldots,N_s}{\arg}\left[\min\left(P_E^{(\ell)}(\mathbf{H})\right)\right] \tag{2.27}$$

where $P_E^{(\ell)}(\mathbf{H})$ is given by the right-side term of (2.26).

Intuitively thinking, it is expected that the proposed method provides transmit-diversity gains besides the multiplexing gain of the SM principle. This is because it involves the selection of the subset with instantaneous SER, which is similar to the selection combining method of conventional schemes [27]. Furthermore, this way of selecting the subset is asymptotically optimal at the high-SNR region due to the tightness of the union bound for high SNRs, but suboptimal in the low-SNR region due to the looseness of the union bound in that region.

Another point to mention is the complexity and energy consumption comparison at the receiver of our proposal with the conventional transmit antenna selection method regarding the required feedback operations, such as estimating the feedback variable and dispatching it to the

terminal. However, in this proposal we are interested in the energy consumption reduction at the terminal side during the uplink phase, which is very important for battery-powered terminals, and therefore we do not consider this comparison study at the receiver. This is left as a topic for future research.

2.2.2.2.2.2 Low-Complexity Suboptimal Selection

Based on [2, Eq. (6)], (2.26) can be re-written as

$$P_E^{(\ell)}(\mathbf{H}) \leqslant P_{E_{signal}}^{(\ell)}(\mathbf{H}) + P_{E_{spatial}}^{(\ell)}(\mathbf{H}) + P_{E_{joint}}^{(\ell)}(\mathbf{H}) \tag{2.28}$$

where

$$\begin{aligned}
P_{E_{signal}}^{(\ell)}(\mathbf{H}) &= \frac{1}{MQ}\sum_{k=1}^{M}\sum_{m=1}^{Q}\sum_{\substack{\widehat{m}=1\\ \widehat{m}\neq m}}^{Q} Q\left(\sqrt{\frac{\gamma}{2}\left\|\mathbf{h}_k^{(\ell)}\right\|_F^2 |s_m - s_{\widehat{m}}|^2}\right)\\
P_{E_{spatial}}^{(\ell)}(\mathbf{H}) &= \frac{1}{MQ}\sum_{k=1}^{M}\sum_{\substack{\widehat{k}=1\\ \widehat{k}\neq k}}^{M}\sum_{m=1}^{Q} Q\left(\sqrt{\frac{\gamma}{2}\left\|\mathbf{h}_k^{(\ell)} - \mathbf{h}_{\widehat{k}}^{(\ell)}\right\|_F^2 |s_m|^2}\right)\\
P_{E_{joint}}^{(\ell)}(\mathbf{H}) &= \frac{1}{MQ}\sum_{k=1}^{M}\sum_{m=1}^{Q}\sum_{\substack{\widehat{k}=1\\ \widehat{k}\neq k}}^{M}\sum_{\substack{\widehat{m}=1\\ \widehat{m}\neq m}}^{Q} Q\left(\sqrt{\frac{\gamma}{2}\left\|\mathbf{h}_k^{(\ell)} s_m - \mathbf{h}_{\widehat{k}}^{(\ell)} s_{\widehat{m}}\right\|_F^2}\right)
\end{aligned} \tag{2.29}$$

According to (2.29), we distinguish three types of minimum squared Euclidean distances, denoted as $ED_{signal}^{2^{(\ell)}}(\mathbf{H})$, $ED_{spatial}^{2^{(\ell)}}(\mathbf{H})$, and $ED_{joint}^{2^{(\ell)}}(\mathbf{H})$, which correspond to $P_{E_{signal}}^{(\ell)}(\mathbf{H})$, $P_{E_{spatial}}^{(\ell)}(\mathbf{H})$, and $P_{E_{joint}}^{(\ell)}(\mathbf{H})$, respectively. In particular,

$$\begin{aligned}
ED_{signal}^{2^{(\ell)}}(\mathbf{H}) &= \frac{\gamma}{2}\min_{k=1,2,\ldots,M}\left\|\mathbf{h}_k^{(\ell)}\right\|_F^2 \min_{\substack{m,\widehat{m}=1,2,\ldots,Q\\ \widehat{m}\neq m}} |s_m - s_{\widehat{m}}|^2\\
ED_{spatial}^{2^{(\ell)}}(\mathbf{H}) &= \frac{\gamma}{2}\min_{\substack{k,\widehat{k}=1,2,\ldots,M\\ k\neq\widehat{k}}}\left\|\mathbf{h}_k^{(\ell)} - \mathbf{h}_{\widehat{k}}^{(\ell)}\right\|_F^2 \min_{m=1,2,\ldots,Q}|s_m|^2\\
ED_{joint}^{2^{(\ell)}}(\mathbf{H}) &= \frac{\gamma}{2}\min_{\substack{k,\widehat{k}=1,2,\ldots,M,\, k\neq\widehat{k}\\ m,\widehat{m}=1,2,\ldots,Q,\, m\neq\widehat{m}}}\left\|\mathbf{h}_k^{(\ell)} s_m - \mathbf{h}_{\widehat{k}}^{(\ell)} s_{\widehat{m}}\right\|_F^2\\
&\geqslant \frac{\gamma}{2}\min_{k,\widehat{k}=1,2,\ldots,M,\, k\neq\widehat{k}}\sigma^{2^{(\ell)}}_{k,\widehat{k}} \min_{\substack{m,\widehat{m}=1,2,\ldots,Q\\ m\neq\widehat{m}}}\left\|\begin{pmatrix} s_m\\ s_{\widehat{m}}\end{pmatrix}\right\|_F^2
\end{aligned} \tag{2.30}$$

where $\min_{k,\widehat{k}=1,2,\ldots,M,\, k\neq\widehat{k}}\sigma^{2^{(\ell)}}_{k,\widehat{k}}$ denotes the minimum squared singular value of the matrix $\left(\mathbf{h}_k^{(\ell)} - \mathbf{h}_{\widehat{k}}^{(\ell)}\right)$. The last inequality follows from the Rayleigh-Ritz theorem [7]. Consequently, for the ℓ_{th}

candidate subset of antennas, the instantaneous minimum squared Euclidean distance can be formulated as follows

$$ED^{2^{(\ell)}}(\mathbf{H}) = \min\left\{ED^{2^{(\ell)}}_{signal}(\mathbf{H}), ED^{2^{(\ell)}}_{spatial}(\mathbf{H}), ED^{2^{(\ell)}}_{joint_{bound}}(\mathbf{H})\right\}, \tag{2.31}$$

where $ED^{2^{(\ell)}}_{joint_{bound}}(\mathbf{H})$ is given by the lower bound of the Rayleigh-Ritz theorem, according to (2.30). Consequently, the selected antenna subset is the one that has that the largest instantaneous minimum squared Euclidean distance among all the candidate subsets. Hence,

$$\widehat{\ell}_{selected} = \underset{\ell=1,2,\ldots,N_s}{\arg\max}\left\{ED^{2^{(\ell)}}(\mathbf{H})\right\} \tag{2.32}$$

2.2.2.2.3 Complexity Comparison

The aim of this section is to present the computational requirements at the receiver, in terms of total number of floating point operations (flops)[1], needed for the schemes under consideration. The optimal subset selection requires an exhaustive search among all possible Euclidean Distance differences and hence in total $\binom{N_t}{2}(5N_r-1)Q^2$ flops are required. The so-called Euclidean Distance Antenna Selection (EDAS)-based algorithm [32], [33], which is an algorithm of lower complexity than the exhaustive search-based, that has been proposed in the literature and it is based on QR decomposition requires [2] $(2N_r-1)$ complex operations for the main diagonal elements of the matrix $\mathbf{D}$ [33]. For computing the off-diagonal elements of $\mathbf{D}$, a QR decomposition needs to be performed on complex matrices of size $2N_r \times 4$, which requires $\left(64N_r - \frac{2}{3}64\right)\frac{Q}{2}$ flops for each element, according to the Householder method [31, Eq. (10.9)]. Hence, by taking into account all the possible combinations of transmit antennas, the total number of flops needed for EDAS is $N_t(2N_r-1) + 64\binom{N_t}{2}\left(N_r - \frac{2}{3}\right)\frac{Q}{2}$.

Based on (2.30), our lower-complexity proposed algorithm imposes a complexity of: i) $N_t(2N_r-1)$ flops for the signal part, ii) $\binom{N_t}{2}(3N_r-1)$ flops for the spatial part, and iii) $\binom{N_t}{2}\left(16N_r - \frac{16}{3}\right)$ flops for the joint part, according to the Householder method [31, Eq. (31.4)] for performing singular value decomposition. Hence, the total number of flops required

[1] Each addition, subtraction, multiplication, division, or square root counts as one flop [31].

[2] For the complexity of EDAS, the reduced complexity proposal of [33] is taken into consideration .

for the proposed method is $N_t\left(2N_r-1\right)+19\binom{N_t}{2}\left(N_r-\frac{1}{3}\right)$. Finally, another algorithm that has been proposed in the literature for the selection of the subset that is called Capacity-based Optimized Antenna Selection (COAS) [32] and the conventional TAS with MRC at the receiver [34] both exhibit a complexity equal to $N_t\left(2N_r-1\right)$ flops.

Table 2.2: Number of flops for antenna selection

Optimal Selection	EDAS	Low-Complexity Proposal	COAS	TAS with MRC
72960	25642	1087	42	42

Table 2.2 shows the numerical values for the complexity requirements of the examined antenna selection schemes for $N_t=6$, $N_r=4$, $M=4$, and $Q=16$. As it can be observed, the reduction in the number of flops needed for the low-complexity proposed method compared to the optimal selection and EDAS algorithms is significant. It approximately achieves 70 and 25 times smaller complexity than the optimal selection and EDAS, respectively. This is due to the fact that its complexity is not dependent on the modulation order, in contrast to the aforementioned algorithms.

2.2.2.2.4 Numerical Results

The aim of this section is: i) To provide a performance comparison in terms of SER of the proposed antenna subset selection for SM against the state-of-the-art antenna selection schemes and ii) To provide the relative energy gain for a target SER of the low-complexity proposed and the EDAS algorithm over the conventional TAS with MRC at the receiver.

2.2.2.2.4.1 Performance Comparison

Fig. 2.9 depicts the performance curves based on Monte Carlo simulations of the TAS scheme with MRC at the receiver together with the optimal selection, EDAS, COAS, and the low-complexity proposed antenna subset selection for SM for $N_t=6$, $M=4$, and a rate of 6 bpcu. In addition, the conventional open-loop SM case has been included in order to illustrate the transmit-diversity gains of the proposed antenna subset selection method. Without loss of generality, we consider a QAM signal constellation diagram. For the TAS scheme, a 64-QAM

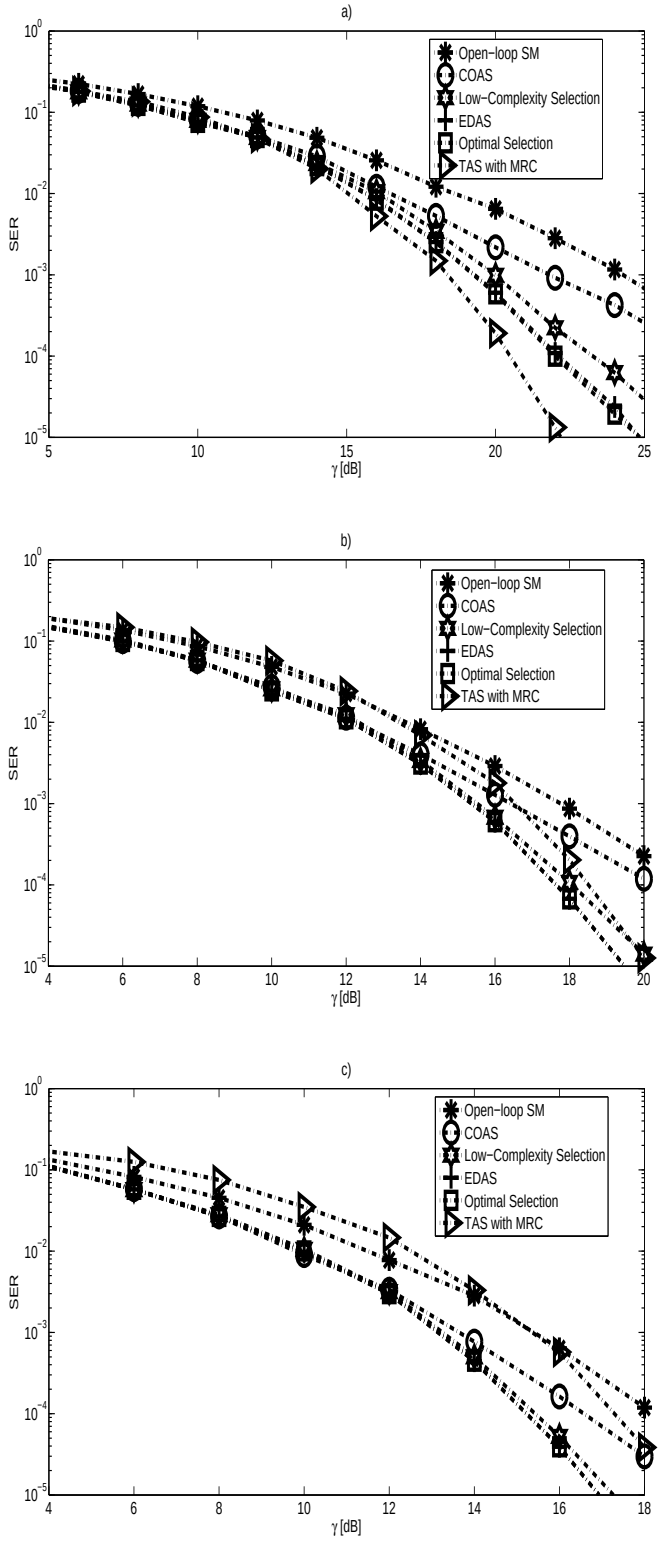

Figure 2.9: SER vs. γ based on Monte Carlo simulations of the TAS with MRC, the different antenna selection methods for SM, and the open-loop SM for a 6 bpcu, $N_t = 6, M = 4$, and a) $N_r = 2$, b) $N_r = 3$, and c) $N_r = 4$.

order is needed to achieve the 6 bpcu, whereas a 16-QAM order is needed for the SM-based schemes since two bits are obtained from the spatial constellation diagram by using a subset of $M = 4$ transmit antennas.

The main conclusions that can be drawn by observing Fig. 2.9 are as follows: i) The proposed optimal and low-complexity antenna subset selection methods for SM benefit more than the TAS with MRC as the number of receive antennas increases, which is due to the multiplexing gain of SM and the use of a smaller modulation order. In fact, we see in Fig. 2.9 b) and c) that they outperform the latter method for SER values up to 10^{-5}. This trend was expected since a similar trend has already been observed in the comparison of conventional open-loop SM with SIMO systems [2]. Consequently, although the TAS with MRC method has a lower complexity, the performance gains of the proposed low-complexity algorithm over the former method provide a promising trade-off between complexity and performance. ii) The performance of the proposed low-complexity algorithm for selection gets closer to the performance of the optimal selection for SER values up to 10^{-5} as the number of receive antennas increases. This is due to the fact that the probability of selecting a subset other than the one that corresponds to the maximum minimum squared Euclidean distance of the system decreases as the number of receive antennas increases. This trend is depicted in Table 2.3, which shows the aforementioned error probability, denoted as subset error probability, for the configurations of Fig. 2.9.

Table 2.3: Subset Error Probability (%)

$N_r = 2$	$N_r = 3$	$N_r = 4$
54	45	40

2.2.2.2.4.2 Energy Gain Comparison

In this section, the relative energy gain of the low-complexity proposal and EDAS over the TAS with MRC is calculated for the configurations of Fig. 2.9 and a target SER of 10^{-4}, which is defined as

$$\left(\gamma^{TAS/MRC} - \gamma^{Ant.\ Selec.\ Spat.\ Mod.}\right)/\gamma^{TAS/MRC}\,[\%] \tag{2.33}$$

where $\gamma^{TAS/MRC}$ and $\gamma^{Ant.\ Selec.\ Spat.\ Mod.}$ are the SNR values that correspond to the TAS with MRC and the proposed low-complexity antenna selection algorithm for SM, respectively.

Table 2.4: Relative energy gain (%) of the proposed and the EDAS algorithm over the TAS with MRC method for SER=10^{-4}

Low-complexity selection			EDAS		
$N_r = 2$	$N_r = 3$	$N_r = 4$	$N_r = 2$	$N_r = 3$	$N_r = 4$
-82	11	35	-36	17	35

Table 2.4 shows the relative energy gain that the low-complexity proposal and the EDAS selection algorithms achieve over the TAS with MRC for the target SER of 10^{-4}. As it can be observed, the higher the number of receive antennas is, the more beneficial the proposed method is compared to TAS with MRC due to its multiplexing gain. Moreover, it practically achieves the same energy gain with EDAS for higher than 2 receive antennas with a much lower complexity, as it was shown in Section 2.2.2.2.3.

2.3 Enhancing the Energy-Efficiency Potentials of Conventional SM/SSK Systems through High Rates

In terms of achieved rates, although a SM system can increase the rate in comparison with a SIMO system by the logarithm of the number of transmit antennas, still this increase can be significantly lower than the offered rate of a conventional spatial multiplexing MIMO system in which the rate increases with the number of transmit antennas [35]. Consequently, it is intuitive that the energy-efficiency potentials of SM in relation to conventional MIMO schemes can increase by devising schemes that are based on the SM principle and offer rates similar to spatial multiplexing MIMO system. In the following, such a scheme is proposed, which is based on the combination of SM with spatial multiplexing, and which we name as multistream SM.

2.3.1 Previous Works

To the best of the author's knowledge, the only proposal to enhance the rate potentials of conventional SM systems is the GSM scheme in which more than one antennas are allowed to be activated for transmission from which the same signal symbol is transmitted [3]. This

way, the rate increases compared to a single-RF SM system since the spatial constellation diagram increases, but, on the other hand, this rate increase is still significantly lower than the corresponding one of a spatial multiplexing system with the same number of transmit antennas.

2.3.2 Multistream SM

2.3.2.1 System Model

A generic MIMO communication system is considered with a transmitter having N_t transmit antennas and N_a RF chains and a receiver with N_r receive antennas and an equal number of RF chains. We assume that the receiver uses a ML detector and is able to estimate the channel impulse responses perfectly during a pilot-based training estimation period prior the data transmission. Consequently, the receiver has perfect CSI. Furthermore, it is assume that a feedback channel does not exist between the receiver and the transmitter, which can be due to a fast fading channel, for instance. Hence, only open-loop transmission techniques can be exploited.

In addition, the channel matrix $\mathbf{H} \in \mathbb{C}^{N_r \times N_t}$ has entries h_{ji}, $j = 1, 2, ...N_r$, $i = 1, 2, ...N_t$, which can be modeled as independent and identically distributed (iid) complex Gaussian random variables with zero-mean and unit variance (Rayleigh fading).

2.3.2.2 Proposed Scheme

The principle of multistream SM is depicted in Fig. 2.10. At the transmitter, the bitstream is divided into blocks containing $\log_2 \left\lfloor \binom{N_t}{N_a} \right\rfloor_2 + N_a \log_2 (M)$ bits each. Each block is further divided into two sub-blocks with the first and second sub-block containing $\log_2 \left\lfloor \binom{N_t}{N_a} \right\rfloor_2$ and $N_a \log_2 (M)$ bits, respectively. The $\log_2 \left\lfloor \binom{N_t}{N_a} \right\rfloor_2$ bits of the first sub-block are used to choose the N_a antennas, out of the possible $\binom{N_t}{N_a}$ combinations, that are activated for transmission. The $N_a \log_2 (M)$ bits of the second sub-block are used to choose the N_a different symbol streams of M-QAM symbols that are emitted from the N_a antennas that are activated

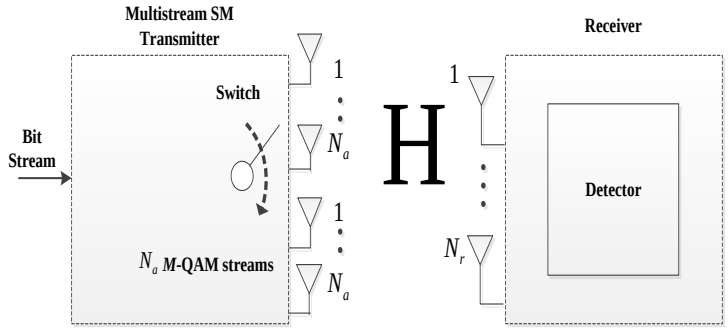

Figure 2.10: Multistream SM principle.

for transmission. Depending on the detection type at the receiver, the active antennas and the constellation symbols that are emitted from them can be jointly estimated by a ML detection. Consequently, the total $\log_2\left\lfloor \binom{N_t}{N_a} \right\rfloor_2 + N_a \log_2(M)$ bits can be recovered at the receiver.

Under the above assumptions, the received signal is given by

$$\mathbf{y} = \sqrt{\frac{E_m}{N_a}}\mathbf{H}_a\mathbf{S} + \mathbf{n} \tag{2.34}$$

where the columns of $\mathbf{H}_a \in \mathbb{C}^{N_r \times N_a}$ correspond to the selected N_a antennas. $\mathbf{H}_a$ can be written as

$$\mathbf{H}_a = \left[\mathbf{h}_{(1)}\mathbf{h}_{(2)}\ldots\mathbf{h}_{(N_a)}\right] \tag{2.35}$$

where $\mathbf{h}_{(l)} \in \mathbb{C}^{N_r \times 1}$ and $(l) \in \{1, 2, ..., N_t\}, l = 1, 2, ..., N_a$, denotes the index of the $l-th$ transmit antenna. The vector $\mathbf{S} = \left[s_1 s_2 \ldots s_{N_a}\right]^T$ consists of the N_a M-QAM streams that are transmitted.

Example: Let us assume that $N_t = 4$, $N_a = 2$, and the transmission rate is 6 bpcu. With this transmit configuration, there are $\binom{4}{2} = 6$ possible combinations of two transmit antennas. In particular, by indexing the transmit antennas as 1, 2, 3, and 4, the possible combinations are: [1,2], [1,3], [1,4], [2,3], [2,4], and [3,4]. From these combinations, $\lfloor 6 \rfloor_2 = 4$ are chosen, which means that $\log_2(4) = 2$ bits can be conveyed, apart from the bits of the signal-constellation diagram, by detecting at the receiver which pair of antennas has been activated for transmission. Specifically, if, for instance, the pairs [1,2], [1,3], [2,3], and [3,4] are chosen as the feasible pairs of antennas we can index them as 00, 01, 10, and 11, respectively. If the bitstream is for instance 00101110, then the first two bits (00) are used to activate the pair [1,2] of transmit antennas from which the 8-QAM streams 101 and 110 will be emitted from them. If the first

two bits are 10, the pair [2,3] will be activated and so on.

2.3.3 Performance Analysis of Multistream SM with ML Detection

2.3.3.1 Derivation of the ABEP Bound

Let us assume that the p_{th} subset of N_a antennas is activated and the q_{th} signal vector is transmitted. Then, the received signal is given by

$$\mathbf{y} = \sqrt{\frac{E_m}{N_a}}\mathbf{H}_{a_p}\mathbf{S}_q + \mathbf{n} \tag{2.36}$$

where $1 \leqslant p \leqslant \left\lfloor \binom{N_t}{N_a} \right\rfloor_2$ and $1 \leqslant q \leqslant M^{N_a}$. For convenience, we denote $B = \left\lfloor \binom{N_t}{N_a} \right\rfloor_2$ and $C = M^{N_a}$. Assuming that the constellation symbols are equally likely, the ML detector is the optimal detector and the estimation of p and q is given by

$$\begin{aligned}\left[\widehat{p}, \widehat{q}\right] &= \arg\max_{p,q} p_{\mathbf{y}}\left(\mathbf{y}\left|\mathbf{H}_{a_p}, \mathbf{S}_q\right.\right) \\ &= \arg\min_{p,q} \sqrt{\frac{E_m}{N_a}}\left\|\mathbf{H}_{a_p}\mathbf{S}_q\right\|_F^2 - 2\,\mathrm{Re}\left\{\mathbf{y}^H\mathbf{H}_{a_p}\mathbf{S}_q\right\} \\ &= d_{pq},\end{aligned} \tag{2.37}$$

where $p_{\mathbf{y}}\left(\mathbf{y}\left|\mathbf{H}_{a_p}, \mathbf{S}_q\right.\right) = \pi^{-N_r}\exp\left(-\left\|\mathbf{y} - \sqrt{\frac{E_m}{N_a}}\mathbf{H}_{a_p}\mathbf{S}_q\right\|_F^2\right)$ is the probabillity density function of $\mathbf{y}$ conditioned on $\mathbf{H}_{a_p}$ and $\mathbf{S}_q$.

For calculating the ABEP of multistream SM with ML detection the union bound formula is used and, particularly, the CUB that closely matches Monte Carlo simulations at the high-SNR region [26]. By using the CUB, the ABEP is bounded as

$$ABEP \leqslant F\sum_{p=1}^{B}\sum_{q=1}^{C}\sum_{\widehat{p}=1}^{B}\sum_{\widehat{q}=1}^{C} N_{b_{pq\to\widehat{p}\,\widehat{q}}} PEP_{pq\to\widehat{p}\,\widehat{q}} \tag{2.38}$$

where $F = \frac{1}{BC}\frac{1}{\log_2(BC)}$. $N_{b_{pq\to\widehat{p}\,\widehat{q}}}$ and $PEP_{pq\to\widehat{p}\,\widehat{q}}$ denote the number of bits in error and the pairwise error probability (PEP) between the constellation symbols $\mathbf{H}_{a_p}\mathbf{S}_q$ and $\mathbf{H}_{a_{\widehat{p}}}\mathbf{S}_{\widehat{q}}$, respectively. The PEP is given by

$$\begin{aligned}PEP_{pq\to\widehat{p}\,\widehat{q}} &= E_{\mathbf{H}}\left\{PEP\left(\mathbf{H}_{a_p}\mathbf{S}_q \to \mathbf{H}_{a_{\widehat{p}}}\mathbf{S}_{\widehat{q}}\left|\mathbf{H}\right.\right)\right\} \\ &= E_{\mathbf{H}}\left\{PEP\left(d_{pq} \to d_{\widehat{p}\,\widehat{q}}\left|\mathbf{H}\right.\right)\right\} \\ &= E_{\mathbf{H}}\left\{Q\left(\sqrt{\frac{\gamma}{2N_a}\left\|\mathbf{H}_{a_p}\mathbf{S}_q - \mathbf{H}_{a_{\widehat{p}}}\mathbf{S}_{\widehat{q}}\right\|_F^2}\right)\right\}\end{aligned} \tag{2.39}$$

In order to provide an insightful analysis, two cases are distinguished according to (2.39): i) Only the signals vectors are different between two constellation symbols in the PEP formula, i.e. $\mathbf{H}_{a_p} = \mathbf{H}_{a_{\widehat{p}}}$ and $\mathbf{S}_q \neq \mathbf{S}_{\widehat{q}}$. The ABEP resulting form this case is denoted as $ABEP_{signal}$. ii) $\mathbf{H}_{a_p}$ and $\mathbf{H}_{a_{\widehat{p}}}$ differ in at least one column, i.e. $\mathbf{H}_{a_p} \neq \mathbf{H}_{a_{\widehat{p}}}$. The ABEP resulting from this case is denoted as $ABEP_{jo\,\mathrm{int}}$ since both the spatial and signal components between two constellation symbols can differ with respect to each other. Based on these considerations, (2.38) can be written as

$$ABEP \leqslant ABEP_{signal} + ABEP_{jo\,\mathrm{int}} \tag{2.40}$$

1) *Analysis of* $ABEP_{signal}$: $ABEP_{signal}$ is given by

$$\begin{aligned} ABEP_{signal} &= \\ &= F\sum_{p=1}^{B}\sum_{q=1}^{C}\sum_{\widehat{q}\neq q=1}^{C} N_{b_{pq\to p\widehat{q}}} PEP_{pq\to p\widehat{q}} \\ &= \frac{1}{B}\frac{\log_2(C)}{\log_2(BC)}\sum_{p=1}^{B} ABEP_{MIMO_{N_a,M}} \\ &= \frac{\log_2(C)}{\log_2(BC)} ABEP_{MIMO_{N_a,M}} \end{aligned} \tag{2.41}$$

where

$$PEP_{pq\to p\widehat{q}} = E_{\mathbf{H}}\left\{Q\left(\sqrt{\frac{\gamma}{2N_a}\left\|\mathbf{H}_{a_p}\left(\mathbf{S}_q - \mathbf{S}_{\widehat{q}}\right)\right\|_F^2}\right)\right\} \tag{2.42}$$

and, consequently, $ABEP_{MIMO_{N_a,M}}$ is the ABEP of a conventional Spatial Multiplexing MIMO setup with ML detection, N_a transmit antennas, and M-QAM symbols emitted from each of them. Assuming that Gray encoding is used for the bit allocation of the signal constellation diagram, $ABEP_{MIMO_{N_a,M}}$ can be approximated as [35, Eq. (15)]

$$ABEP_{MIMO_{N_a,M}} \approx \frac{\beta_{MIMO}}{\log_2(M)}(2\gamma)^{-N_r}\begin{pmatrix} 2N_r - 1 \\ N_r - 1 \end{pmatrix} \tag{2.43}$$

where $\beta_{MIMO} = M^{-N_a}\sum_m\sum_j\left(\sum_i \beta_{s_q,ij}^{-N_r}\right)$ and $\beta_{s_q,ij} = \|d_i - d_j\|_F^2/2E_m$. d_i and d_j are defined in [Section III] [35].

2) *Analysis of* $ABEP_{joint}$: $ABEP_{joint}$ is given by

$$ABEP_{jo\,\mathrm{int}} = F\sum_{p=1}^{B}\sum_{q=1}^{C}\sum_{\widehat{p}\neq p=1}^{B}\sum_{\widehat{q}=1}^{C} N_{b_{pq\to\widehat{p}\,\widehat{q}}} PEP_{pq\to\widehat{p}\,\widehat{q}} \tag{2.44}$$

where $PEP_{pq\to\widehat{p}\,\widehat{q}}$ is given by (2.39). $PEP_{pq\to\widehat{p}\,\widehat{q}}$ can also be written as

$$PEP_{pq\to\widehat{p}\,\widehat{q}} = E_{\mathbf{h}}\left\{Q\left(\sqrt{\frac{\gamma}{2N_a}\left\|\sum_{i}^{d_{p,\widehat{p}}}\mathbf{h}_{p(i)}\left(s_{q_i}-s_{\widehat{q}_i}\right)+\sum_{j,j\neq i}^{N_a-d_{p,\widehat{p}}}\mathbf{h}_{p(j)}s_{q_j}-\mathbf{h}_{\widehat{p}(j)}s_{\widehat{q}_j}\right\|_F^2}\right)\right\}$$
$$= E_{\mathbf{h}}\left\{Q\left(\sqrt{u}\right)\right\}, \tag{2.45}$$

where $d_{p,\widehat{p}}$ is the number of common columns between the matrices $\mathbf{H}_{a_p}$ and $\mathbf{H}_{a_{\widehat{p}}}$. If, for instance, $\mathbf{H}_{a_p}=\left[\mathbf{h}_1\mathbf{h}_2\mathbf{h}_3\right]$ and $\mathbf{H}_{a_{\widehat{p}}}=\left[\mathbf{h}_1\mathbf{h}_2\mathbf{h}_4\right]$, then $d_{p,\widehat{p}}=2$.

By direct inspection of (2.45), it canbe observed that the argument of the square root inside the Q-function, which is denoted as u, is a chi-squared distributed random variable with $2N_r$ degrees of freedom. Hence, its probabillity density function (pdf), is given by [28, page 41] $p_{\mathbf{h}}(u)=\frac{u^{N_r-1}\exp\left(-\frac{u}{2\sigma^2_{pq,\widehat{p}\,\widehat{q}}}\right)}{\left(2\sigma^2_{pq,\widehat{p}\,\widehat{q}}\right)^{N_r}\Gamma(\mathrm{N}_r)}$ where $\Gamma(\cdot)$ denotes the Gamma function. $\sigma^2_{pq,\widehat{p}\,\widehat{q}}$ is given by

$$\sigma^2_{pq,\widehat{p}\,\widehat{q}}=\frac{\gamma}{4N_a}\left[\sum_{i}^{d_{p,\widehat{p}}}\left|s_{q_i}-s_{\widehat{q}_i}\right|^2+\sum_{j,j\neq i}^{N_a-d_{p,\widehat{p}}}\left(\left|s_{q_j}\right|^2+\left|s_{\widehat{q}_j}\right|^2\right)\right] \tag{2.46}$$

. Now, $PEP_{pq\to\widehat{p}\,\widehat{q}}$ can be derived as

$$PEP_{pq\to\widehat{p}\,\widehat{q}}=\int_0^\infty Q\left(\sqrt{u}\right)p_{\mathbf{h}}(u)\,du$$
$$=\mu^{N_r}_{pq,\widehat{p}\,\widehat{q}}\sum_{k=0}^{N_r-1}\binom{N_r-1+k}{k}\left(1-\mu_{pq,\widehat{p}\,\widehat{q}}\right)^k \tag{2.47}$$

where $\mu_{pq,\widehat{p}\,\widehat{q}}=\frac{1}{2}\left(1-\sqrt{\frac{\sigma^2_{pq,\widehat{p}\,\widehat{q}}}{1+\sigma^2_{pq,\widehat{p}\,\widehat{q}}}}\right)$.

2.3.3.2 Diversity Analysis

According to (2.40), the achievable diversity order of multistream SM with ML detection is the minimum between the diversity orders of $ABEP_{signal}$ and $ABEP_{joint}$. Based on (2.43) and by considering the notion of diversity, we conclude that the diversity order of $ABEP_{signal}$ is equal to N_r since the exponent of γ is equal to $-N_r$.

According to (2.44), the diversity order of $ABEP_{joint}$ is equal to the diversity order of each of the $PEP_{pq\to\widehat{p}\,\widehat{q}}$. However, (2.47) does not directly indicate the diversity order of

$PEP_{pq\to\widehat{p}\,\widehat{q}}$. To this end, the upper bound of the Q-function will be used, i.e. $Q(u) \leqslant (1/2)\exp(-u^2/2)$. As a result, $PEP_{pq\to\widehat{p}\,\widehat{q}}$ can be upper-bounded as

$$\begin{aligned} PEP_{pq\to\widehat{p}\,\widehat{q}} &\leqslant \frac{1}{2}\int_0^{\infty} \exp(-u/2) p_{\mathbf{h}}(u)\, du \\ &= \frac{1}{2}\left(1+\sigma^2_{pq,\widehat{p}\,\widehat{q}}\right)^{-N_r} \\ &\overset{\gamma\gg 1}{\simeq} \frac{1}{2}\left(\sigma^2_{pq,\widehat{p}\,\widehat{q}}\right)^{-N_r}. \end{aligned} \tag{2.48}$$

From (2.48), it is concluded that the diversity order of $ABEP_{jo\,\mathrm{int}}$ is also equal to N_r, which means that the ML detection for multistream SM offers full receive diversity, equal to N_r.

2.3.4 Numerical Results

The aim of this section is: i) To provide for different MIMO configurations and rates a performance comparison of multistream SM with ML detection with well-known schemes that exist in literature. ii) To also provide for these configurations an energy efficiency assessment at the transmitter, for a target ABEP, of multistream SM with the proposed optimal detection over those SOTA methods.

2.3.4.1 Performance Comparison

Fig. 2.11 shows the performance curves of multistream SM with ML detection, its counterpart with a suboptimal detector that was proposed in [36], the Alamouti scheme [37], conventional Spatial Multiplexing [35], and oprn-loop SM. For the latter two schemes, we used the optimal ML detection. We assumed a rate equal to 6 bpcu, $N_t = 4$, $N_a = 2$, and $N_r = 4$. Such a transmit MIMO setup can find implementation on next generation terminals, which are likely to be equipped with multiple antennas, but only a limited number of RF chains due mainly to size constraints, apart from complexity and cost issues.

Out of the possible $\binom{4}{2} = 6$ combinations of two active transmit antennas, we randomly select four of them for the multistream SM concept. Hence, 2 bits can be obtained from the spatial constellation diagram. The optimal choice of the subsets is left as a topic for future research. As it can be observed from Fig. 2.11, the presented analytical model of the ABEP

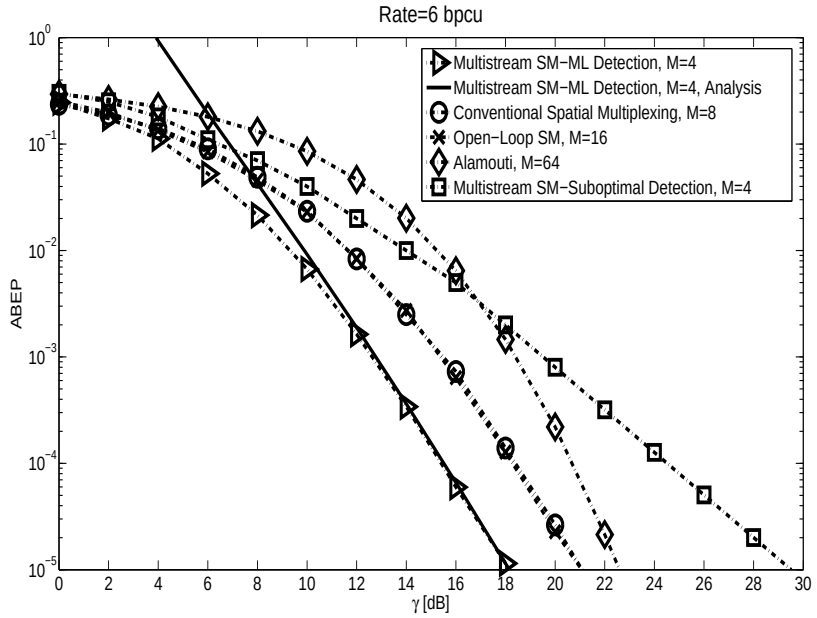

Figure 2.11: ABEP vs. γ for $N_t = 4$, $N_a = 2$, $N_r = 4$, and a rate of 6 bpcu. The dotted lines with markers represent Monte Carlo simulations.

of multistream SM perfectly matches the Monte Carlo simulations in the high-SNR region. In addition, it is observed that multistream SM with ML detection significantly outperforms the SOTA methods in the that region. Regarding its comparison with conventional Spatial Multiplexing and conventional SM, such high performance gains can be intuitively explained by considering the SNR advantage that the use of a smaller modulation order offers, especially for a high number of receive antennas. A similar trend has been observed in the comparison of SM with single-antenna systems [2].

As far as the comparison of multistream SM with ML detection with the Alamouti scheme is concerned, we see in Fig. 2.11 that although Alamouti has a higher total diversity due to its transmit diversity gain, the crossing point occurs for an ABEP lower than 10^{-5}, which is much lower than the ABEP requirements of many systems. Due to this, multistream SM with ML detection is the preferred choice, even though it has a smaller diversity than Alamouti. Finally, its full receive diversity in contrast to the SOTA multistream SM with the suboptimal detector, enables it to significantly outperform the latter method.

Fig. 2.12 shows the performance curves for the same MIMO setup as Fig. 2.11, but for a rate of 8 bpcu. As it can be observed, multistream SM with ML detection and conventional Spatial Multiplexing have a smaller performance difference than for the 6 bpcu rate case. Log-

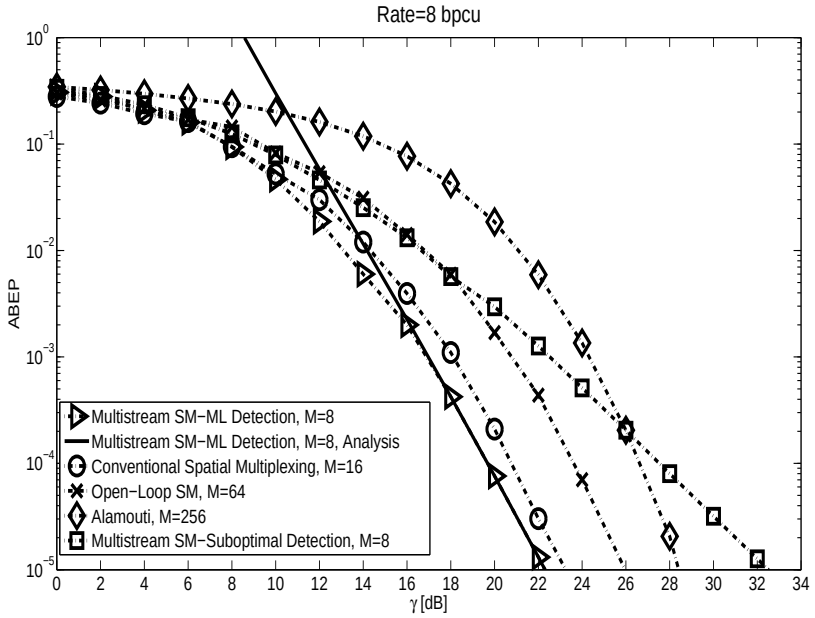

Figure 2.12: ABEP vs. γ for $N_t = 4$, $N_a = 2$, $N_r = 4$, and a rate of 8 bpcu. The dotted lines with markers represent Monte Carlo simulations.

ically thinking, this is attributed to the fact that the difference between the minimum Euclidean distances between 8-QAM and 16-QAM is smaller than the respective difference when QPSK and 8-QAM are employed for multistream SM and conventional Spatial Multiplexing, respectively, in the case of a 6 bpcu rate. Although their SNR difference is not significant, it is still advantageous to employ multistream SM instead of conventional Spatial Multiplexing due to the smaller modulation order used, which alleviates the problem of designing highly efficient RF amplifiers in the case of a high QAM modulation order.

2.3.4.2 Energy Gain Comparison

Now, the values for a target ABEP equal to 10^{-5} of the relative energy gain are presented, regarding the energy consumption at the transmitter, of multistream SM with ML detection over the Alamouti, conventional Spatial Multiplexing, SM, and multistream SM with the suboptimal detector methods. The relative energy gain is defined as $100\% \times \frac{\gamma_{SOTA} - \gamma_{Multis.\ SM-ML}}{\gamma_{SOTA}}$ and the respective values are given in Table 2.5. As it is observed, multistream SM achieves various energy efficiency gains over the SOTA methods that can reach up to almost 100%.

Table 2.5: Relative EE gain of multistream SM with ML detection over SOTA methods for a target ABEP=10^{-5}.

Rate = 6 bpcu			
Alamouti	Spat. Multip.	SM	Multistream SM-Suboptimal Detection
65%	50%	50%	93%
Rate = 8 bpcu			
Alamouti	Spat. Multip.	SM	Multistream SM-Suboptimal Detection
75%	21%	58%	90%

2.4 Conclusions

Motivated by the small amount of literature works regarding SM schemes that provide either transmit diversity or higher rates than the conventional open-loop approach, which can boost its energy-efficiency potentials, in this chapter:

1) Firstly, two transmit-diversity achieving closed-loop and SM-based schemes were proposed. In particular, the first scheme is designed for MISO channels and is based on the GSSK concept, in which more than one antennas can be activated for transmission and no constellation symbol (PSK/QAM) is conveyed. The proposed scheme relies on the feedback of the channel phases from the receiver to the transmitter, which are used for the design of the transmit precoding vectors in a way that the instantaneous BER is minimized. Numerical results show that the proposal not only achieves transmit diversity, but it can also significantly outperform several competitive closed-loop MISO transmission approaches in terms of both ABEP and transmit energy efficiency for various configurations.

The second closed-loop scheme proposed retains the basic single RF at the transmitter feature of conventional SM and is based on the selection of a subset of antennas at the transmitter for which SM is employed. The criterion is the selection of the subset that results in the minimum instantaneous SER. Two selection schemes are examined:

i) The optimal selection, which is based on an exhaustive search and results in a high computational burden at the receiver for the selection of the subset.

ii) A suboptimal selection, which is based on SVD decomposition and significantly alle-

viates the complexity of the optimal selection.

The results show that the two proposed algorithms can significantly outperform in terms of error rate and energy efficiency at the transmitter the conventional single-RF TAS with MRC at the receiver as the number of receive antennas increases. This is important from a practical point of view, since until recently single RF TAS with MRC was the most well known single RF scheme.

2) Secondly, an open-loop method for increasing the achievable rate of conventional SM was proposed, which is based on the merge of SM with Spatial Multiplexing. A tight high-SNR analytical framework for the error rate of the proposed scheme was proposed and it was observed in the numerical results that the proposal can outperform in terms of error rate and energy-efficiency at the transmitter competitive open-loop technologies, such as the open-loop SM, the Alamouti scheme, and the conventional Spatial Multiplexing.

APPENDIX

Let us consider two constellation points, $x_p(t)$ and $x_k(t)$, $p, k = 1, 2, ..., N_H$, of the proposed AGSSK-TOSD concept. According to (2.4), $x_p(t) = \sqrt{\frac{E_m}{N_a}} \left(\sum_{l=1}^{N_a} \left| h_{p(l)} \right| \right) e^{j\phi_p} u_p(t)$ and $x_k(t) = \sqrt{\frac{E_m}{N_a}} \left(\sum_{l=1}^{N_a} \left| h_{k(l)} \right| \right) e^{j\phi_k} u_k(t)$. Now, let us assume that the point $x_p(t)$ is conveyed, which means that $y(t) = x_p(t) + n(t)$. The decision metric is given by

$$D_i = \mathrm{Re}\left\{ \int_0^{T_m} y(t)\, x_i^*(t)\, dt \right\} - \frac{1}{2} \int_0^{T_m} x_i(t) x_i^*(t)\, dt, \quad i = p, k \tag{2.49}$$

where T_m is the symbol duration. Consequently, the probability that the p_{th} constellation point is detected instead of k_{th}, conditioned on the channel statistics, is given by

$$P_r\left(D_p < D_k \,|h\right) = P_r\left(\begin{array}{l} \frac{1}{2}\frac{E_m}{N_a}\left(\sum_{l=1}^{N_a}\left|h_{p(l)}\right|\right)^2 + \frac{1}{2}\frac{E_m}{N_a}\left(\sum_{l=1}^{N_a}\left|h_{k(l)}\right|\right)^2 \\ +\sqrt{\frac{E_m}{N_a}}\sum_{l=1}^{N_a}\left|h_{p(l)}\right|\mathrm{Re}\left\{\int_0^{T_m} n\left(t\right)e^{-j\phi_p}u_p^*\left(t\right)dt\right\} \\ < \frac{E_m}{N_a}\sum_{l=1}^{N_a}\left|h_{p(l)}\right|\sum_{l=1}^{N_a}\left|h_{k(l)}\right|e^{j\phi_p}e^{-j\phi_k}\int_0^{T_m} u_p\left(t\right)u_k^*\left(t\right)dt \\ +\sqrt{\frac{E_m}{N_a}}\sum_{l=1}^{N_a}\left|h_{k(l)}\right|\mathrm{Re}\left\{\int_0^{T_m} n\left(t\right)e^{-j\phi_k}u_k^*\left(t\right)dt\right\} \end{array}\right) \tag{2.50}$$

Case 1: $k = p + \frac{N_H}{2}$. Then, $\phi_k = \pi + \phi_p$ according to the bi-time-orthogonal design of (2.16). Consequently, from (2.50) we get

$$P_r\left(D_p < D_k \,|h\right) = Q\left(\sqrt{\frac{\gamma}{2N_a}}\left[\sum_{l=1}^{N_a}\left[\left|h_{p(l)}\right| + \left|h_{k(l)}\right|\right]\right]\right) \tag{2.51}$$

Case 2: $k \neq p + \frac{N_H}{2}$. Then, $u_p\left(t\right)$ and $u_k\left(t\right)$ are time-orthogonal and so we get from (2.50)

$$P_r\left(D_p < D_k \,|h\right) = P_r\left(\begin{array}{l} \frac{1}{2}\frac{E_m}{N_a}\left(\sum_{l=1}^{N_a}\left|h_{p(l)}\right|\right)^2 + \frac{1}{2}\frac{E_m}{N_a}\left(\sum_{l=1}^{N_a}\left|h_{k(l)}\right|\right)^2 \\ < \sqrt{\frac{E_m}{N_a}}\sum_{l=1}^{N_a}\left|h_{k(l)}\right|\mathrm{Re}\left\{\int_0^{T_m} n\left(t\right)e^{-j\phi_k}u_k^*\left(t\right)dt\right\} \\ -\sqrt{\frac{E_m}{N_a}}\sum_{l=1}^{N_a}\left|h_{p(l)}\right|\mathrm{Re}\left\{\int_0^{T_m} n\left(t\right)e^{-j\phi_p}u_p^*\left(t\right)dt\right\} \end{array}\right) =$$
$$Q\left(\sqrt{\frac{\gamma}{2N_a}\left[\left(\sum_{l=1}^{N_a}\left|h_{p(l)}\right|\right)^2 + \left(\sum_{l=1}^{N_a}\left|h_{k(l)}\right|\right)^2\right]}\right) \tag{2.52}$$

which is due to the fact that the factors $\mathrm{Re}\left\{\int_0^{T_m} n\left(t\right)e^{-j\phi_p}u_p^*\left(t\right)dt\right\}$ and $\mathrm{Re}\left\{\int_0^{T_m} n\left(t\right)e^{-j\phi_k}u_k^*\left(t\right)dt\right\}$ are independent zero-mean normally distributed processes with variance equal to $N_0/2$ each. The uncorrelatedness (and, consequently, independence) between them is due to the orthogonality of $u_p\left(t\right)$ and $u_k\left(t\right)$ [32, p. 234].

Bibliography

[1] Jeganathan, J.; Ghrayeb, A.; Szczecinski, L., "Spatial modulation: optimal detection and performance analysis," Communications Letters, IEEE , vol.12, no.8, pp.545,547, Aug. 2008.

[2] Di Renzo, M.; Haas, H., "Bit Error Probability of SM-MIMO Over Generalized Fading Channels," Vehicular Technology, IEEE Transactions on , vol.61, no.3, pp.1124,1144, March 2012.

[3] Younis, A.; Serafimovski, N.; Mesleh, R.; Haas, H., "Generalised spatial modulation," Signals, Systems and Computers (ASILOMAR), 2010 Conference Record of the Forty Fourth Asilomar Conference on , vol., no., pp.1498,1502, 7-10 Nov. 2010.

[4] Jeganathan, J.; Ghrayeb, A.; Szczecinski, L.; Ceron, A., "Space shift keying modulation for MIMO channels," Wireless Communications, IEEE Transactions on , vol.8, no.7, pp.3692,3703, July 2009.

[5] Jeganathan, J.; Ghrayeb, A.; Szczecinski, L., "Generalized space shift keying modulation for MIMO channels," Personal, Indoor and Mobile Radio Communications, 2008. PIMRC 2008. IEEE 19th International Symposium on , vol., no., pp.1,5, 15-18 Sept. 2008.

[6] Love, D.J.; Heath, R.W., "Equal gain transmission in multiple-input multiple-output wireless systems," Communications, IEEE Transactions on , vol.51, no.7, pp.1102,1110, July 2003.

[7] Heath, R.W.; Paulraj, A., "Antenna selection for spatial multiplexing systems based on minimum error rate," Communications, 2001. ICC 2001. IEEE International Conference on , vol.7, no., pp.2276,2280 vol.7, 2001.

[8] GORE, D.A.; Paulraj, A.J., "MIMO antenna subset selection with space-time coding," Signal Processing, IEEE Transactions on , vol.50, no.10, pp.2580,2588, Oct 2002.

[9] Ping Yang; Yue Xiao; Lei Li; Qian Tang; Yi Yu; Shaoqian Li, "Link Adaptation for Spatial Modulation With Limited Feedback," Vehicular Technology, IEEE Transactions on , vol.61, no.8, pp.3808,3813, Oct. 2012.

[10] Handte, T.; Muller, A.; Speidel, J., "BER Analysis and Optimization of Generalized Spatial Modulation in Correlated Fading Channels," Vehicular Technology Conference Fall (VTC 2009-Fall), 2009 IEEE 70th , vol., no., pp.1,5, 20-23 Sept. 2009.

[11] Tarokh, Vahid; Jafarkhani, Hamid; Calderbank, A.R., "Space-time block codes from orthogonal designs," Information Theory, IEEE Transactions on , vol.45, no.5, pp.1456,1467, Jul 1999.

[12] Di Renzo, M.; Haas, H., "Transmit-Diversity for Spatial Modulation (SM): Towards the Design of High-Rate Spatially-Modulated Space-Time Block Codes," Communications (ICC), 2011 IEEE International Conference on , vol., no., pp.1,6, 5-9 June 2011.

[13] Basar, E.; Aygolu, U.; Panayirci, E.; Poor, H.V., "Space-Time Block Coded Spatial Modulation," Communications, IEEE Transactions on , vol.59, no.3, pp.823,832, March 2011.

[14] Sugiura, S.; Sheng Chen; Hanzo, L., "Coherent and Differential Space-Time Shift Keying: A Dispersion Matrix Approach," Communications, IEEE Transactions on , vol.58, no.11, pp.3219,3230, November 2010.

[15] Sugiura, S.; Sheng Chen; Hanzo, L., "Generalized Space-Time Shift Keying Designed for Flexible Diversity-, Multiplexing- and Complexity-Tradeoffs," Wireless Communications, IEEE Transactions on , vol.10, no.4, pp.1144,1153, April 2011.

[16] Rajashekar, R.; Hari, K.V.S., "Modulation diversity for Spatial Modulation using Complex Interleaved Orthogonal Design," TENCON 2012 - 2012 IEEE Region 10 Conference , vol., no., pp.1,6, 19-22 Nov. 2012.

[17] Ali Khan, M.Z.; Rajan, B.S., "Single-symbol maximum likelihood decodable linear STBCs," Information Theory, IEEE Transactions on , vol.52, no.5, pp.2062,2091, May 2006.

[18] Ping Yang; Yue Xiao; Yi Yu; Shaoqian Li, "Adaptive Spatial Modulation for Wireless MIMO Transmission Systems," Communications Letters, IEEE , vol.15, no.6, pp.602,604, June 2011.

[19] Wei-Ho Chung; Cheng-Yu Hung, "Multi-Antenna Selection Using Space Shift Keying in MIMO Systems," Vehicular Technology Conference (VTC Spring), 2012 IEEE 75th , vol., no., pp.1,5, 6-9 May 2012.

[20] Ning Ma; Anguo Wang; Changcai Han; Yuchu Ji, "Adaptive joint mapping generalised spatial modulation," Communications in China (ICCC), 2012 1st IEEE International Conference on , vol., no., pp.520,523, 15-17 Aug. 2012.

[21] Di Renzo, M.; Haas, H., "Performance Comparison of Different Spatial Modulation Schemes in Correlated Fading Channels," Communications (ICC), 2010 IEEE International Conference on , vol., no., pp.1,6, 23-27 May 2010.

[22] Di Renzo, M.; Haas, H., "Space Shift Keying (SSK−) MIMO over Correlated Rician Fading Channels: Performance Analysis And a New Method for Transmit-Diversity," Communications, IEEE Transactions on , vol.59, no.1, pp.116,129, January 2011.

[23] Di Renzo, M.; De Leonardis, D.; Graziosi, F.; Haas, H., "Space Shift Keying (SSK−) MIMO with Practical Channel Estimates," Communications, IEEE Transactions on , vol.60, no.4, pp.998,1012, April 2012.

[24] Di Renzo, M.; Haas, H., "Space Shift Keying (SSK) Modulation: On the Transmit-Diversity / Multiplexing Trade-Off," Communications (ICC), 2011 IEEE International Conference on , vol., no., pp.1,6, 5-9 June 2011.

[25] Du Yang; Chao Xu; Lie-Liang Yang; Hanzo, L., "Transmit-Diversity-Assisted Space-Shift Keying for Colocated and Distributed/Cooperative MIMO Elements," Vehicular Technology, IEEE Transactions on , vol.60, no.6, pp.2864,2869, July 2011.

[26] Di Renzo, M.; Haas, H., "A General Framework for Performance Analysis of Space Shift Keying (SSK) Modulation for MISO Correlated Nakagami-m Fading Channels," Communications, IEEE Transactions on , vol.58, no.9, pp.2590,2603, September 2010.

[27] A Goldsmith, *Wireless Communications*, Cambridge University Press 2005.

[28] J Proakis, *Digital Communications*, 4th ed., McGraw−Hill, New York, 2000.

[29] Ney da Silva, J.A.; de Campos, M.L.R., "Spectrally Efficient UWB Pulse Shaping With Application in Orthogonal PSM," Communications, IEEE Transactions on , vol.55, no.2, pp.313,322, Feb. 2007.

[30] Shang-Ho Tsai, "Equal Gain Transmission with Antenna Selection in MIMO Communications," Wireless Communications, IEEE Transactions on , vol.10, no.5, pp.1470,1479, May 2011

[31] L. N. Trefethen and D. Bau III, *Numerical Linear Algebra*, Siam, June 1997.

[32] Rajashekar, R.; Hari, K.V.S.; Hanzo, L., "Antenna Selection in Spatial Modulation Systems," Communications Letters, IEEE , vol.17, no.3, pp.521,524, March 2013.

[33] Pillay, N.; Hongjun Xu, "Comments on "Antenna Selection in Spatial Modulation Systems"," Communications Letters, IEEE , vol.17, no.9, pp.1681,1683, September 2013.

[34] Zhuo Chen; Jinhong Yuan; Vucetic, B., "Analysis of Transmit Antenna Selection/Maximal-Ratio Combining in Rayleigh Fading Channels," Vehicular Technology, IEEE Transactions on , vol.54, no.4, pp.1312,1321, July 2005.

[35] Xu Zhu; Murch, R.D., "Performance analysis of maximum likelihood detection in a MIMO antenna system," Communications, IEEE Transactions on , vol.50, no.2, pp.187,191, Feb 2002.

[36] Jintao Wang; Shuyun Jia; Jian Song, "Generalised Spatial Modulation System with Multiple Active Transmit Antennas and Low Complexity Detection Scheme," Wireless Communications, IEEE Transactions on , vol.11, no.4, pp.1605,1615, April 2012.

[37] Alamouti, S., "A simple transmit diversity technique for wireless communications," Selected Areas in Communications, IEEE Journal on , vol.16, no.8, pp.1451,1458, Oct 1998.

Chapter 3

ANC in the MARC and the Two-Way Relaying Channel

3.1 Introduction

As discussed in Chapter 1, ANC is the simplest NC type since the relays do not have to decode the incoming signals from the sources, but they only need to amplify and forward them to the destination. The need of employing amplify-and-forward relays becomes evident if the relays are battery-powered mobile terminals that can afford complicated operations on the incoming signals due to energy constraints. Due to this, ANC is considered as a promising approach for next generation wireless networks in which the complexity of operations at the relays should be kept as low as possible. Hence, in this chapter the aim is to present two interesting scenarios where ANC can find implementation in future wireless networks as an energy-efficient and low-complexity approach. Towards this:

Contribution:

i) Firstly, the MARC is presented, in which multiple sources want to communicate with a common destination through the use of multiple relays, and it is discussed how ANC can be employed. Subsequently, for the optimal detector at the destination an error rate analytical framework is derived that is shown to be tight in the high-SNR region with respect to Monte Carlo simulations. Based on this framework, an energy efficiency comparison of ANC in the MARC with the conventional Time Division Multiple Access (TDMA) approach and prove that the possibility of ANC being more energy efficient than TDMA increases as the number

of sources, or the number of relays, or the modulation order increases. This analysis, which to the best of the author's knowledge has not been considered elsewhere in the literature, indicates the potentials of ANC as a promising approach in future networks. Furthermore, to alleviate the complexity burden of performing optimal detection, especially for a relatively high number of sources, analytical error rate frameworks for two widely considered linear detectors, the Zero Forcing (ZF) and the Minimum Mean Square Error (MMSE) [1], are presented which are shown to be tight in the high-SNR region for various scenarios. In addition, the problem of optimally allocating an assumed available budget in the network to the sources and the relays so that the error rate is minimized is formulated. In addition, it is proved that this problem is convex for the 3 receivers under consideration and, moreover, its solution is provided for the ZF and MMSE receivers.

ii) Secondly, the two-way relaying channel with ANC is investigated. In this scenario, two sources want to exchange information through the use of one amplify-and-forward relay. For this system model, an error rate analytical framework for the optimal receiver that takes into account imperfect channel estimates and also realistic modeling of interference coming from other networks is derived. In particular, the interference is modeled as a Poisson Point Process (PPP) [2], which is a more plausible scenario, as it will be explained, than modeling the interference as Gaussian, which the majority of literature works consider. The presented framework is tight under various scenarios with respect to Monte Carlo simulation, as it will be shown in the results. In addition, the energy gain that can be achieved for the two sources as the the radius of the region where the interferers cannot be found increases is substantiated.

3.2 The MARC with ANC

3.2.1 The Scenario

The MARC depicted in Fig. 3.1 is considered, which is a typical uplink scenario for next generation cellular networks and also included in the LTE-Advanced wireless standard [3]. In particular, K sources want to communicate with a common destination through the use of M fixed-gain and half-duplex relays. All the nodes are equipped with a single antenna and no direct links exist between the sources and the destination, which can be attributed to a large distance or a heavy-shadowing environment between the sources and the destination.

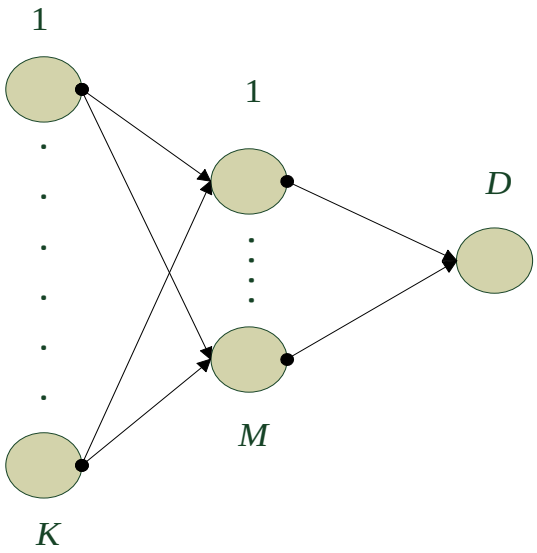

Figure 3.1: The MARC.

3.2.2 Previous Works

Few research works have investigated the performance of ANC in the MARC, especially from an information-theoretic point of view [7]- [11] (and references therein). In particular, in [7] the authors prove that ANC achieves the optimal diversity-multiplexing tradeoff at high multiplexing gains, as well as that it outperforms compress-and-forward and decode-and-forward relaying at low and high multiplexing gains, respectively. In [8], a family of optimal distributed space-time codes [9] for the two-user MARC is proposed, which achieve the optimal diversity-multiplexing tradeoff. In [10], the authors characterize the optimal relay amplification factor and the resulting optimal rate regions in multihop MARCs. Finally, in [11] expressions of the outage probability and ergodic capacity are obtained when distributed relay selection is applied.

Besides these notable information-theoretic results on the capabilities of ANC applied to the MARC, designers of practical systems are also interested in the expected system diversity and error probabilities when employing practical modulation schemes. Towards this end, the authors of [12] present a diversity analysis of ANC in the MARC, however no error rate framework is provided. Such a framework is important because it can provide estimates on the required power needed from the sources and relays to achieve a target error rate and, furthermore, it can enable the energy efficiency comparison of ANC with competitive approaches, such as TDMA. This is still an open issue.

3.2.3 System Model

A narrowband block-fading channel is assumed and let $h_{km} \sim CN(0,1)$ be the channel coefficient from the k_{th} source to the m_{th} relay and $f_m \sim CN(0,1)$ be the channel coefficient from the m_{th} relay to the destination, $k = 1, 2, ..., K$, $m = 1, 2, ..., M$. In addition, σ^2_{km} and $\sigma^2_{m_D}$ denote the path-loss coefficients of the source-relay and relay-destination links, respectively, which depend on both the distance between nodes and the shadowing environment between them. To simplify the notations and for analytical tractability of the derivations in the following sections, it is assumed that $\sigma^2_{km} = \sigma^2_{SR}$ and $\sigma^2_{m_D} = \sigma^2_{RD}$. Physically speaking, this means that the sources and the relays constitute two clusters (the nodes of the same cluster are located relatively close with each other in the same geographical area and, hence, under the same shadowing effect) and, hence, the path-loss coefficients of the source-relay and relay-destination links can be considered equal, respectively. Furthermore, it is assumed that: i) The channel coefficients that correspond to source-relay and relay-destination links are perfectly known to the destination (which can be possible via pilot-based channel estimation prior to data transmission) together with the corresponding path-loss coefficients, ii) The relays have statistical knowledge of the source-relay links, which means that they are aware of σ^2_{SR}, and iii) No feedback channel exists in the system (open-loop system). Finally, without loss of generality, it is considered that the sources and the relays have equal transmission powers, P_S and P_R, respectively, and all the sources employ the same modulation order Q.

The communication protocol consists of two transmission phases:

1st Phase - Transmission from the sources to the relays: During the first phase, which has a duration of 1 time slot, the K sources simultaneously transmit their modulated packets s_k to the relays. Hence, the received signal y_m at the m_{th} relay is given by

$$y_m = \sum_{k=1}^{K} \sqrt{P_S \sigma^2_{SR}} h_{km} s_k + n_m, \tag{3.1}$$

where $n_m \sim CN(0,1)$ is the AWGN at the m_{th} relay. This signal models assumes that there is perfect synchronization at the relays of the incoming signals from the sources, which can be achieved in real systems by following the method of [4, Section 7.2].

2nd Phase - Transmission from the relays to the destination: During the second phase, the fixed-gain relays amplify their received signal and forward it to the destination. As a case-study, the time-orthogonal transmission protocol from the relays is considered, which means that they

forward their signal to the destination sequentially in M non-overlapping time slots. Based on this protocol, $M+1$ time slots are required for the end-to-end communication between the sources and the destination.

The gain r_m of the relays, which normalizes their average transmission power with respect to the average received power of the sources, is given by [5]

$$r_m = \sqrt{\frac{1}{KP_S\sigma_{SR}^2 + 1}}. \tag{3.2}$$

Consequently, the received signal at the destination from each of the relays is

$$y_{D_m} = \sqrt{P_R\sigma_{RD}^2}r_m y_m f_m + n_D = \sqrt{\frac{P_S\sigma_{SR}^2 P_R\sigma_{RD}^2}{KP_S\sigma_{SR}^2 + 1}} f_m \sum_{k=1}^{K} h_{km}s_k + \tilde{n}_{Dm}, \tag{3.3}$$

where $n_D \sim CN(0,1)$ and $\tilde{n}_{Dm} \sim CN\left(0, \frac{P_R\sigma_{RD}^2}{KP_S\sigma_{SR}^2+1}|f_m|^2 + 1\right)$. In matrix form, (3.3) can be written as

$$\mathbf{y} = \sqrt{\frac{P_S\sigma_{SR}^2 P_R\sigma_{RD}^2}{KP_S\sigma_{SR}^2 + 1}}\mathbf{FHs} + \tilde{\mathbf{n}}_D, \tag{3.4}$$

where $\mathbf{F} \in \mathbb{C}^{M\times M}$ is a diagonal matrix with $f_1, ..., f_M$ being the elements of its main diagonal, $\mathbf{H} \in \mathbb{C}^{M\times K}$ with h_{km} as entries, $\mathbf{s} = \left(s_1 \cdots s_K\right)^T$, and $\tilde{\mathbf{n}}_D = \left(\tilde{n}_{D_1} \cdots \tilde{n}_{D_M}\right)^T$.

Remark 1 From (3.4), it is clear that the MARC with ANC and time-orthogonal transmission from the relays is equivalent to a spatial multiplexing MIMO system [6] with channel matrix $\mathbf{FH}$, where sources and relays are the equivalent to transmit and receive antennas, respectively. However, there are two main differences with respect to a conventional direct-link MIMO system: i) The channel consists of the product of two matrices with random elements, in particular $\mathbf{F}$ and $\mathbf{H}$. ii) The noise is dependent on random variables, in particular the relay-to-destination channel gains, as it can be observed from (3.4). Consequently, due to the new statistics created by this type of MIMO channel, compared to the direct-link MIMO counterpart, novel analytical expressions are needed to characterize the achievable error rate of ANC in the MARC. This is the main contribution of this work.

3.2.4 Error Rate Analysis for the Optimal ML Detector and Energy Efficiency Comparison with TDMA

3.2.4.1 SER with ML Detection

By employing the ML-optimal detection criterion, the destination can jointly detect the transmitted symbols from the sources as

$$\mathbf{s}_{det} = \arg\min_{\hat{s}_k} \sum_{m=1}^{M} \frac{\left| y_{D_m} - \sqrt{\frac{P_S\sigma_{SR}^2 P_R\sigma_{RD}^2}{KP_S\sigma_{SR}^2+1}} f_m \sum_{k=1}^{K} h_{km}\hat{s}_k \right|^2}{\frac{P_R\sigma_{RD}^2}{KP_S\sigma_{SR}^2+1}|f_m|^2 + 1}, \tag{3.5}$$

where $\mathbf{s}_{det} = \left(s_{1_{det}} \cdots s_{K_{det}}\right)^T$ is the detected symbol vector.

Based on (3.5), the aim is to derive an analytical closed-form framework for the union bound [6] of the SER per source. To this end, let $\{s_q\}$ denote the set of all possible Q symbols transmitted from a particular source, which are assumed to be equally probable. Furthermore, let $\{\mathbf{s}\}$ denote the set of the Q^K symbol vectors to be transmitted form the K sources, where $\{\mathbf{s}_i\}$ defines a subset of $\{\mathbf{s}\}$ in which the symbol vectors have s_q transmitted from the k_{th} source. Thus, in total there are Q^{K-1} such vectors. Also, let $\{\mathbf{s}_j\}$ denote the set of $Q^K - Q^{K-1}$ symbol vectors in which the symbol transmitted from the k_{th} source is different from s_q. Assuming that all the sources employ the same modulation order Q, the union bound of the SER for ML detection, which is denoted as SER_{ML}, is given by [6, Eq. (5)]

$$SER_{ML} \leqslant Q^{-K} \sum_{q=1}^{Q} \sum_{i=1}^{Q^{K-1}} \sum_{j=1}^{Q^K - Q^{K-1}} PEP_{s_q,ij}, \tag{3.6}$$

where $PEP_{s_q,ij}$ denotes the PEP of detecting the symbol vector $\mathbf{s}_j$ when the vector $\mathbf{s}_i$ is transmitted.

Proposition 1 $PEP_{s_q,ij}$ can be approximated in closed-form as

$$PEP_{s_q,ij} \approx \frac{1}{12}\left[\frac{1}{b+1} + \frac{bc}{a(b+1)^2} Z\left(\frac{c}{a\,(b+1)}\right)\right]^M + \frac{1}{6}\left[\frac{3}{4b+3} + \frac{12bc}{a(4b+3)^2} Z\left(\frac{3c}{a\,(4b+3)}\right)\right]^M, \tag{3.7}$$

where $Z\,(x) = e^x E_1\,(x)$, $a = P_R\sigma_{RD}^2$, $b = \frac{1}{4}P_S\sigma_{SR}^2 \left\|\mathbf{\Delta s}_{i,j}\right\|_F^2$, and $c = KP_S\sigma_{SR}^2 + 1$.

Proof: See APPENDIX A.1.

Consequently, by plugging (3.7) into (3.6) the union bound of the SER per source for ML detection is obtained.

Proposition 2 As $P_S, P_R \to \infty$, the pair-wise coding gain, which is denoted as $G_{Pair_{ij}}^{ML}$, and diversity order, which is denoted as G_{ML}^{div}, of the ML detector are given by

$$G_{Pair_{ij}}^{ML} = \left[\frac{1}{\left(\sigma_{RD}^2 \|\mathbf{\Delta s}_{i,j}\|_F^2\right)^M} \left[\frac{(4K)^M}{12} + \frac{(3K)^M}{6} \right] \right]^{-\frac{1}{M}}, \quad G_{ML}^{div} = M. \tag{3.8}$$

Proof: See APPENDIX A.2.

Remark 2 From (3.8), the following two observations for the ML detector in the high-SNR regime are made: i) A full diversity gain, equal to the number of relays, is achieved, regardless of the number of sources. ii) $G_{Pair_{ij}}^{ML}$ (and, consequently, SER_{ML}) decreases as the number of sources increases and, moreover, increases as σ_{RD}^2 increases. In particular, it can be observed that it only depends on σ_{RD}^2 and not on σ_{SR}^2. Hence, as σ_{RD}^2 increases, which means that the quality of the relay-destination links becomes better, SER_{ML} decreases.

3.2.4.2 Energy Efficiency Comparison with TDMA

Without performing network coding operations at the relays and by considering that only time is available as a resource and not bandwidth, which is a plausible scenario when there are many sources (users) inside a cell, then one known way to serve all the sources is by the TDMA approach. In this case, the sources are served sequentially and at any given time the bandwidth resources are used only by one source. Since in TDMA $M+1$ time slots are required for the end-to-end transmission of one source, in total $K(M+1)$ time slots are required for the end-to-end transmission of the K sources. Assuming that the sources and relays use the same power level, denoted as P_{TDMA}, without loss of generality, the total power used in the network in these $K(M+1)$ time slots, which we denote as P_{total}^{TDMA}, is given by

$$P_{total}^{TDMA} = K(M+1) P_{TDMA}. \tag{3.9}$$

On the other hand, since in ANC there is simultaneous transmission from the sources to the relays, only $M+1$ time slots are required for the end-to-end transmission of the K sources. Hence, in $K(M+1)$ time slots that are required for the end-to-end transmission of the K sources in TDMA, K rounds of end-to-end transmission occur in the ANC case. Consequently,

by assuming the same power level of the sources and the relays, which is denoted as P_{ANC}, the total power used in the network in these $K(M+1)$ time slots, which is denoted as P_{total}^{ANC}, is given by

$$P_{total}^{ANC} = K^2 P_{ANC} + KMP_{ANC} = K(K+M)P_{ANC}. \tag{3.10}$$

In addition, if Q_{ANC} is the modulation order of the sources used in the ANC case, then in the TDMA protocol the sources need to employ a modulation order Q_{TDMA} that is given by

$$Q_{TDMA} = Q_{ANC}^{K} \tag{3.11}$$

to match the same number of bits per source transmitted with the one of the ANC case.

Now, to make a fair energy requirement comparison of ANC with TDMA it is assumed that the total available power in both cases is the same, which means that

$$\begin{aligned} P_{total}^{ANC} &= P_{total}^{TDMA} \\ &\overset{(3.9),\,(3.10)}{\Rightarrow} (K+M)P_{ANC} = (M+1)P_{TDMA}. \end{aligned} \tag{3.12}$$

Considering (3.12), if ANC achieves a smaller BER per source than TDMA, then it achieves better energy efficiency or the other way round if the opposite happens. Consequently, to examine the energy saving prospects of ANC with respect to the TDMA protocol, the ratio

$$r_{TDMA/ANC} = \frac{BER_{TDMA}}{BER_{ANC}}. \tag{3.13}$$

If $r_{TDMA/ANC} > 1$, ANC is the preferred choice, energy-wise, otherwise TDMA is the preferred solution. BER_{ANC} is obtained from (3.6) as

$$BER_{ANC} \leqslant \frac{Q^{-K} \sum_{q=1}^{Q} \sum_{i=1}^{Q^{K-1}} \sum_{j=1}^{Q^K - Q^{K-1}} PEP_{s_q,ij}}{\log_2(Q)} \tag{3.14}$$

is formulated. BER_{TDMA} is obtained from (3.14) by setting $K = 1$ at the enumerator and $Q_{TDMA} = Q_{ANC}^{K}$ at the denominator, since the transmission takes place sequentially among the sources.

Theorem 1 $r_{TDMA/ANC}$ is a monotonically increasing function of i) K, ii) M, and ii) Q_{ANC}. This means that the possibility of using ANC instead of TDMA increases for increasing K, M, and Q_{ANC}.

Proof: See APPENDIX B.1.

3.2.5 Error Rate Analysis for the Suboptimal ZF and MMSE Detectors

3.2.5.1 ZF Detector

Due to the high complexity of the non-linear ML detector, even for a moderate number of sources and relays, it is of practical importance to consider low-complexity linear detectors that lead to individual source detection instead of a joint one, like the ML detector. Considering that the MARC with ANC is equivalent to a spatial multiplexing MIMO channel with channel matrix $\mathbf{FH}$, as it is shown in Section 3.2.1, a simple detector that falls to this category is the ZF detector [1]. In this case, the constraint $K \leqslant M$ needs to hold due to matrix inversion properties. Such a scenario requires an abundance of nodes acting as relays, which can be a real-world case considering that the relays can be inactive mobile terminals [15] or even the base stations of several underutilized femtocells overlaid in a macro-cell area with relaying capabilities [16], [17]. In the latter case, they can help, for instance, some macro-cell users that are scheduled to be analog network-coded in the uplink.

With a ZF receiver and considering that the channel matrix is $\mathbf{FH}$, the ZF-equalized received signal vector $\mathbf{y}_{eq}^{ZF}$ is given by [1]

$$\mathbf{y}_{eq}^{ZF} \overset{(a)}{=} \mathbf{G}_{ZF}\mathbf{y} = \sqrt{\frac{P_S\sigma_{SR}^2 P_R\sigma_{RD}^2}{KP_S\sigma_{SR}^2+1}}\mathbf{s} + \mathbf{G}_{ZF}\tilde{\mathbf{n}}_D = \sqrt{\frac{P_S\sigma_{SR}^2 P_R\sigma_{RD}^2}{KP_S\sigma_{SR}^2+1}}\mathbf{s} + \tilde{\mathbf{n}}_{ZF}, \tag{3.15}$$

where in (a) we use (3.4) and, moreover,

$$\mathbf{G}_{ZF} = \left[(\mathbf{FH})^H \mathbf{FH}\right]^{-1}(\mathbf{FH})^H, \quad \tilde{\mathbf{n}}_{ZF} = \mathbf{G}_{ZF}\tilde{\mathbf{n}}_D. \tag{3.16}$$

Proposition 3 Let $KP_S\sigma_{SR}^2+1 \gg P_R\sigma_{RD}^2$. Then, an approximate expression in the high-SNR regime for the SER of the ZF detector, which we denote as SER_{ZF}, is given by

$$SER_{ZF} \approx c_1\left[\frac{1}{3}\left[\frac{1}{c_2\bar{\gamma}}e^{\frac{1}{c_2\bar{\gamma}}}E_1\left(\frac{1}{c_2\bar{\gamma}}\right)\right]^{M-K+1} + \frac{2}{3}\left[\frac{1}{c_3\bar{\gamma}}e^{\frac{1}{c_3\bar{\gamma}}}E_1\left(\frac{1}{c_3\bar{\gamma}}\right)\right]^{M-K+1}\right], \tag{3.17}$$

where $\bar{\gamma}$ is the average pre-processing received SNR per source, given by

$$\bar{\gamma} = \frac{P_S\sigma_{SR}^2 P_R\sigma_{RD}^2}{KP_S\sigma_{SR}^2 + P_R\sigma_{RD}^2+1}. \tag{3.18}$$

and

$$c_1 = 1-\frac{1}{\sqrt{Q}}, \quad c_2 = \frac{3}{2\left(Q-1\right)}, \quad c_3 = \frac{2}{Q-1}. \tag{3.19}$$

Proof: See APPENDIX A.3.

Proposition 4 As $\bar{\gamma} \to \infty$, the coding gain and diversity order of the ZF detector, which we denote as G_{ZF}^{cod} and G_{ZF}^{div}, respectively, are given by

$$G_{ZF}^{cod} = \left[\frac{c_1}{3}\left({c_2}^{-(M-K+1)} + 2{c_3}^{-(M-K+1)}\right)\right]^{-\frac{1}{(M-K+1)}}, \quad G_{ZF}^{div} = M - K + 1. \tag{3.20}$$

Proof: See APPENDIX A.4.

Remark 3 From (3.20), we observe that G_{ZF}^{div} depends on the number of sources, as it was expected based on the ZF detector analysis in non-relay MIMO channels [1] and, specifically, it decreases as the number of sources increases. Hence, it is expected that the performance gap between the ML and ZF detectors increases as the number of sources increases.

In addition, although the derived analytical framework of (3.17) has been obtained by assuming that $KP_S\sigma_{SR}^2+1 \gg P_R\sigma_{RD}^2$ holds, it also performs reasonably well for the $KP_S\sigma_{SR}^2+1 > P_R\sigma_{RD}^2$ case, as it will be shown in the numerical results of Section 3.2.7.

Finally, we remark that the Rayleigh-product nature of the MARC with ANC, based on (3.4), together with the approximation of (3.109), makes the derived SER expression for the ZF receiver of (3.17) valid also for the special category of channels that are called Rayleigh-product or multi-keyhole [18].[1]

3.2.5.2 MMSE Detector

As in the ZF detector case, MMSE detection requires $K \leqslant M$ to work. For a general channel matrix $\mathbf{A}$, the equalizing receive filter for the k_{th} source, which we denote as $\mathbf{g}_{MMSE,k}$ is given by $\left(\mathbf{A}\mathbf{A}^H + \frac{1}{\bar{\gamma}}\mathbf{I}_M\right)^{-1}\mathbf{a}_k$ [19], where $\mathbf{a}_k$ is the k_{th} column of $\mathbf{A}$. In our case, $\mathbf{A} = \mathbf{F}\mathbf{H}$. Hence,

$$\mathbf{g}_{MMSE,k} = \left(\mathbf{F}\mathbf{H}\mathbf{H}^H\mathbf{F}^H + \frac{1}{\bar{\gamma}}\mathbf{I}_M\right)^{-1}\mathbf{F}\mathbf{h}_k, \tag{3.21}$$

where $\bar{\gamma}$ is given by (3.18).

[1] In [18] the authors derive closed-formed expressions for the ergodic sum rate of the ZF and MMSE receivers in Rayleigh-product channels, but not for the error rate of these receivers, which constitutes the main contribution in this work.

By considering (3.21), the MMSE-equalized received signal for the k_{th} source, which is denoted as $y_{eq,k}^{MMSE}$, is given by

$$y_{eq,k}^{MMSE} = \mathbf{g}_{MMSE,k}^{H}\mathbf{y} \overset{(f)}{=} \sqrt{\frac{P_S\sigma_{SR}^2 P_R\sigma_{RD}^2}{KP_S\sigma_{SR}^2+1}}\mathbf{g}_{MMSE,k}^{H}\mathbf{FHs} + \mathbf{g}_{MMSE,k}^{H}\tilde{\mathbf{n}}_D$$
$$= \sqrt{\frac{P_S\sigma_{SR}^2 P_R\sigma_{RD}^2}{KP_S\sigma_{SR}^2+1}}\mathbf{g}_{MMSE,k}^{H}\mathbf{Fh}_k s_k + \tilde{n}_k^{MMSE}, \tag{3.22}$$

where in (f) we use (3.4) and

$$\tilde{n}_k^{MMSE} = \sum_{i\neq k}\mathbf{g}_{MMSE,k}^{H}\mathbf{Fh}_i s_i + \mathbf{g}_{MMSE,k}^{H}\tilde{\mathbf{n}}_D. \tag{3.23}$$

As it can be observed from (3.23), $\tilde{n}_k^{MMSE}$ consists of the interference term $\sum\limits_{i\neq k}\mathbf{g}_{MMSE,k}^{H}\mathbf{Fh}_i s_i$ and the noise term $\mathbf{g}_{MMSE,k}^{H}\tilde{\mathbf{n}}_D$.

Proposition 5 Let $KP_S\sigma_{SR}^2+1 \gg P_R\sigma_{RD}^2$. Then, an approximate expression in the high-SNR regime for the SER of the MMSE detector, which we denote as SER_{MMSE}, is given by

$$SER_{MMSE} \approx \frac{c_1}{3}(K-1)\binom{M}{M-K+1}\left[A(c_2)+2A(c_3)\right], \tag{3.24}$$

where c_1, c_2, and c_3 are given by (3.19), and

$$A(c) = \left[\frac{1}{c\bar{\gamma}}e^{\frac{1}{c\bar{\gamma}}}E_1\left(\frac{1}{c\bar{\gamma}}\right)\right]^{M-K+1} e^c\sum_{k=0}^{K-2}(-1)^k\binom{K-2}{k}E_{M-K+3+k}(c). \tag{3.25}$$

Proof: See APPENDIX A.5.

Proposition 6 As $\bar{\gamma}\to\infty$, the coding gain and diversity order of the MMSE detector, which is denoted as G_{MMSE}^{cod} and G_{MMSE}^{div}, respectively, are given by

$$G_{MMSE}^{cod} = \left[\frac{c_1}{3}(K-1)\binom{M}{M-K+1}\left[C(c_2)+2C(c_3)\right]\right]^{-\frac{1}{M-K+1}}, \quad G_{MMSE}^{div} = M-K+1, \tag{3.26}$$

where

$$C(c) = c^{-(M-K+1)}e^c\sum_{k=0}^{K-2}(-1)^k\binom{K-2}{k}E_{M-K+3+k}(c). \tag{3.27}$$

Proof: See APPENDIX A.6.

Remark 4 From (3.26), we observe that the MMSE detector achieves the same diversity order as the ZF detector, but it has a different coding gain, as expected.

In addition, it is again noted, as in the case of the ZF detector, that although the derived analytical framework of (3.24) has been obtained by assuming that $KP_S\sigma_{SR}^2 + 1 \gg P_R\sigma_{RD}^2$ holds, it also works well for the $KP_S\sigma_{SR}^2 + 1 > P_R\sigma_{RD}^2$ case, as it will be shown in the numerical results of Section 3.2.7.

Finally, it can be noted, as in the case of the ZF detector, that the Rayleigh-product nature of the MARC with ANC, based on (3.4), together with the approximation of (3.109), makes the derived SER expression for the MMSE receiver of (3.24) valid also for the Rayleigh-product type of channels [18].

3.2.5.3 Comparison Between the ZF and MMSE Detectors

Since the ZF and MMSE detectors achieve the same diversity order, as we have proved in Section 3.2.5, it is interesting to examine how the ratio of their coding gains, which is denoted as $\frac{G_{MMSE}^{cod}}{G_{ZF}^{cod}}$, is affected by the number of sources, the number of relays, and the modulation order. From (3.20) and (3.26), we have

$$\frac{G_{MMSE}^{cod}}{G_{ZF}^{cod}} = \left[\frac{c_2^{-(M-K+1)} + 2c_3^{-(M-K+1)}}{(K-1)\binom{M}{M-K+1}\left[C\left(c_2\right) + 2C\left(c_3\right)\right]}\right]^{\frac{1}{M-K+1}}. \tag{3.28}$$

Theorem 2 $\frac{G_{MMSE}^{cod}}{G_{ZF}^{cod}}$ is: i) A monotonically increasing function of K. ii) A monotonically decreasing function of M. iii) A monotonically decreasing function of Q.

Proof: See APPENDIX B.2.

These trends validate and, furthermore, corroborate the findings of [1], which was the first work presenting the surprising result that there is a non-vanishing gap between the performance of the ZF and MMSE receivers in a non-relay MIMO setup, as the SNR tends to infinity. Consequently, it is proved that the non-vanishing performance gap between these receivers behaves monotonically with respect to the number of sources, the number of relays, and the modulation order.

3.2.6 Optimal Power Allocation in the High-SNR Regime

Let us assume that there is a total power budget in the network, denoted as P_{budget}, to be allocated to source and relay nodes. By considering this, the aim of optimal power allocation policies is to distribute P_{budget} between source and relay nodes in such a way that the SER per source is minimized. This is the main objective of this section.

In particular, the optimal power allocation problem can be formulated as

$$\begin{aligned} \underset{P_S,P_R}{\text{minimize}} \quad & SER\left(P_S,P_R\right) \\ \text{subject to} \quad & P_{budget} = KP_S + MP_R. \end{aligned} \tag{3.29}$$

In the following, i) It is proved that (3.29) is a convex problem for the three receivers under analysis and, consequently, it has a unique solution. ii) For the ZF and MMSE receivers, the solution of (3.29) is provided in closed form.

3.2.6.1 ML detector

For the ML receiver, the PEP $PEP_{s_q,ij}$ between the symbol vectors $\mathbf{s}_i$ and $\mathbf{s}_j$ is given by (3.7). To make the optimal power allocation problem analytically tractable, the optimal power allocation in the high-SNR regime is considered, which means that $P_S,\ P_R \gg 1$. Then, (3.7) can be upper bounded as

$$PEP_{s_q,ij} \lessapprox \frac{1}{\left[\left\|\Delta\mathbf{s}_{i,j}\right\|_F^2\right]^M}\left[\frac{(4K)^M}{12}+\frac{(3K)^M}{6}\right]\left[\frac{1}{\sigma_{SR}^2\left(P_{budget}-MP_R\right)}+\frac{\log\left(1+\sigma_{RD}^2P_R\right)}{\sigma_{RD}^2P_R}\right]^M, \tag{3.30}$$

where we have used $P_S = \frac{P_{budget}-MP_R}{K}$ and the inequality $E_1\left(z\right) < e^{-z}\log\left(1+\frac{1}{z}\right)$ [14, 5.1.20]. As it is observed from (3.30), the factor that is included in all the pairwise error probabilities and depends on the power allocation is $\left[\frac{1}{\sigma_{SR}^2\left(P_{budget}-MP_R\right)}+\frac{\log\left(1+\sigma_{RD}^2P_R\right)}{\sigma_{RD}^2P_R}\right]^M$. Hence, the objective function of the SER bound to be included in the power allocation problem so as to minimize the SER is

$$D_{ML}\left(P_R\right) = \frac{1}{\sigma_{SR}^2\left(P_{budget}-MP_R\right)}+\frac{\log\left(1+\sigma_{RD}^2P_R\right)}{\sigma_{RD}^2P_R}. \tag{3.31}$$

Based on (3.31), in the case of ML detection (3.29) is formulated as follows:

$$\begin{aligned} \underset{P_R}{\text{minimize}} \quad & D_{ML}\left(P_R\right) \\ \text{subject to} \quad & P_R \in \left(0, \frac{P_{budget}}{M}\right). \end{aligned} \tag{3.32}$$

Theorem 3 (3.32) is a convex optimization problem since $D_{ML}\left(P_R\right)$ is a convex function in $P_R \in \left(0, \frac{P_{budget}}{M}\right)$.

Proof: See APPENDIX B.3.

Due to the fact that the $D_{ML}\left(P_R\right)$ includes the term $\log\left(1+\sigma_{RD}^2 P_R\right)$, it is not possible to find a closed-form expression for the value of P_R that minimizes it. However, since $D_{ML}\left(P_R\right)$ is convex and a single-variable function, a line-search in any computational software program can be performed for finding this value. Subsequently, P_S is obtained as $\frac{P_{budget}-MP_R}{K}$, for the given P_{budget}.

3.2.6.2 ZF detector

From (3.107) and by using $E_1\left(z\right) < e^{-z}\log\left(1+\frac{1}{z}\right)$ [14, 5.1.20], we get

$$SER_{ZF} \lessapprox \frac{c_1}{3}\left[\left(\frac{\log\left(1+c_2\bar{\gamma}\right)}{c_2\bar{\gamma}}\right)^{M-K+1} + 2\left(\frac{\log\left(1+c_3\bar{\gamma}\right)}{c_3\bar{\gamma}}\right)^{M-K+1}\right]. \tag{3.33}$$

From (3.33), it follows that the objective function to be minimized is

$$D_{ZF}\left(P_R\right) = \frac{\log\left(1+\bar{\gamma}\right)}{\bar{\gamma}} \overset{(p)}{=} \frac{\log\left(1+\frac{\sigma_{SR}^2\sigma_{RD}^2}{K}\frac{\left(P_{budget}-MP_R\right)P_R}{\sigma_{SR}^2 P_{budget}-P_R\left(M\sigma_{SR}^2-\sigma_{RD}^2\right)+1}\right)}{\frac{\sigma_{SR}^2\sigma_{RD}^2}{K}\frac{\left(P_{budget}-MP_R\right)P_R}{\sigma_{SR}^2 P_{budget}-P_R\left(M\sigma_{SR}^2-\sigma_{RD}^2\right)+1}}, \tag{3.34}$$

where in (p) (3.18) and $P_S = \frac{P_{budget}-MP_R}{K}$ is used. In addition, in (3.34) excluded the multiplicative factors $c_2,\ c_3 > 0$ that exist in (3.33) are excluded since a P_R value that minimizes the term $\frac{\log(1+\bar{\gamma})}{\bar{\gamma}}$ also minimizes $\frac{\log(1+c\bar{\gamma})}{c\bar{\gamma}}\ \forall c > 0$, since c is a multiplicative constant. Hence, for ZF detection (3.29) becomes

$$\begin{aligned} \underset{P_R}{\text{minimize}} \quad & R\left(P_R\right) = \frac{\log\left(1+S\left(P_R\right)\right)}{S\left(P_R\right)} \\ \text{subject to} \quad & P_R \in \left(0, \frac{P_{budget}}{M}\right), \end{aligned} \tag{3.35}$$

where

$$S\left(P_R\right)=\frac{\left(P_{budget}-MP_R\right)P_R}{\sigma_{SR}^2P_{budget}-P_R\left(M\sigma_{SR}^2-\sigma_{RD}^2\right)+1}. \tag{3.36}$$

Now, Lemma 1 is presented, which will be used for proving Theorem 4 that is subsequently presented.

Lemma 1 Assuming two continuous functions $f\left(x\right)$ and $g\left(x\right)$, where $f\left(x\right)$ is concave and $g\left(x\right)$ is convex and non-increasing (monotonically decreasing), it holds that $h\left(x\right)=g\left(f\left(x\right)\right)$ is a convex function.

Proof: See [21, (3.10)].

Theorem 4 $R\left(P_R\right)$ is a convex function in $P_R\in\left(0,\frac{P_{budget}}{M}\right)$ and, hence, (3.35) is a convex optimization problem with solution $P_{R_{sol}}$ given by

$$P_{R_{sol}}=\begin{cases}\frac{M\left(1+\sigma_{SR}^2P_{budget}\right)-\sqrt{M^2\left(1+\sigma_{SR}^2P_{budget}\right)^2-M\left(M\sigma_{SR}^2-\sigma_{RD}^2\right)\left(P_{budget}+P_{budget}^2\sigma_{SR}^2\right)}}{M\left(M\sigma_{SR}^2-\sigma_{RD}^2\right)}, & \text{if} \quad M\sigma_{SR}^2\neq\sigma_{RD}^2.\\ \frac{P_{budget}}{2M}, & \text{otherwise.}\end{cases} \tag{3.37}$$

Proof: See APPENDIX B.4.

3.2.6.3 MMSE detector

From (3.24) and by using $E_1\left(z\right)<e^{-z}\log\left(1+\frac{1}{z}\right)$ [14, 5.1.20], we have

$$SER_{MMSE}\lessapprox\frac{c_1}{3}\left(K-1\right)\binom{M}{M-K+1}\left[P\left(c_2\right)+P\left(c_3\right)\right], \tag{3.38}$$

where

$$P\left(c\right)=\left[\frac{\log\left(1+c\bar{\gamma}\right)}{c\bar{\gamma}}\right]^{M-K+1}e^c\sum_{k=0}^{K-2}\left(-1\right)^k\binom{K-2}{k}E_{M-K+3+k}\left(c\right). \tag{3.39}$$

Due to fact that (3.38) contains the same term $\frac{\log(1+c\bar{\gamma})}{c\bar{\gamma}}$, $c>0$, that exists in the case of the ZF detector, the same optimal power allocation applies to the MMSE detector as the one for the ZF detector. Hence, $P_{R_{sol}}$ for the MMSE case is again given by (3.37).

3.2.7 Numerical Results

The aim in this section is threefold: i) To substantiate the close match, with respect to Monte Carlo simulations, of the derived analytical error rate frameworks for the examined ML, ZF, and MMSE receivers for ANC and to examine under which scenarios the optimal power allocation policy can be beneficial compared to the equal one. ii) To numerically validate Theorem 1. iii) To numerically validate Theorem 2.

3.2.7.1 SER Curves and Energy Gain of the Optimal Power Allocation Policy

In Figs. 3.2, 3.3, 3.4, and 3.5, we illustrate the SER vs. $\frac{P_{budget}}{(K+M)}$ curves for the examined three receivers for ANC in balanced ($\sigma_{SR}^2 = \sigma_{RD}^2$) and unbalanced ($\sigma_{SR}^2 \neq \sigma_{RD}^2$) scenarios and for different number of sources. Both the equal power allocation policy, denoted as EPA, and the optimal one, denoted as OPA, based on Section IV are considered. From these Figures, in most scenarios the close match in the high-SNR regime (equivalently, for SER$\leqslant 10^{-2}$, as it could be seen) of the derived analytical frameworks with the Monte Carlo simulations is observed, with the only exception for ZF and MMSE receivers when $K = 2$, $\sigma_{SR}^2 = 1$ and $\sigma_{RD}^2 = 4$, for which it holds that $KP_S\sigma_{SR}^2 + 1 < P_R\sigma_{RD}^2$. This looseness of the framework for this scenario was expected due to the approximation of the channel noise, according to (3.109). However, it is noted that the need for employing the suboptimal ZF and MMSE receivers becomes greater as K increases, due to the high complexity of the ML detection, and, hence, it is expected that in real-world scenarios $KP_S\sigma_{SR}^2 + 1 > P_R\sigma_{RD}^2$ applies, which makes the derived SER frameworks for the ZF and MMSE receivers being in close agreement with the simulations results, as it is observed in Fig. 3.5. Furthermore, error rates lower or equal to 10^{-2} are typical error rate requirements from the system designer in uncoded systems (which is what we consider in our case), since with channel coding the error rates can be significantly reduced. Hence, although the derived SER formulas for the three examined receivers are based on high-SNR considerations, their close match with the Monte Carlo simulations for SER$\leqslant 10^{-2}$ verifies their practical importance.

In addition, from Figs. 3.2, 3.3, 3.4, and 3.5 the following regarding the optimal power allocation policy is observed:

i) The performance gains over the EPA are practically the same for both the case where the

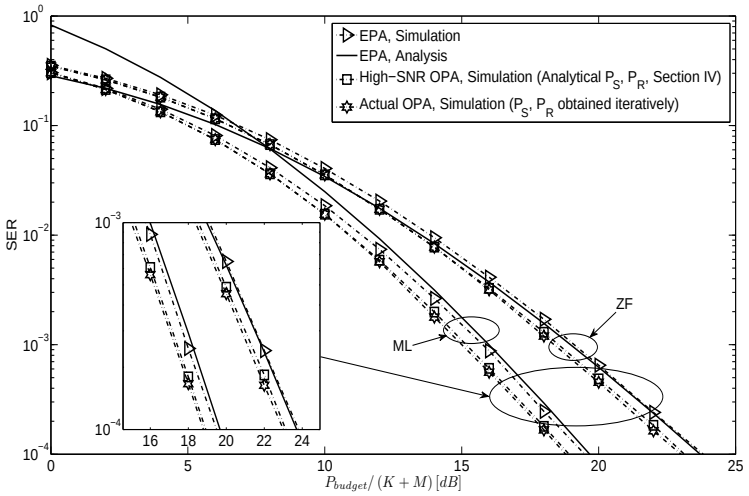

(a)

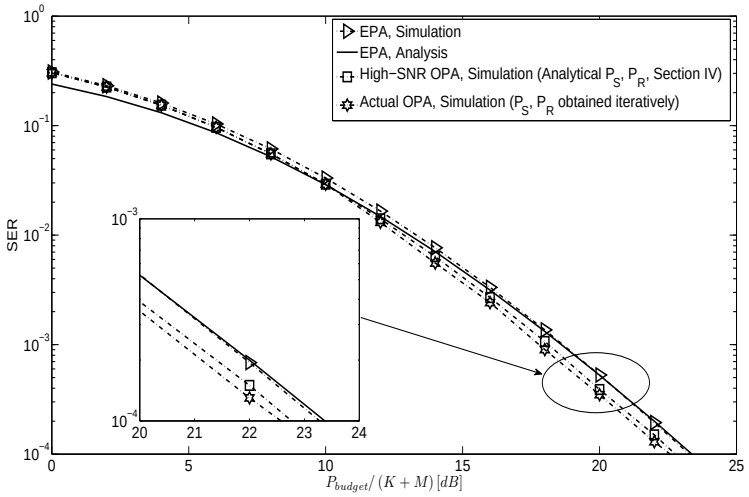

(b)

Figure 3.2: SER vs. $\frac{P_{budget}}{(K+M)}$ [dB] for $K = 2$, $M = 4$, and $Q = 4$, and (a) ML and ZF for $\sigma_{SR}^2 = 4$ and $\sigma_{RD}^2 = 1$, (b) MMSE for $\sigma_{SR}^2 = 4$ and $\sigma_{RD}^2 = 1$.

optimal values of P_S and P_R are obtained analytically (Section 3.2.6) and iteratively through linear search (actual optimal power allocation). This validates the accuracy and importance of the analytically derived optimal power allocation of Section 3.2.6.

ii) The policy is more beneficial when $\sigma_{SR}^2 > \sigma_{RD}^2$ (the quality of the source-relay links is better than the corresponding one of the relay-destination links). In particular, noticeable gains can be observed for this case. To understand why this happens, let us, for instance, examine the SER formula in the high-SNR regime of the ML receiver, according to (3.106). It can be seen that when $P_S,\ P_R \to \infty$, the SER of the ML detector depends only on P_R and σ_{SR}^2, which means that the higher these values are, the lower the SER is. Hence, if, for instance,

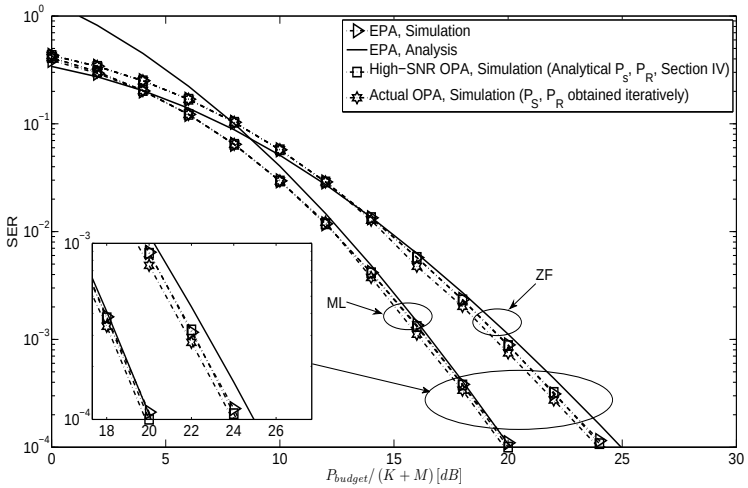

(a)

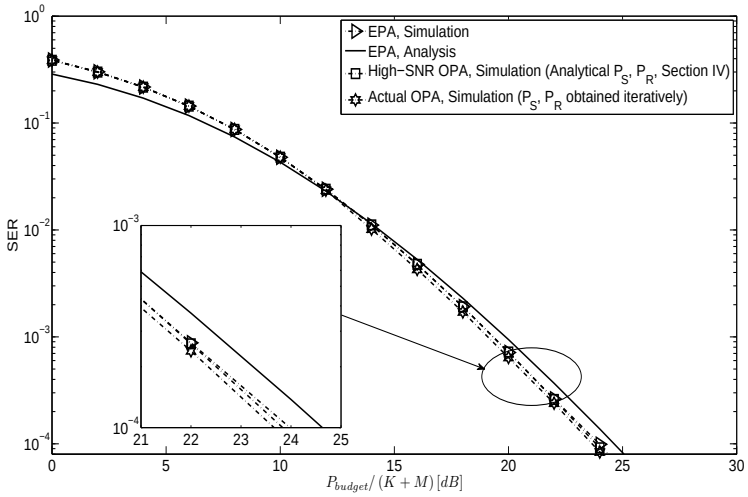

(b)

Figure 3.3: SER vs. $\frac{P_{budget}}{(K+M)}$ [dB] for $K = 2$, $M = 4$, and $Q = 4$, and (a) ML and ZF for $\sigma_{SR}^2 = 1$ and $\sigma_{RD}^2 = 1$, (b) MMSE for $\sigma_{SR}^2 = 1$ and $\sigma_{RD}^2 = 1$.

$\sigma_{SR}^2 > \sigma_{RD}^2$ and $P_S = P_R$ (EPA), the minimization of the SER per source entails allocating more power to the relays so that the factor $P_R\sigma_{RD}^2$ increases, based on (3.106). On the other hand, if $\sigma_{SR}^2 < \sigma_{RD}^2$, then the factor $P_R\sigma_{RD}^2$ has an adequate value to give a low enough SER and, consequently, the optimal power allocation policy provides minimal gains, as we see in Fig. 3.4 and Fig. 3.5. A similar conclusion can be drawn by examining the high-SNR SER analytical framework of the ZF and MMSE detectors.

iii) The higher the number of sources is, the higher the gain with respect to the equal power allocation policy is. This can be explained by the fact that the sub-optimality of the latter policy becomes more pronounced as the number of nodes increases.

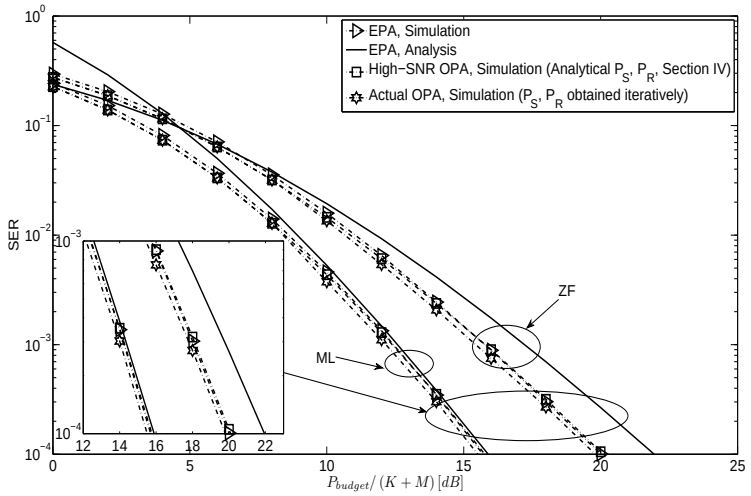

(a)

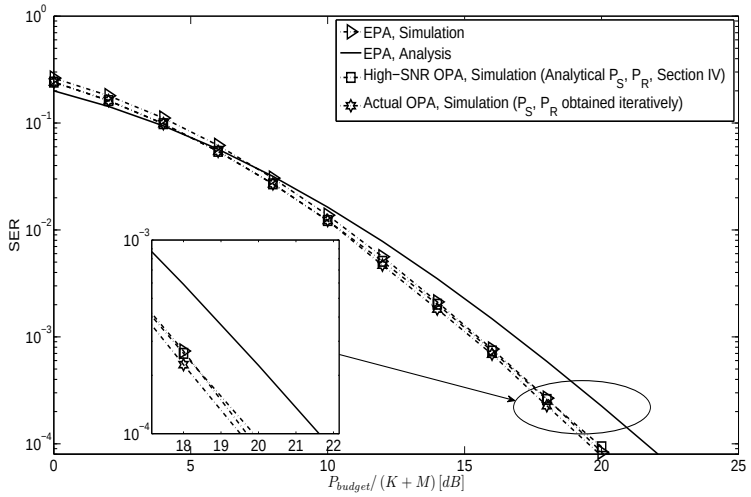

(b)

Figure 3.4: SER vs. $\frac{P_{budget}}{(K+M)}$ [dB] for $K = 2$, $M = 4$, and $Q = 4$, and (a) ML and ZF for $\sigma^2_{SR} = 1$ and $\sigma^2_{RD} = 4$, (b) MMSE for $\sigma^2_{SR} = 4$ and $\sigma^2_{RD} = 1$.

Now, to numerically substantiate the optimal power allocation policy energy gains over the equal power allocation policy, which are observed in Figs. 3.2, 3.3, 3.4, and 3.5, the relative energy gain between these two policies is formulated, which is denoted as E_{gain}, and it is given by

$$E_{gain} = \frac{P^{EPA}_{budget} - P^{OPA}_{budget}}{P^{EPA}_{budget}} \, [\%] \, , \tag{3.40}$$

where P^{EPA}_{budget} and P^{OPA}_{budget} denote the total power needed among the sources and relays to achieve a target SER for the equal and the optimal power allocation policy, respectively. Table 3.1 shows both the E_{gain} and $P^{EPA}_{budget} - P^{OPA}_{budget}$ values, where P^{EPA}_{budget} and P^{OPA}_{budget} have been obtained by Monte Carlo simulations, for the examined configurations of Figs. 3.2, 3.3, 3.4, 3.5 and for

a target SER=10^{-4}.

Table 3.1: $P_{budget}^{EPA} - P_{budget}^{OPA}$ and E_{gain} for $M = 4$, $Q = 4$, and target SER=10^{-4}.

$\sigma_{SR}^2 = 4$ and $\sigma_{RD}^2 = 1$		$\sigma_{SR}^2 = 1$ and $\sigma_{RD}^2 = 1$		$\sigma_{SR}^2 = 1$ and $\sigma_{RD}^2 = 4$	
ML	ZF/MMSE	ML	ZF/MMSE	ML	ZF/MMSE
$P_{budget}^{EPA} - P_{budget}^{OPA}$ [dB] & E_{gain} (%)					
$K = 2$					
0.7 & 14.9	0.7 & 14.9	0 & 0	0 & 0	0 & 0	0 & 0
$K = 3$					
1.5 & 29	1.4 & 27.6	0.7 & 14.9	0.7 & 14.9	0.1 & 2.3	0 & 0
$K = 4$					
2 & 36.9	2 & 36.9	1.2 & 24.1	1 & 20.1	0.2 & 4.5	0 & 0

As it is observed from Table 3.1, for $K = M = 4$, $\sigma_{SR}^2 = 4$, and $\sigma_{RD}^2 = 1$, E_{gain} is close to 40 %, which clearly indicates how important the optimal power allocation policy is for some configurations. Moreover, we see that approximately the same gains are achieved with the optimal power allocation over the equal one for all the examined receivers, as it was expected. This constitutes an indication that the noise approximation of (3.109), which was used in the performance analysis of both the ZF and MMSE detector, does not lead to a suboptimal power allocation in the high-SNR regime.

Finally, it can be noted that the simulation results show that the performance gap between the ML and ZF/MMSE detectors increases with increasing number of sources, which was expected, as it is aforementioned in Section 3.2.5.1, due to the dependency of the diversity order of the latter receivers on the number of sources in contrast to the ML detector.

Now, in order to get some insights of how the power is allocated to the sources and the relays in the OPA case, in Table 3.2 P_S an P_R are showed in the EPA an OPA cases for a P_{budget} that gives a SER of 10^{-4} in the EPA case and for balanced and unbalanced settings. As it can be observed form Table 3.2, when the channel quality of the source-relay links is better or the same with the one of the relay-destination links, substantially less power should be allocated to the sources than the relays to minimize the SER. This is a very important result from a practical point of view since the sources are likely to be battery-powered mobile terminals in the uplink

and, hence, significant energy gains and, consequently, expansion of operational duration for those devices are expected by employing the OPA policy. On the other hand, although the power of the relays needs to increase in most scenarios compared to the EPA case, this may not pose a problem since the relays are likely to be connected to the power network (since it is more likely to be larger devices, such as femto base stations, as it was justified in Section 3.2.5).

Table 3.2: EPA and OPA (in dB) for $K = M = 4$, $Q = 4$, and P_{budget} that gives SER=10^{-4} in the EPA case.

ML		ZF		MMSE	
EPA	OPA	EPA	OPA	EPA	OPA
$\sigma_{SR}^2 = 4$ and $\sigma_{RD}^2 = 1$					
$P_S = P_R = 23.8$	$P_S = 16.8$ $P_R = 26.4$	$P_S = P_R = 56$	$P_S = 52$ $P_R = 58$	$P_S = P_R = 51.5$	$P_S = 47.5$ $P_R = 53.5$
$\sigma_{SR}^2 = 1$ and $\sigma_{RD}^2 = 1$					
$P_S = P_R = 24.1$	$P_S = 19.7$ $P_R = 26.2$	$P_S = P_R = 56.3$	$P_S = 54.5$ $P_R = 57.5$	$P_S = P_R = 51.8$	$P_S = 50$ $P_R = 53$
$\sigma_{SR}^2 = 1$ and $\sigma_{RD}^2 = 4$					
$P_S = P_R = 22$	$P_S = 19.7$ $P_R = 23.5$	$P_S = P_R = 52$	$P_S = 52$ $P_R = 52$	$P_S = P_R = 48$	$P_S = 48$ $P_R = 48$

3.2.7.2 Numerical Validation of Theorem 1

Assuming that P_{total}^{TDMA} and P_{total}^{ANC} are the total power of the sources and relays required to achieve a target BER in the TDMA and ANC case, respectively, based on Section 3.2.4.2, the relative energy gain that is achieved by the use of ANC instead of TDMA for the particular target BER is defined as

$$relative\ energy\ gain = \frac{P_{total}^{TDMA} - P_{total}^{ANC}}{P_{total}^{TDMA}}\,[\%]\,. \tag{3.41}$$

In Tables 3.3 and 3.4, this gain is illustrated for a target BER of 10^{-4}, $\sigma_{SR}^2 = \sigma_{RD}^2 = 1$, different number of sources, relays, and two values for the modulation order. To obtain the

P_{total}^{TDMA} and P_{total}^{ANC} values to achieve this target BER, the analytical framework for the BER of (3.14) is used.

Table 3.3: Relative Energy Gain (%) of Analog Network Coding over TDMA for $Q_{ANC} = 2$ (BPSK).

$K = 2$	$K = 3$	$K = 4$	$K = 5$	$K = 6$
$M = 1$				
-100	-100	-100	-58	-20
$M = 2$				
-32	-5	37	65	84
$M = 3$				
-15	26	63	83	93
$M = 4$				
-5	37	72	89	96

The values of Tables 3.3 and 3.4 corroborate the proven monotonic trends of $r_{TDMA/ANC}$ of (3.13) with respect to the number of sources, the number of relays, and the modulation order. In particular, it can be seen that the higher the number of sources or the number of relays or the modulation order of the sources is, the better it is for ANC, energy-wise, as expected. From these Tables it can be also observed that ANC is less energy efficient than TDMA only for few cases, in particular when the value Q_{ANC} is small and when the value of either K or M or both is small as well. This is because on one hand the multiplexing gain become more beneficial for high M (similar to the case when the coding gain of a spatial multiplexing MIMO system significantly increases as the number of receive antennas increases) and on the other hand, when either K or Q_{ANC} or both increase then the Q_{TDMA} needs to increase as well, which makes the error rate of TDMA to substantially decrease due to the small among constellation points in the scheme.

Finally, it should also be noted that in Tables 3.3 and 3.4 results are presented for number of sources up to 8 and 4, respectively, since this means that the employed modulation order for TDMA to keep the same rate per source for these number of sources is 64 QAM, based on (3.11), which is the highest modulation order allowed according to the current wireless

Table 3.4: Relative Energy Gain (%) of ANC over TDMA for $Q_{ANC} = 4$ (QPSK).

$K = 2$	$K = 3$
$M = 1$	
9	48
$M = 2$	
58	91
$M = 3$	
72	95
$M = 4$	
77	97

standards, such as LTE.

3.2.7.3 Numerical Validation of Theorem 2

To numerically validate Theorem 2, the ratio $\frac{SER_{ZF}}{SER_{MMSE}}$ of the SER of the ZF and MMSE detectors is considered. In Fig. 3.6, it is showed how $\frac{SER_{ZF}}{SER_{MMSE}}$ is affected by K, M, and Q, by keeping two of these parameters fixed and varying the remaining one. SER_{ZF} and SER_{MMSE} have been obtained by means of Monte Carlo simulations for the same P_S and P_R. Furthermore, considered values of P_S and P_R that give SER_{ZF}, $SER_{MMSE} < 10^{-4}$ are considered since such low SER values correspond to the high-SNR regime, where the coding gain and diversity order are achieved.

As it is observed from Fig. 3.6, $\frac{SER_{ZF}}{SER_{MMSE}}$: i) Increases with increasing K. ii) Decreases with increasing M and increasing Q. Consequently, these trends numerically validate Theorem 2. From a practical point of view, the message that Fig. 3.6 conveys is that when K is notably lower than M or the modulation order is high ($Q > 16$, for instance), it is practically not more beneficial to employ the MMSE receiver instead of the less complex ZF since the ratio $\frac{SER_{ZF}}{SER_{MMSE}}$ tends to 0 dB.

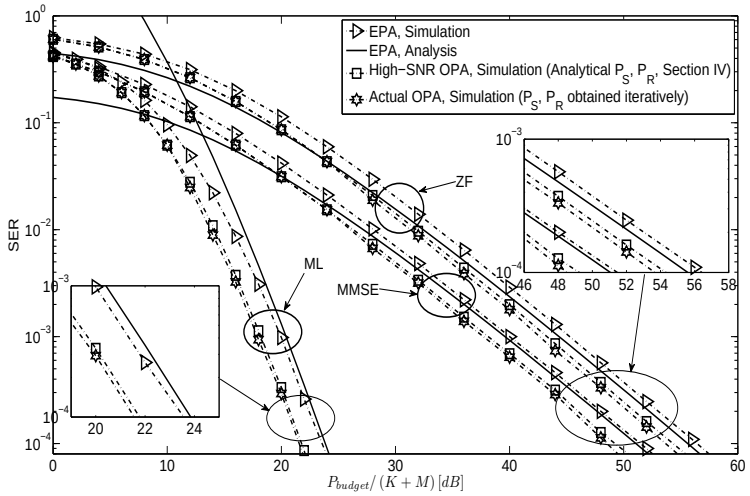

(a)

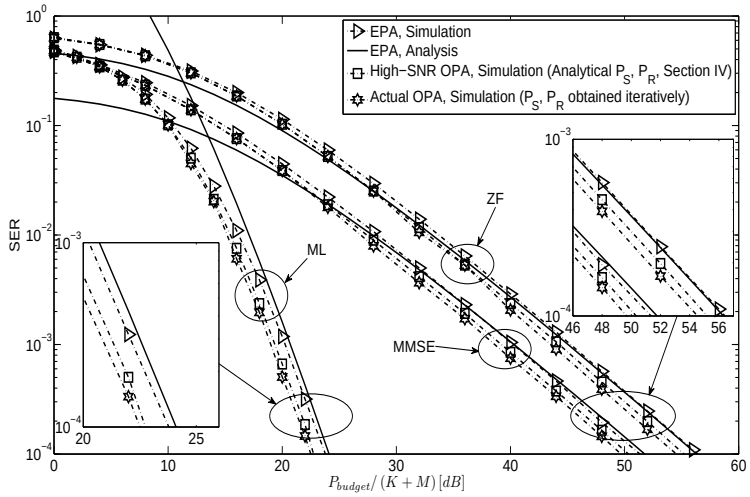

(b)

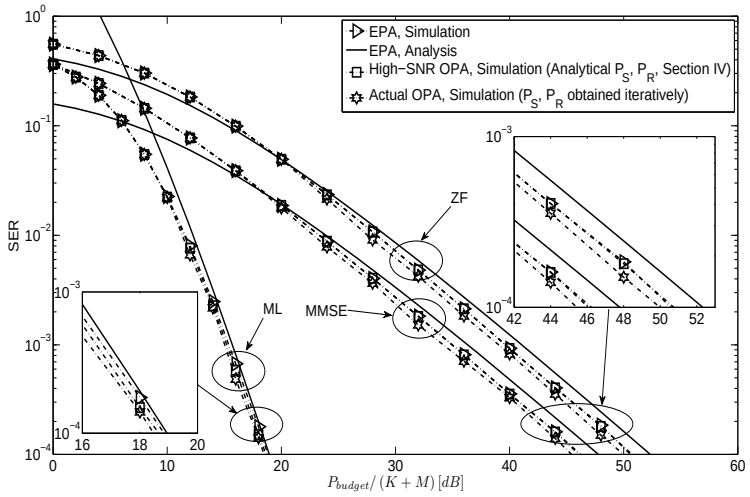

(c)

Figure 3.5: SER vs. $\frac{P_{budget}}{(K+M)}$ [dB] for $K = 4$, $M = 4$, and $Q = 4$, and (a) ML, ZF, and MMSE for $\sigma_{SR}^2 = 4$ and $\sigma_{RD}^2 = 1$, (b) ML, ZF, and MMSE for $\sigma_{SR}^2 = 1$ and $\sigma_{RD}^2 = 1$, and (c) ML, ZF, and MMSE for $\sigma_{SR}^2 = 1$ and $\sigma_{RD}^2 = 4$.

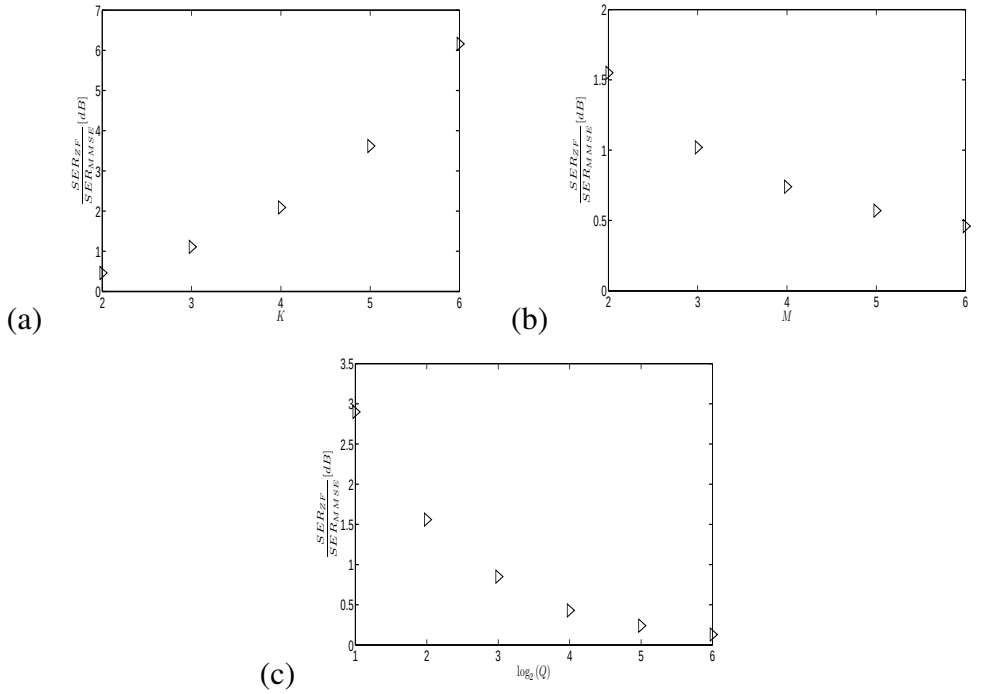

Figure 3.6: $\frac{SER_{ZF}}{SER_{MMSE}}$ in the high-SNR regime (SER_{ZF}, $SER_{MMSE} < 10^{-4}$) vs. (a) K for $M = 6$ and $Q = 4$, (b) M for $K = 2$ and $Q = 4$, and (c) $\log_2(Q)$ for $K = M = 2$. For all the plots, we used $\sigma^2_{SR} = \sigma^2_{RD} = 1$.

3.3 Two-Way Relaying with ANC under the Effect of Network Interference

3.3.1 The Scenario

It is assumed that two fixed single-antenna sources, A and B, want to exchange packets via a half-duplex, single-antenna, amplify-and-forward, and variable-gain relay. For a better utilization of the network resources the two packets are allowed to be network-coded and so the end-to-end communication occurs in two phases: i) During the first phase, which has a duration of one time slot, the two sources simultaneously send their packets to the relay. ii) During the second phase, which also has a duration of one time slot, the relay amplifies the summed signal received from the two sources and sends it to the sources. Then, each source detects its intended packet after subtracting its self-interfering signal from the received signal. For this, it is assumed that each source is able to estimate, not perfectly, its channel coefficient from the relay. In addition, it is considered that the relay has imperfect channel estimates of the channel coefficients from the sources to itself.

Moreover, it is assumed that both the relay and the sources are affected by interference and for simplification, without loss of generality, that the relay is located at the origin of the network and that sources A and B are at a distance d_A and d_B from the relay, respectively. In addition, it is considered that no interferer (node that uses the same frequency with the two-way system under consideration) is located inside a circle with radius $R_{exc} > \max(d_A, d_B)$ measured from the origin. Hence, it is assumed that there is an exclusion region regarding the interference. This system model is depicted in Fig. 3.7, where the triangles represent the possible sources of interference. Furthermore, it is assumed that the two sources transmit with the same power level, which is denoted as P_S.

3.3.2 Previous Works

Up until now, there have been several works on the two-way relaying channel with ANC that deal with different aspects. For instance, as far its information-theoretic capabilities are concerned, in [22] the authors study the optimal beamformers that maximize the achievable rate

region in a scenario with multiple relays and they also find the strategies with which the optimal diversity-multiplexing tradeoff is achieved in a scenario with one relay. In addition, in [23] the case of a full-duplex AF relay is studied and it is shown that this case achieves a higher rate than the half-duplex case when the residual self-interference is kept under a certain threshold. Regarding precoding design, [24] studies the joint source and relay precoding design based on the mean-square-error criterion with both the sources and the relay equipped with multiple antennas and in [25] the same authors study a multi-pair of users scenario, which exchange information though a multi-antenna relay with the aim of maximizing the minimum achievable rate among all the users subject to a peak power constraint. For the case of multiple relays that can assist the two-way communication, performance enhancement implementations compared to the single-relay case can be found in the indicative works of [26] and [27] in which relay selection is considered.

All the aforementioned works consider perfect channel state information (CSI) knowledge at the source nodes, which means that they can perfectly cancel the self-interfering part of the forwarded analog signal from the relay. However, in real world scenarios the CSI needs to be estimated through the use of pilot signals prior to data transmission and, hence, estimation errors are expected, which means that the two sources cannot perfectly eliminate the self-interference of the ANC signal. To this end, the first work considering CSI errors and their effect on the two-way relaying channel is the work of [28] in which the authors derive analytical frameworks for the outage probability and the bit error rate by considering multiple relays, where either maximum ratio combining [29] or relay selection is employed. Furthermore, apart from not considering CSI errors, the aforementioned works do not also consider the effect of co-channel interference, which is another performance limitation factor expected to exist in real-world scenarios. Indicative works of two-way relaying systems considering the impact of Gaussian co-channel interference can be found in [30]- [33]. In particular, in [30] and [31] the outage probability is analytically studied, whereas in [32] besides the outage probability the authors derive analytical expressions for the error probability and the achievable rate. However, these works that consider the impact of co-channel interference assume a perfect CSI knowledge. To the best of our knowledge, the only work that considers the impact of both channel estimation errors and co-channel interference is [33] in which the authors derive analytical expressions for the system outage probability, error rate, and achievable sum rate in a two-way multiple relaying system where the relays dispatch their ANC signal sequen-

tially to the destination or the relay with the best channel conditions is selected to assist the communication.

Although the consideration of the effect of co-channel interference makes the system analysis more practical, the previously mentioned co-channel interference related works rely on the assumption of Gaussian interference resulting from a finite number of interference. For this to hold, the complex channel coefficients of the interferers should be Gaussian and their position known a priori, which can occur only in planned cellular systems. Consequently, the Gaussian interference assumption seems an implausible case for next generation cellular systems, which are expected to be of heterogeneous nature [34], [35] with several small cells, cognitive radios, and Wi-Fi access points, for instance, overlaid in the area covered by a macro cell. These nodes can act as interferers to the macro-cell users and their number and position are unknown a priori. Hence, the resulting interference is not expected to be Gaussian distributed. To model it, the most common approach in the literature is the stochastic geometry approach in which the location of the interferers and their number are distributed according to a Poisson Point Process (PPP) [36]- [38][2].

In light of an increasing amount of works investigating the impact of the PPP interference model in future wireless networks, some papers have recently started investigating the performance of one way relay-based systems in the presence of this interference type [40]-[45]. In [40], the outage probability of optimal, maximum ratio and selection combining [29] is investigated. In [41], the outage probability and error rate of AF-based dual-hop relaying is studied without the inclusion of the direct link from the source to the destination. In [42], the achievable spatial-contention diversity order of cooperative relaying is computed. In [41], the error probability and diversity order of multi-hop relaying are studied with single-antenna nodes. In [44], the analysis of [41] is extended by considering also the direct link from the source to the destination where maximum ratio combining is used to combine the direct and the relay-forwarded signal. Finally, in [45] the authors consider the same system model as the one in [44], but the selection combining scheme is used at the destination.

As aforementioned, these works consider one-way relay systems and to the best of our knowledge there is no work in the literature considering the impact of co-channel interference

[2]Although it is not the most realistic stochastic geometry model to describe the expected interference in emerging heterogeneous networks [39], PPP modeling is preferred due to its analytical tractability and the important insights that the system designer can obtain by its theoretical analysis.

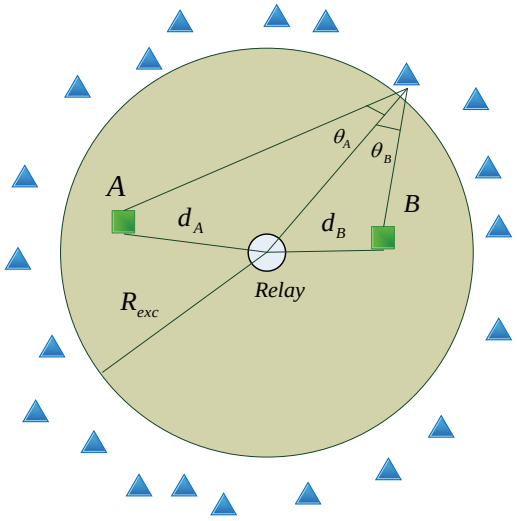

Figure 3.7: Two-Way Relaying with Network Interference.

in the two-way relaying scenario that is characterized by a PPP.

3.3.3 System Model

Two phases are distinguished:

First phase: The signal received at the relay in the first slot, which we denote as y_R, is given by:

$$y_R = \sqrt{\frac{P_S}{d_A^a}} h_A s_A + \sqrt{\frac{P_S}{d_B^a}} h_B s_B + n_R + i_R, \tag{3.42}$$

where h_A, $h_B \sim CN(0,1)$ denote the channel coefficients of the source A-relay and source B-relay links, respectively, $n_R \sim CN(0,1)$ is the Additive White Gaussian Noise at the destination, i_R represents the interfering signal at the relay, and a is the path-loss exponent. In addition, it is assumed that:

$$h_A = \hat{h}_A + e_{h_A} \tag{3.43}$$

and

$$h_B = \hat{h}_B + e_{h_B}, \tag{3.44}$$

where $\hat{h}_A$ and $\hat{h}_B$ denote the estimated channel coefficients at the relay and the sources and e_{h_A}, $e_{h_B} \sim CN(0, \sigma_{\mathrm{E}}^2)$ denote the channel estimation errors of the source A-relay and source B-relay links, respectively, which are assumed to be independent of h_A and h_B. Hence, $\hat{h}_A$,

$\hat{h}_B \sim CN(0, 1-\sigma_{\mathrm{E}}^2)$. One question of course is how it is possible that both the relay and the sources have exactly the same erroneous channel estimates. Simply, it is assumed that the relay is the one that performs channel estimation and subsequently forwards these erroneous channel estimates to the sources prior to data transmission.

Second phase: In the second phase, the variable-gain relay first amplifies y_R after proper power scaling. By assuming that the relay is unaware of the interference statistics, its amplification factor, which we denote as G_R, is given by

$$G_R = \sqrt{\frac{P_R}{\frac{P_S}{d_A^a}\left|\hat{h}_A\right|^2 + \frac{P_S}{d_B^a}\left|\hat{h}_B\right|^2 + P_S\sigma_{\mathrm{E}}^2\left(\frac{1}{d_A^a}+\frac{1}{d_B^a}\right)}}, \tag{3.45}$$

where P_R is the power at the relay and for simplicity the scaling of G_R with the unit variance of the noise at the relay is excluded due to the fact that its effect is negligible for high P_S. Then, after amplification, the relay sends the received signal to the sources. Let us examine one of the two sources, source A for instance. The received signal of source A, which is denoted as y_A, is given by:

$$y_A = G_R y_R \frac{h_A}{\sqrt{d_s^a}} + n_A + i_A, \tag{3.46}$$

where $n_A \sim CN(0,1)$ and i_A denote the Additive White Gaussian Noise and interference, respectively, that affect source A at the second time slot. By having the channel estimate $\hat{h}_A$, source A performs imperfect self-interference cancellation and, hence, the resulting signal, which is denoted as y'_A, is given by:

$$y'_A = y_A - G_R\sqrt{\frac{P_S}{d_s^a}}\hat{h}_A s_A. \tag{3.47}$$

3.3.4 Characterization of the Network Interference

In this section, we characterize the interference processes i_R and i_A that affect the relay and source A, respectively. Assuming that sources A and B represent macro-cell users and that there is a heterogeneous cellular network where, e.g., cognitive radios, wi-fi access points, and small cell base stations are overlaid with the macro cells, these nodes act as interferers to the two sources. Furthermore, their position and number is unknown. Taking this into account, the resulting interference statistics are different than the widely considered Gaussian distributed interference statistics, which can only apply to carefully planned networks. The

normal approach in these cases is to consider that the spatial positions of the interferers follow a PPP with a particular intensity $\lambda \left(\frac{nodes}{m^2}\right)$ [2].

Now, regarding i_R and i_A, the most generic and logical assumption is that i_R and i_A are correlated since some interferers that are active at the 1st time slot are also active at the 2nd time slot. In addition, some interferers that are active at the 1st time slot are not at the 2nd one and, in the same way, there are new interferers generated at the 2nd slot that are not active at the 1st one. By considering the superposition and thinning property of a PPP process [2], i_R and i_A can be modeled by three independent PPP processes as

$$i_R = i_1^{first\ slot} + i_2 \quad and \quad i_A = i_1^{second\ slot} + i_3, \tag{3.48}$$

where $i_1^{first\ slot}$ and $i_1^{second\ slot}$ correspond to the interferers that are active at both time slots and so affect the relay and source A, i_2 corresponds to the interferers that are active only at the 1st time slot and so affect only the relay, and i_3 to the ones that are active only at the 2nd time slot and so affect only source A. In addition, by assuming that $i_1^{first\ slot}$ and $i_1^{second\ slot}$ have intensity $\lambda_1 = m_1\lambda$, the intensity of i_2 and i_3 is $\lambda_2 = m_2\lambda$, where $m_2 = 1 - m_1$ and $0 \leqslant m_1,\, m_2 \leqslant 1$. λ is the total intensity of the PPP interference at each time slot. Hence, from the above we understand that i_R and i_A are correlated because of the correlation of $i_1^{first\ slot}$ with $i_1^{second\ slot}$. In mathematical terms, we have

$$i_1^{first\ slot} = \sum_i \sqrt{\frac{P_I}{d_i^a}} h_i, \quad i_1^{\text{sec}\,ond\ slot} = \sum_i \sqrt{\frac{P_I}{\left(\sqrt{d_i^2 + d_A^2 - 2d_i d_A \cos\theta_{A_i}}\right)^a}} h_i'. \tag{3.49}$$

$$i_2 = \sum_k \sqrt{\frac{P_I}{d_k^a}} h_k. \tag{3.50}$$

$$i_3 = \sum_p \sqrt{\frac{P_I}{\left(\sqrt{d_p^2 + d_A^2 - 2d_p d_A \cos\theta_{A_p}}\right)^a}} h_p, \tag{3.51}$$

where P_I is the power level of each interferer and d_i, d_k, and d_p represent the distances form the corresponding interferers to the origin of the network, where it is assumed that the relay is located. By assuming that the fading channels h_i, h_i', h_k, and h_p of all the interferers to source A and the relay are distributed as $CN\,(0, 1)$, then conditioned on the distances of the interferers to source A and the relay, $i_1^{first\ slot}$, $i_1^{second\ slot}$, i_2, and i_3 are Gaussian random variables with variances $I_1^{first\ slot}$, $I_1^{second\ slot}$, I_2, and I_3, respectively, which are given by

$$I_1^{first\ slot} = \sum_i \frac{P_I}{d_i^a}, \quad I_1^{second\ slot} = \sum_i \frac{P_I}{\left(\sqrt{d_i^2 + d_A^2 - 2d_i d_A \cos\theta_i}\right)^a}. \tag{3.52}$$

$$I_2 = \sum_k \frac{P_I}{d_k^a}. \tag{3.53}$$

$$I_3 = \sum_p \frac{P_I}{\left(\sqrt{d_p^2 + d_A^2 - 2d_p d_A \cos\theta_{A_p}}\right)^a}. \tag{3.54}$$

3.3.5 Performance Analysis

The analytical derivation of the SER of the two sources consists of two steps:

i) Firstly, the distribution of the SINR for each of the two sources in the high-SINR region is derived.

ii) Secondly, based on the analytical expression of the distribution of the SINR of the two sources, the analytical expression for the SER is derived by using the Moment Generating Function (MGF) approach.

3.3.5.1 SINR Distribution

By substituting (3.46) into (3.47), we get

$$\begin{aligned} y'_A = {} & 2G_R \frac{\sqrt{P_S}}{d_A^a}\hat{h}_A e_{h_A} s_A + G_R \frac{\sqrt{P_S}}{d_A^a} e_{h_A}^2 s_A + G_R \sqrt{\frac{P_S}{d_A^a d_B^a}}\hat{h}_A \hat{h}_B s_B + G_R \sqrt{\frac{P_S}{d_A^a d_B^a}}\hat{h}_B e_{h_A} s_B \\ & + G_R \sqrt{\frac{P_S}{d_A^a d_B^a}}\hat{h}_A e_{h_B} s_B + G_R \sqrt{\frac{P_S}{d_A^a d_B^a}} e_{h_A} e_{h_B} + G_R \frac{n_R \hat{h}_A}{\sqrt{d_A^a}} + G_R \frac{n_R e_{h_A}}{\sqrt{d_A^a}} \\ & + G_R \frac{i_R \hat{h}_A}{\sqrt{d_A^a}} + G_R \frac{i_R e_{h_A}}{\sqrt{d_A^a}} + n_A + i_A. \end{aligned} \tag{3.55}$$

Based on (3.55), the useful signal is the term $G_R \sqrt{\frac{P_S}{d_A^a d_B^a}}\hat{h}_A \hat{h}_B s_B$ and the rest of terms constitute the interference plus the noise. In addition, due to the fact that in practical cases it holds that $\sigma_{\mathrm{E}}^2 \ll 1$, it is logically assumed that the terms $G_R \frac{\sqrt{P_S}}{d_A^a} e_{h_A}^2 s_A$, $G_R \sqrt{\frac{P_S}{d_A^a d_B^a}} e_{h_A} e_{h_B}$, and $G_R \frac{n_R e_{h_A}}{\sqrt{d_A^a}}$ of (3.55) are much smaller compared to other terms of the same equation, and, thus,

can be excluded from (3.55). Hence, we have

$$y'_A \approx 2G_R\frac{\sqrt{P_S}}{d_A^a}\hat{h}_A e_{h_A} s_A + G_R\sqrt{\frac{P_S}{d_A^a d_B^a}}\hat{h}_A\hat{h}_B s_B + G_R\sqrt{\frac{P_S}{d_A^a d_B^a}}\hat{h}_B e_{h_A} s_B + G_R\sqrt{\frac{P_S}{d_A^a d_B^a}}\hat{h}_A e_{h_B} s_B + G_R\frac{n_R\hat{h}_A}{\sqrt{d_A^a}} + G_R\frac{i_R\hat{h}_A}{\sqrt{d_A^a}} + G_R\frac{i_R e_{h_A}}{\sqrt{d_A^a}} + n_A + i_A. \quad (3.56)$$

Now, it can be observed from (3.56) that conditioned on the distances of the interferers to the relay and source A and on $\hat{h}_A$ and $\hat{h}_B$ the interference plus noise term is Gaussian, since it is assumed that the fast fading channel coefficients form the interferers to the relay and source A are Gaussian (Rayleigh fading). By considering (3.45), the SINR of source A, which is denoted as $SINR_A$, that results from (3.56) is given by:

$$SINR_A \approx \frac{\frac{P_S P_R\left|\hat{h}_A\right|^2\left|\hat{h}_B\right|^2}{d_A^a d_B^a}}{\left(\frac{4P_S P_R\sigma_E^2}{d^{2a}} + \frac{P_S P_R\sigma_E^2}{d_A^a d_B^a} + \frac{P_R}{d_A^a} + \frac{P_R I_R}{d_A^a} + \frac{P_S}{d_A^a} + \frac{P_S I_A}{d_A^a}\right)\left|\hat{h}_A\right|^2 + \left(\frac{P_S P_R\sigma_E^2}{d_A^a d_B^a} + \frac{P_S}{d_B^a} + \frac{P_S I_A}{d_B^a}\right)\left|\hat{h}_B\right|^2 + \mu}, \quad (3.57)$$

where $I_R = I_1^{first\ slot} + I_2$, $I_A = I_1^{second\ slot} + I_3$, and $\mu = \frac{P_R I_R\sigma_E^2}{d_A^a} + P_S\sigma_E^2\left(\frac{1}{d_A^a} + \frac{1}{d_B^a}\right) + P_S\sigma_E^2\left(\frac{1}{d_A^a} + \frac{1}{d_B^a}\right) I_A$. Due to the fact that $\sigma_{\mathrm{E}}^2 \ll 1$, the constant term μ can be excluded form the denominator of (3.57). Hence, by multiplying the enumerator and denominator of (3.57) with $d_A^a d_B^a$, we get

$$SINR_A \approx \frac{P_S P_R\left|\hat{h}_A\right|^2\left|\hat{h}_B\right|^2}{C\left|\hat{h}_A\right|^2 + D\left|\hat{h}_B\right|^2}, \quad (3.58)$$

where

$$C = 4P_S P_R\sigma_E^2\frac{d_A^a}{d_B^a} + P_S P_R\sigma_E^2 + P_R d_B^a + P_R I_R d_B^a + P_S d_B^a + P_S I_A d_B^a \quad (3.59)$$

and

$$D = P_S P_R\sigma_E^2 + P_S d_A^a + P_S I_A d_A^a. \quad (3.60)$$

Based on the SINR expression for the source A of (3.58), the aim is to derive a closed-form formula of the SER per source of the system. Towards this, for the high-SINR region the Cumulative Density Function (CDF) in closed-form of $SINR_A$ is firstly derived is derived, which is denoted as $F_A(x)$, in a two-step procedure: i) Firstly, the CDF of $SINR_A$ conditioned on the network interference (the statistics of the distances) is derived, which is denoted as $F_A(x\,|I)$ by averaging over $\left|\hat{h}_A\right|^2$ and $\left|\hat{h}_B\right|^2$. ii) Subsequently, $F_A(x)$ is derived by averaging over the statistics of the network interference.

i) $F_A\left(x\left|I\right.\right)$: We have that

$$F_A\left(x|I\right) \overset{(3.58)}{=} \Pr\left(\frac{P_S P_R\left|\hat{h}_A\right|^2\left|\hat{h}_B\right|^2}{C\left|\hat{h}_A\right|^2 + D\left|\hat{h}_B\right|^2} \leqslant X\right) = \Pr\left(\left|\hat{h}_A\right|^2\left(P_S P_R\left|\hat{h}_B\right|^2 - CX\right) \leqslant D\left|\hat{h}_B\right| X\right)$$
$$= \Pr\left(P_S P_R\left|\hat{h}_B\right|^2 - CX \leqslant 0\right)$$
$$+ \Pr\left(\left|\hat{h}_A\right|^2 \leqslant \frac{D\left|\hat{h}_B\right| X}{P_S P_R\left|\hat{h}_B\right|^2 - CX} | P_S P_R\left|\hat{h}_B\right|^2 - CX > 0\right). \tag{3.61}$$

For the first term of (3.61), we have:

$$\Pr\left(P_S P_R\left|\hat{h}_B\right|^2 - CX \leqslant 0\right) = \Pr\left(\left|\hat{h}_B\right|^2 \leqslant \frac{CX}{P_S P_R}\right) = 1 - e^{\left(1-\sigma_E^2\right)\frac{CX}{P_S P_R}}. \tag{3.62}$$

For the second term of (3.61), we have:

$$\Pr\left(\left|\hat{h}_A\right|^2 \leqslant \frac{D\left|\hat{h}_B\right| X}{P_S P_R\left|\hat{h}_B\right|^2 - CX} | P_S P_R\left|\hat{h}_B\right|^2 - CX > 0\right)$$
$$= \int_{\frac{CX}{P_S P_R}}^{\infty}\left(1 - e^{\left(1-\sigma_E^2\right)\frac{DyX}{P_S P_R y - CX}}\right)\left(1-\sigma_E^2\right)e^{\left(1-\sigma_E^2\right)y}dy$$
$$\overset{(u=P_S P_R y - CX)}{=} \frac{1-\sigma_E^2}{P_S P_R} e^{-\left(1-\sigma_E^2\right)\frac{CX}{P_S P_R}} \int_0^{\infty} e^{-\left(1-\sigma_E^2\right)\frac{u}{P_S P_R}} du$$
$$- \frac{1-\sigma_E^2}{P_S P_R} e^{-\frac{(D+C)X}{P_S P_R}} \int_0^{\infty} e^{-\left(1-\sigma_E^2\right)\left(\frac{CDX^2}{u} + \frac{u}{P_S P_R}\right)} du$$
$$= e^{-\left(1-\sigma_E^2\right)\frac{CX}{P_S P_R}} - \frac{1-\sigma_E^2}{P_S P_R} e^{-\left(1-\sigma_E^2\right)\frac{(D+C)X}{P_S P_R}} 2\sqrt{CDX^2} K_1\left(\frac{2\left(1-\sigma_E^2\right)}{P_S P_R}\sqrt{CDX^2}\right), \tag{3.63}$$

where the second term of (3.63) follows from [13, 3.478.4] and $K_1\left(\cdot\right)$ denotes the modified Bessel function of the second kind and first order. By considering the high-SINR regime ($P_S, P_R >> 1$), the small argument approximation of $K_1\left(\cdot\right)$, i.e. $K_1\left(z\right) \approx \frac{1}{z},\ z << 1$ can be used. Hence, (3.63) becomes

$$\Pr\left(\left|\hat{h}_A\right|^2 \leqslant \frac{D\left|\hat{h}_B\right| X}{P_S P_R\left|\hat{h}_B\right|^2 - CX} | P_S P_R\left|\hat{h}_B\right|^2 - CX > 0\right) \approx e^{-\left(1-\sigma_E^2\right)\frac{CX}{P_S P_R}} - e^{-\left(1-\sigma_E^2\right)\frac{(D+C)X}{P_S P_R}}. \tag{3.64}$$

By plugging (3.62) and (3.64) into (3.61), we get

$$F_A\left(x|I\right) \approx 1 - e^{-\left(1-\sigma_E^2\right)\frac{(D+C)x}{P_S P_R}} \overset{P_S, P_R >> 1}{\approx} \left(1-\sigma_E^2\right)\frac{(D+C)\,x}{P_S P_R}. \tag{3.65}$$

The small argument approximation ($e^{-x} \approx 1-x,\ x \ll 1$) of the exponential function in (3.65) is considered since the error probability in the high-SINR region is dominated by the behavior of the probability (or cumulative) density function (pdf) as x (SINR) tends to 0 [46]. Hence, in the region of interest (high-SINR region) it holds that $(1-\sigma_E^2)\frac{(D+C)x}{P_S P_R} << 1$ (the exponent in (3.65)).

ii) $F_A(x)$: From (3.65), we have

$$\begin{aligned} F_A(x) &= E_I\{F_A(x|I)\} \\ &\approx \left(1-\sigma_E^2\right)\left[\frac{d_B^a}{P_S}E_I\{I_R\} + \frac{d_A^a + d_B^a}{P_R}E_I\{I_A\} + Z\right]x, \end{aligned} \tag{3.66}$$

where

$$E_I\{I_R\} = E_I\left(I_1^{first\ slot}\right) + E_I(I_2) \quad and \quad E_I\{I_A\} = E_I\left(I_1^{\text{sec}\,ond\ slot}\right) + E_I(I_3), \tag{3.67}$$

and

$$Z = 4\sigma_E^2\frac{d_B^a}{d_A^a} + 2\sigma_E^2 + \left(\frac{1}{P_S}+\frac{1}{P_R}\right)d_B^a + \frac{d_A^a}{P_R}. \tag{3.68}$$

Proposition 7 In the high-SINR region, the two extreme cases of independence ($m_1 = 0$) and full correlation ($m_1 = 1$) between i_R and i_A result in the same $F_A(x)$ in that region.

Proof: i) For $m_1 = 0$ (independence between i_R and i_A), we get from (3.66)

$$\begin{aligned} F_A(x) &= E_I\{F_A(x|I)\} \\ &\approx \left(1-\sigma_E^2\right)\left[\frac{d_B^a}{P_S}E_I\{I_2\}|_{m_1=0} + \frac{d_A^a + d_B^a}{P_R}E_I\{I_3\}|_{m_1=0} + Z\right]x. \end{aligned} \tag{3.69}$$

ii) For $m_1 = 1$ (full correlation between i_R and i_A), we get from (3.66)

$$\begin{aligned} F_A(x) &= E_I\{F_A(x|I)\} \\ &\approx \left(1-\sigma_E^2\right)\left[\frac{d_B^a}{P_S}E_I\left\{I_1^{first\ slot}\right\}|_{m_1=1} + \frac{d_A^a + d_B^a}{P_R}E_I\left\{I_2^{first\ slot}\right\}|_{m_1=1} + Z\right]x. \end{aligned} \tag{3.70}$$

By considering that $E_I\{I_1^{first\ slot}\} = E_I\{I_2\}$ and $E_I\{I_1^{\text{sec}\,ond\ slot}\} = E_I\{I_3\}$, according to (3.52), (3.53), and (3.54), the proof of Proposition 7 is concluded.

Remark 5 Due to the fact that in the high-SINR region $F_A(x)$ has the same expression regardless of whether i_R and i_A are independent or fully correlated, it is straightforward that any other

intermediate case ($0 < m_1 < 1$) between these two extreme cases results in the same $F_A(x)$. This means that the distribution of $SINR_A$ in the high-SINR region (and, consequently, the corresponding error probability in the same region) is determined by the total power effect of the interferers to the relay and source A (which, in turn, is determined by the parameter λ of the PPP interference, which it is assumed that remains the same at each time slot) and not on the amount of correlation between i_R and i_A.

Now, we have that [47, Eq. (8)] (which is a result of Campbell's Theorem for a PPP process [2])

$$E_I\left\{I_1^{first\ slot}\right\} = \frac{2\pi m_1 \lambda P_I}{a-2} R_{exc}^{2-a} \quad and \quad E_I\left\{I_2\right\} = \frac{2\pi m_2 \lambda P_I}{a-2} R_{exc}^{2-a}. \tag{3.71}$$

Furthermore, again according to Campbell's Theorem, we have

$$E_I\left\{I_1^{\text{sec}\,ond\ slot}\right\} = m_1 \lambda P_I \int_{R_{exc}}^{\infty} l_1 dl_1 \int_0^{2\pi} \frac{1}{\left(\sqrt{l_1^2 + d_A^2 - 2l_1 d_A \cos\theta}\right)^a} d\theta. \tag{3.72}$$

By setting $l_2^2 = l_1^2 + d_A^2 - 2l_1 d_A \cos\theta$, we have

$$\cos\theta = \frac{l_1^2 + d_A^2 - l_2^2}{2l_1 d_A} \Rightarrow \theta = \cos^{-1}\left(\frac{l_1^2 + d_A^2 - l_2^2}{2l_1 d_A}\right) \Rightarrow d\theta = \frac{2l_2}{\sqrt{l_2^2 - (l_1^2 - d_A^2)}\sqrt{(l_1^2 + d_A^2) - l_2^2}} dl_2. \tag{3.73}$$

By plugging (3.73) into (3.72), we get

$$\begin{aligned}
E_I\left\{I_1^{\text{sec}\,ond\ slot}\right\} &= 2m_1 \lambda P_I \int_{R_{exc}}^{\infty} l_1 dl_1 \int_{l_1 - d_A}^{l_1 + d_A} l_2^{-a} \frac{2l_2}{\sqrt{l_2^2 - (l_1 - d_A)^2}\sqrt{(l_1 + d_A)^2 - l_2^2}} dl_2 \\
&\overset{t = l_2^{-2}}{=} 2m_1 \lambda P_I \int_{R_{exc}}^{\infty} l_1 dl_1 \int_{\frac{1}{(l_1 + d_A)^2}}^{\frac{1}{(l_1 - d_A)^2}} \frac{t^{\frac{a}{2} - 2}}{\sqrt{\frac{1}{t} - (l_1 - d_A)^2}\sqrt{(l_1 + d_A)^2 - \frac{1}{t}}} dt \\
&= 2m_1 \lambda P_I \int_{R_{exc}}^{\infty} \frac{l_1}{(l_1 - d_A)(l_1 + d_A)} dl_1 \int_{\frac{1}{(l_1 + d_A)^2}}^{\frac{1}{(l_1 - d_A)^2}} \frac{t^{\frac{a}{2} - 1}}{\sqrt{\frac{1}{(l_1 - d_A)^2} - t}\sqrt{t - \frac{1}{(l_1 + d_A)^2}}} dt \\
&\overset{u = t - \frac{1}{(l_1 + d_A)^2}}{=} 2m_1 \lambda P_I \int_{R_{exc}}^{\infty} \frac{l_1}{(l_1 - d_A)(l_1 + d_A)} dl_1 \\
&\times \int_0^{\frac{1}{(l_1 - d_A)^2} - \frac{1}{(l_1 + d_A)^2}} \frac{\left(u + \frac{1}{(l_1 + d_A)^2}\right)^{\frac{a}{2} - 1}}{\sqrt{u}\sqrt{\frac{1}{(l_1 - d_A)^2} - \frac{1}{(l_1 + d_A)^2} - u}} du.
\end{aligned} \tag{3.74}$$

Now, from (3.74) we distinguish two cases:

1) $a = 2m$, where $m = 2, 3, 4, ...$In this case, for the second integral of (3.74) we can take the binomial expansion of the enumerator. This gives

$$\begin{aligned}
&\int_0^{\frac{1}{(l_1-d_A)^2}-\frac{1}{(l_1+d_A)^2}} \frac{\left(u+\frac{1}{(l_1+d_A)^2}\right)^{\frac{a}{2}-1}}{\sqrt{u}\sqrt{\frac{1}{(l_1-d_A)^2}-\frac{1}{(l_1+d_A)^2}-u}}du \\
&= \sum_{k=0}^{\frac{a}{2}-1}\binom{\frac{a}{2}-1}{k}\left[\frac{1}{(l_1+d_A)^2}\right]^{\frac{a}{2}-1-k}\int_0^{\frac{1}{(l_1-d_A)^2}-\frac{1}{(l_1+d_A)^2}} \frac{u^{k-\frac{1}{2}}}{\sqrt{\frac{1}{(l_1-d_A)^2}-\frac{1}{(l_1+d_A)^2}-u}}du \\
&= \sum_{k=0}^{\frac{a}{2}-1}\binom{\frac{a}{2}-1}{k}\left[\frac{1}{(l_1+d_A)^2}\right]^{\frac{a}{2}-1-k}\left[\frac{4l_1d_A}{(l_1-d_A)^2(l_1+d_A)^2}\right]^k B\left(\frac{1}{2},k+\frac{1}{2}\right), \qquad (3.75)
\end{aligned}$$

which follows from [13, 3.191.1]. $B(\cdot,\cdot)$ is the beta function. By plugging (3.75) into (3.74), we get

$$\begin{aligned}
E_I\left\{I_1^{\text{sec}\,ond\ slot}\right\} &= 2m_1\lambda P_I\sum_{k=0}^{\frac{a}{2}-1}\binom{\frac{a}{2}-1}{k}B\left(\frac{1}{2},k+\frac{1}{2}\right)(4d_A)^k\int_{R_{exc}}^{\infty}\frac{l_1^{k+1}}{(l_1-d_A)^{2k+1}(l_1+d_A)^{a-1}}dl_1 \\
&\overset{p=l_1-R_{exc}}{=} 2m_1\lambda P_I\sum_{k=0}^{\frac{a}{2}-1}\binom{\frac{a}{2}-1}{k}B\left(\frac{1}{2},k+\frac{1}{2}\right)(4d_A)^k \\
&\times\int_0^{\infty}\frac{(p+R_{exc})^{k+1}}{(p+R_{exc}-d_A)^{2k+1}(p+R_{exc}+d_A)^{a-1}}dp \\
&= 2m_1\lambda P_I\sum_{k=0}^{\frac{a}{2}-1}\binom{\frac{a}{2}-1}{k}B\left(\frac{1}{2},k+\frac{1}{2}\right)(4d_A)^k \\
&\times\sum_{w=0}^{k+1}\binom{k+1}{w}R_{exc}^{k+1-w}\int_0^{\infty}\frac{p^w}{(p+R_{exc}-d_A)^{2k+1}(p+R_{exc}+d_A)^{a-1}}dp \\
&= 2m_1\lambda P_I\sum_{k=0}^{\frac{a}{2}-1}\binom{\frac{a}{2}-1}{k}B\left(\frac{1}{2},k+\frac{1}{2}\right)(4d_A)^k\sum_{w=0}^{k+1}\binom{k+1}{w} \\
&\times R_{exc}^{k+1-w}(R_{exc}+d_A)^{1-a}(R_{exc}-d_A)^{w-2k}B(w+1,a+2k-w-1) \\
&\times {}_2F_1\left(a-1,w+1,a+2k,\frac{2d_A}{R_{exc}+d_A}\right), \qquad (3.76)
\end{aligned}$$

which follows from [13, 3.197.1]. ${}_2F(\cdot,\cdot,\cdot,\cdot)$ is the Gaussian hypergeometric function. In the same way, $E_I\{I_3\}$ is given by (3.76) with m_1 replaced by m_2.

2) $a \neq 2m$, where $m = 2, 3, 4, ...$ In this case, the exponent $\frac{a}{2}-1$ of the enumerator of the second integral in (3.74) is fractional and so we cannot rely on the known binomial expansion formula that works only for integer exponents. Instead, we can rely on Newton's generalized

binomial expansion formula for fractional exponents. In particular, if x and y are real numbers with $|x| > |y|$, and r is an complex number, it holds that

$$(x+y)^r = \sum_{k=0}^{\infty} \frac{(r)_k}{k!} x^{r-k} y^k, \tag{3.77}$$

where $(r)_k = r\,(r-1)\cdots(r-k+1)$ is the falling factorial. Let us look again the second integral of (3.74):

$$\int_0^{\frac{1}{(l_1-d_A)^2}-\frac{1}{(l_1+d_A)^2}} \frac{\left(u+\frac{1}{(l_1+d_A)^2}\right)^{\frac{a}{2}-1}}{\sqrt{u}\sqrt{\frac{1}{(l_1-d_A)^2}-\frac{1}{(l_1+d_A)^2}-u}} du. \tag{3.78}$$

The problem in developing the enumerator $\left(u+\frac{1}{(l_1+d_A)^2}\right)^{\frac{a}{2}-1}$ of (3.78), according to (3.77), is that the term u inside the parenthesis is a variable that takes values in the interval $\left[0,\ \frac{1}{(l_1-d_A)^2}-\frac{1}{(l_1+d_A)^2}\right]$, based on the limits of the integral, not a fixed number. Hence, we distinguish two subcases:

i) The maximum value that u takes, which is $\frac{1}{(l_1-d_A)^2}-\frac{1}{(l_1+d_A)^2}$, is smaller than the second term inside the parenthesis of the enumerator of (3.78), which means that

$$\frac{1}{(l_1-d_A)^2}-\frac{1}{(l_1+d_A)^2} < \frac{1}{(l_1+d_A)^2} \Rightarrow l_1^2 - 6l_1d_A + d_A^2 > 0. \tag{3.79}$$

The two roots of the second degree polynomial of (3.79) are

$$l_{1_{1,2}} = \left(3 \pm 2\sqrt{2}\right) d_A. \tag{3.80}$$

Hence,

$$l_1^2 - 6l_1d_A + d_A^2 > 0 \Rightarrow l_1 < \left(3-2\sqrt{2}\right) d_A \quad or \quad l_1 > \left(3+2\sqrt{2}\right) d_A. \tag{3.81}$$

Due to the fact that l_1 takes values in the interval $[R_{exc},\ \infty)$, according to the first integral of (3.74), only the right-side root of (3.81) satisfies our condition. Hence,

$$\frac{1}{(l_1-d_A)^2}-\frac{1}{(l_1+d_A)^2} < \frac{1}{(l_1+d_A)^2} \Rightarrow l_1^2 - 6l_1d_A + d_A^2 > 0 \Rightarrow R_{exc} > \left(3+2\sqrt{2}\right) d_A. \tag{3.82}$$

When (3.82) holds, the enumerator of (3.78) can be expanded according to (3.77), which means

that

$$\int_0^{\frac{1}{(l_1-d_A)^2}-\frac{1}{(l_1+d_A)^2}} \frac{\left(u+\frac{1}{(l_1+d_A)^2}\right)^{\frac{a}{2}-1}}{\sqrt{u}\sqrt{\frac{1}{(l_1-d_A)^2}-\frac{1}{(l_1+d_A)^2}-u}}du$$
$$=\sum_{k=0}^{\infty}\frac{\left(\frac{a}{2}-1\right)_k}{k!}\left[\frac{1}{(l_1+d_A)^2}\right]^{\frac{a}{2}-1-k}\int_0^{\frac{1}{(l_1-d_A)^2}-\frac{1}{(l_1+d_A)^2}}\frac{u^{k-\frac{1}{2}}}{\sqrt{\frac{1}{(l_1-d_A)^2}-\frac{1}{(l_1+d_A)^2}-u}}du$$
$$=\sum_{k=0}^{\infty}\frac{\left(\frac{a}{2}-1\right)_k}{k!}\left[\frac{1}{(l_1+d_A)^2}\right]^{\frac{a}{2}-1-k}\left[\frac{4l_1d_A}{(l_1-d_A)^2(l_1+d_A)^2}\right]^k B\left(\frac{1}{2},k+\frac{1}{2}\right), \tag{3.83}$$

which follows from [13, 3.191.1]. By plugging (3.83) into (3.74) and following the same steps as in (3.76), we get

$$E_I\left\{I_1^{\text{sec}\,ond\ slot}\right\}=2m_1\lambda P_I\sum_{k=0}^{\infty}\frac{\left(\frac{a}{2}-1\right)_k}{k!}B\left(\frac{1}{2},k+\frac{1}{2}\right)(4d_A)^k\sum_{w=0}^{k+1}\binom{k+1}{w}R_{exc}^{k+1-w}(R_{exc}+d_A)^{1-a}$$
$$\times(R_{exc}-d_A)^{w-2k}B\left(w+1,a+2k-w-1\right){}_2F_1\left(a-1,w+1,a+2k,\frac{2d_A}{R_{exc}+d_A}\right). \tag{3.84}$$

Obviously, (3.84) is not in closed-form since the first series grows to infinity. However, we can truncate it and take a finite number of terms, which we denote as N_{trunc}. Hence, we have that

$$E_I\left\{I_1^{\text{sec}\,ond\ slot}\right\}\approx 2m_1\lambda P_I\sum_{k=0}^{N_{trunc}}\frac{\left(\frac{a}{2}-1\right)_k}{k!}B\left(\frac{1}{2},k+\frac{1}{2}\right)(4d_A)^k\sum_{w=0}^{k+1}\binom{k+1}{w}R_{exc}^{k+1-w}(R_{exc}+d_A)^{1-a}$$
$$\times(R_{exc}-d_A)^{w-2k}B\left(w+1,a+2k-w-1\right){}_2F_1\left(a-1,w+1,a+2k,\frac{2d_A}{R_{exc}+d_A}\right). \tag{3.85}$$

In the Numerical Results section it is numerically shown that a value of N_{trunc} as low as 10 is adequate so that the error probability that results from the approximation of (3.85) matches the Monte Carlo simulations in the high-SINR region.

ii) The maximum value $\frac{1}{(l_1-d_A)^2}-\frac{1}{(l_1+d_A)^2}$ of u is greater or equal than the second term inside the parenthesis of the enumerator of (3.78), which means that

$$\frac{1}{(l_1-d_A)^2}-\frac{1}{(l_1+d_A)^2}\geqslant\frac{1}{(l_1+d_A)^2}\Rightarrow l_1^2-6l_1d_A+d_A^2\leqslant 0\Rightarrow R_{exc}\leqslant\left(3+2\sqrt{2}\right)d_A, \tag{3.86}$$

since l_1 takes values in the interval $[R_{exc},\,\infty)$. Supposedly, we can deal with this case by decomposing the integral (3.78) into two integrals that correspond to the range of values where

u is smaller and greater than $\frac{1}{(l_1+d_A)^2}$, which is the second term inside the parenthesis of the enumerator in (3.78). This means that

$$\int_0^{\frac{1}{(l_1-d_A)^2}-\frac{1}{(l_1+d_A)^2}} \frac{\left(u+\frac{1}{(l_1+d_A)^2}\right)^{\frac{a}{2}-1}}{\sqrt{u}\sqrt{\frac{1}{(l_1-d_A)^2}-\frac{1}{(l_1+d_A)^2}-u}}du$$

$$= \int_0^{\frac{1}{(l_1+d_A)^2}} \frac{\left(u+\frac{1}{(l_1+d_A)^2}\right)^{\frac{a}{2}-1}}{\sqrt{u}\sqrt{\frac{1}{(l_1-d_A)^2}-\frac{1}{(l_1+d_A)^2}-u}}du + \int_{\frac{1}{(l_1+d_A)^2}}^{\frac{1}{(l_1-d_A)^2}-\frac{1}{(l_1+d_A)^2}} \frac{\left(u+\frac{1}{(l_1+d_A)^2}\right)^{\frac{a}{2}-1}}{\sqrt{u}\sqrt{\frac{1}{(l_1-d_A)^2}-\frac{1}{(l_1+d_A)^2}-u}}du$$

$$\overset{(3.77)}{=} \sum_{k=0}^{\infty} \frac{\left(\frac{a}{2}-1\right)_k}{k!}\left[\frac{1}{(l_1+d_A)^2}\right]^{\frac{a}{2}-1-k} \int_0^{\frac{1}{(l_1+d_A)^2}} \frac{u^{k-\frac{1}{2}}}{\sqrt{\frac{1}{(l_1-d_A)^2}-\frac{1}{(l_1+d_A)^2}-u}}du$$

$$+ \sum_{k=0}^{\infty} \frac{\left(\frac{a}{2}-1\right)_k}{k!}\left[\frac{1}{(l_1+d_A)^2}\right]^{k} \int_{\frac{1}{(l_1+d_A)^2}}^{\frac{1}{(l_1-d_A)^2}-\frac{1}{(l_1+d_A)^2}} \frac{u^{\frac{a}{2}-\frac{3}{2}-k}}{\sqrt{\frac{1}{(l_1-d_A)^2}-\frac{1}{(l_1+d_A)^2}-u}}du. \tag{3.87}$$

Due to the fact that there are no closed-form expressions in [13] for the limits of these two integrals, we need to consider an approximation to end up with a closed-form expression of $E_I\left\{I_1^{\text{sec}\,ond\ slot}\right\}$. By looking at Fig. 3.7, it can be observed that source A is under the effect of asymmetric interference since it is not located at the center of the circle with radius R_{exc}. In particular, due to this asymmetry there are two values of the smallest possible distance between source A and any interferer that are diametrically opposite. The first distance (smallest one), as it is observed from Fig. 3.7, is equal to $R_{exc}-d_A$ and the second one is equal to $R_{exc}+d_A$. Hence, we can consider two bounds of the interference that affects source A. The first bound corresponds to assumption that the source A is located at the center of a circular exclusion region with radius $R_{exc}-d_A$ and the second bound corresponds to the assumption that source A is located at the center of a circular exclusion region with radius $R_{exc}+d_A$. The first bound, which corresponds to the radius $R_{exc}-d_A$, gives a higher value than the actual interference that source A experiences, whereas the second bound, which corresponds to the radius $R_{exc}+d_A$, gives a smaller value than the actual one. Under these considerations, we can denote these two bounds of the interference as Higher Value (HV), which corresponds to the exclusion region with radius $R_{exc}-d_A$, and Lower Value (LV), which corresponds to the exclusion region with radius $R_{exc}+d_A$. This means that [47, Eq. (8)] (which is a result of Campbell's Theorem for a

PPP process)

$$E_I\left\{I_1^{second\ slot}\right\}_{HV}=\frac{2\pi m_1\lambda P_I}{a-2}\left(R_{exc}-d_A\right)^{2-a}\quad and\quad E_I\left\{I_1^{second\ slot}\right\}_{LV}=\frac{2\pi m_1\lambda P_I}{a-2}\times\left(R_{exc}+d_A\right)^{2-a}. \tag{3.88}$$

We again note that $E_I\left\{I_3\right\}$ is given by the expression of $E_I\left\{I_1^{second\ slot}\right\}$ with m_1 replaced by m_2.

Let us now recapitulate regarding what we have. $F_A\left(x\right)$ in the high-SINR region is given by (3.66), where $E_I\left\{I_R\right\}=E_I\left(I_1^{first\ slot}\right)+E_I\left(I_2\right)$ and $E_I\left\{I_A\right\}=E_I\left(I_1^{second\ slot}\right)+E_I\left(I_3\right)$. For $E_I\left(I_1^{first\ slot}\right)$ and $E_I\left(I_2\right)$ it holds that

$$E_I\left\{I_1^{first\ slot}\right\}=m_1A_I\quad and\quad E_I\left\{I_2\right\}=m_2A_I, \tag{3.89}$$

where

$$A_I=\frac{2\pi\lambda P_I}{a-2}R_{exc}^{2-a}. \tag{3.90}$$

Regarding $E_I\left(I_1^{second\ slot}\right)$ and $E_I\left(I_3\right)$, it holds that

$$E_I\left\{I_1^{second\ slot}\right\}=m_1B_I\quad and\quad E_I\left\{I_3\right\}=m_2B_I, \tag{3.91}$$

where for B_I we distinguish 3 cases:

Case 1)

$a=2m$, where $m=2,3,4,....$In this case,

$$B_I=2\lambda P_I\sum_{k=0}^{\frac{a}{2}-1}\binom{\frac{a}{2}-1}{k}B\left(\frac{1}{2},k+\frac{1}{2}\right)\left(4d_A\right)^k\sum_{w=0}^{k+1}\binom{k+1}{w}R_{exc}^{k+1-w}(R_{exc}+d_A)^{1-a}\times\left(R_{exc}-d_A\right)^{w-2k}B\left(w+1,a+2k-w-1\right){}_2F_1\left(a-1,w+1,a+2k,\frac{2d_A}{R_{exc}+d_A}\right). \tag{3.92}$$

Case 2)

$a\neq 2m$, where $m=2,3,4,...$, and $R_{exc}>\left(3+2\sqrt{2}\right)d_A$. In this case,

$$B_I\approx 2m_1\lambda P_I\sum_{k=0}^{N_{trunc}}\frac{\left(\frac{a}{2}-1\right)_k}{k!}B\left(\frac{1}{2},k+\frac{1}{2}\right)\left(4d_A\right)^k\sum_{w=0}^{k+1}\binom{k+1}{w}R_{exc}^{k+1-w}(R_{exc}+d_A)^{1-a}\times\left(R_{exc}-d_A\right)^{w-2k}B\left(w+1,a+2k-w-1\right){}_2F_1\left(a-1,w+1,a+2k,\frac{2d_A}{R_{exc}+d_A}\right). \tag{3.93}$$

Case 3)

$a \neq 2m$, where $m = 2, 3, 4, ...$, and $R_{exc} \leqslant \left(3 + 2\sqrt{2}\right) d_A$. In this case, we need to take the two bounds of the interference due to the analytical intractability, as we aforementioned. Hence,

$$B_{I_{HV}} = \frac{2\pi\lambda P_I}{a-2} \left(R_{exc} - d_A\right)^{2-a} \quad and \quad B_{I_{LV}} = \frac{2\pi\lambda P_I}{a-2} \left(R_{exc} + d_A\right)^{2-a}. \tag{3.94}$$

3.3.5.2 SER

The instantaneous SER of a coherent detection system, which is denoted as P_S, in Additive White Gaussian Noise (or noise+interference that is Gaussian distributed) is given by [29, Eq. (6.73)]

$$P_S = \frac{c}{\pi} \int_0^{\pi/2} e^{-\frac{g\gamma_{SINR}}{\sin^2\phi}} d\phi, \tag{3.95}$$

where c and g are constants that depend on the modulation that is used. γ_{SINR} is the instantaneous SINR. As it was aforementioned in Section 3.3.1, conditioned on the distances of the interferers to the relay and source A and on $\hat{h}_A$ and $\hat{h}_B$ the interference plus noise term is Gaussian, since we assumed that the fast fading channel coefficients form the interferers to the relay and source A are Gaussian (Rayleigh fading). Hence, (3.95) holds in the considered system model with γ_{SINR} given by (3.58). From (3.95), the average SER of source A, which is denoted as $\bar{P}_{S_A}$ is given by [29, Eq. (6.74)]

$$\bar{P}_{S_A} = \frac{c}{\pi} \int_0^{\pi/2} M_{\gamma_A}\left(\frac{g}{\sin^2\varphi}\right) d\varphi, \tag{3.96}$$

where $M_{\gamma_A}(s)$ denotes the MGF of the instantaneous SINR of source A and it is given by

$$M_{\gamma_A}(s) = E_{\gamma_A}\left\{e^{-s\gamma_A}\right\} = \int_0^{\infty} e^{-sx} f_A(x)\, dx. \tag{3.97}$$

$f_A(x)$ is the pdf of the instantaneous SINR of source A. In the high-SINR region, we have that

$$\begin{aligned} f_A(x) &= \frac{dF_A(x)}{dx} \\ &\approx \left(1 - \sigma_E^2\right) \left[\frac{d_B^a}{P_S}\left(E_I\left\{I_1^{first\ slot}\right\} + E_I\left\{I_2\right\}\right) + \frac{d_A^a + d_B^a}{P_R}\left(E_I\left\{I_1^{\text{second slot}}\right\} + E_I\left\{I_3\right\}\right) + Z\right]. \end{aligned} \tag{3.98}$$

By substituting (3.98) into (3.97), we get

$$M_{\gamma_A}(s) \approx \frac{\left(1 - \sigma_E^2\right) \left[\frac{d_B^a}{P_S}\left(E_I\left\{I_1^{first\ slot}\right\} + E_I\left\{I_2\right\}\right) + \frac{d_A^a + d_B^a}{P_R}\left(E_I\left\{I_1^{\text{second slot}}\right\} + E_I\left\{I_3\right\}\right) + Z\right]}{s}, \tag{3.99}$$

where $E_I\left\{I_1^{first\ slot}\right\}$, $E_I\{I_2\}$, $E_I\left\{I_1^{f\sec ond\ slot}\right\}$, and $E_I\{I_3\}$ have been previously defined. By having the MGF of the SINR in closed form in the high-SINR region, according to (3.99), we can calculate the average SER of source A from (3.96). Especially, for PSK modulation (3.96) becomes

$$P_{SER_A}^{PSK} = \frac{1}{\pi}\int_0^{\pi\frac{(\mathrm{M}-1)}{M}} M_{\gamma_A}\left(\frac{\sin^2\left(\frac{\pi}{M}\right)}{\sin^2(\theta)}\right)d\theta. \tag{3.100}$$

It can be noted that Case 3) results in two bounds of the SER. The 1st bound (upper bound) corresponds to $B_{I_{HV}}$ and the second bound (lower bound) corresponds to $B_{I_{LV}}$. We can take the average value of these two bounds as the average SER of the system. It can also be noted that due to symmetry the average SER analysis for source B gives exactly the same formulas as for source A with the only difference that d_A should be replaced by d_B and d_B by d_A in the corresponding formulas.

3.3.6 Numerical Results

The aim of this section is to compare the SER obtained by Monte Carlo simulations with the analytically derived one and to substantiate the energy gains per source that can be achieved as the radius of the exclusion region increases. The simulation parameters used are $d_A = 120$ m, $d_B = 60$ m, $\sigma_E^2 = 0.001$, $\lambda = 10^{-4}\ \frac{nodes}{m^2}$, $m_1 = 0.5$, radius of the circular simulation area=3000 m (the theoretical infinity), $P_S = P_R = P_T$, and QPSK modulation used by the two sources.

3.3.6.1 SER

Fig. 3.8, illustrates the SER vs. P_T/P_I curves for $a = 4$ (that means we are in Case 1)) and different values of R_{exc}. As it is observed from Fig. 3.8, there is a close match of the analytical model with the Monte Carlo simulations in the high-SINR region. Then, the value $a = 3.2$ is considered and the SER vs. P_T/P_I curves for $R_{exc} = 200$ m is illustrated in Fig. 3.9 (that means that we are in Case 3) since it holds that $R_{exc} < \left(3+2\sqrt{2}\right)d_A$) , $R_{exc} = 500$ m in Fig. 3.10 (again we are in Case 3) since $R_{exc} < \left(3+2\sqrt{2}\right)d_A$), and $R_{exc} = 800$ m in Fig. 3.11 (Now, we are in Case 2) since it holds that $R_{exc} > \left(3+2\sqrt{2}\right)d_A$. In addition, $N_{trunc} = 10$ is used). Again, the close match of the Monte Carlo simulation with the analytical model in the high-SINR region can be observed, as expected.

3.3.6.2 Energy Gain

With reference the value $R_{exc} = 200$ m, in Table 3.5 the relative energy gain achieved is presented as R_{exc} increases and for a target SER=10^{-2}. This gain is defined as

$$relative\ energy\ gain = \frac{P_T^{200\,m} - P_T^{500/800\,m}}{P_T^{200\,m}}\ [\%]\,. \tag{3.101}$$

As we observe from Table 3.5, significant energy gains can be achieved, which were expected, since increasing the radius of the exclusion region means that less volume of interference is affecting the two sources.

Table 3.5: Relative Energy Gain (%) with respect to the value $R_{exc} = 200$ m.

$R_{exc} = 500$ m	$R_{exc} = 800$ m
$a = 3.2$	
87.4	90
$a = 4$	
93.7	98

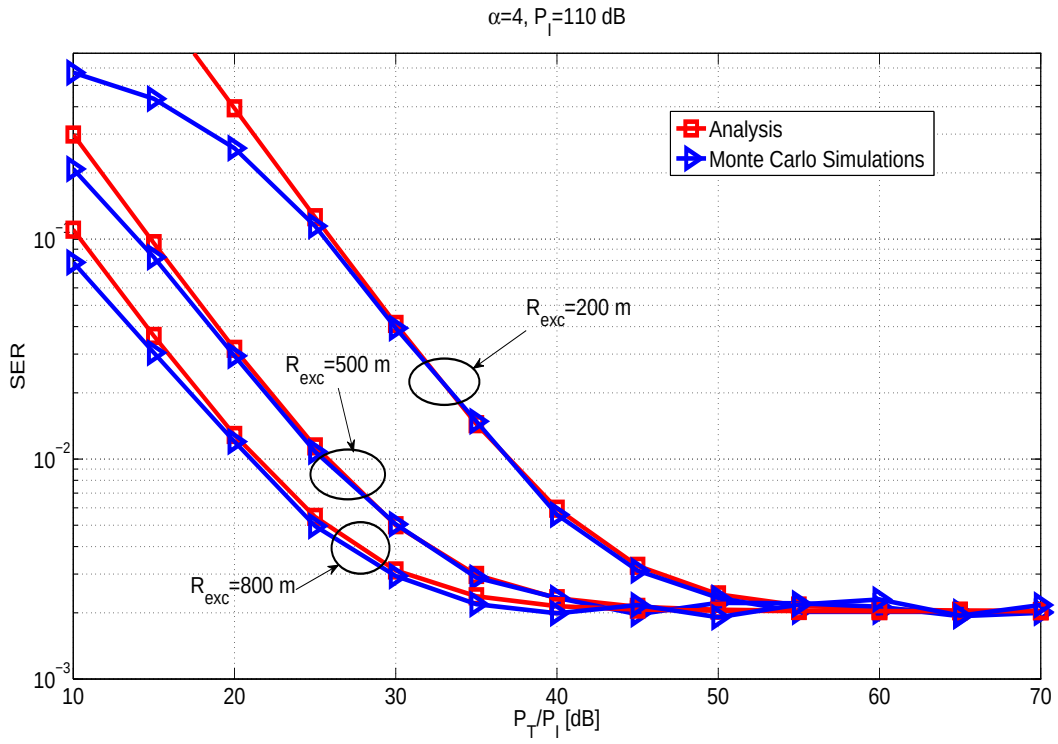

Figure 3.8: SER vs. P_T/P_I for $a = 4$ and $P_I = 110$ dB.

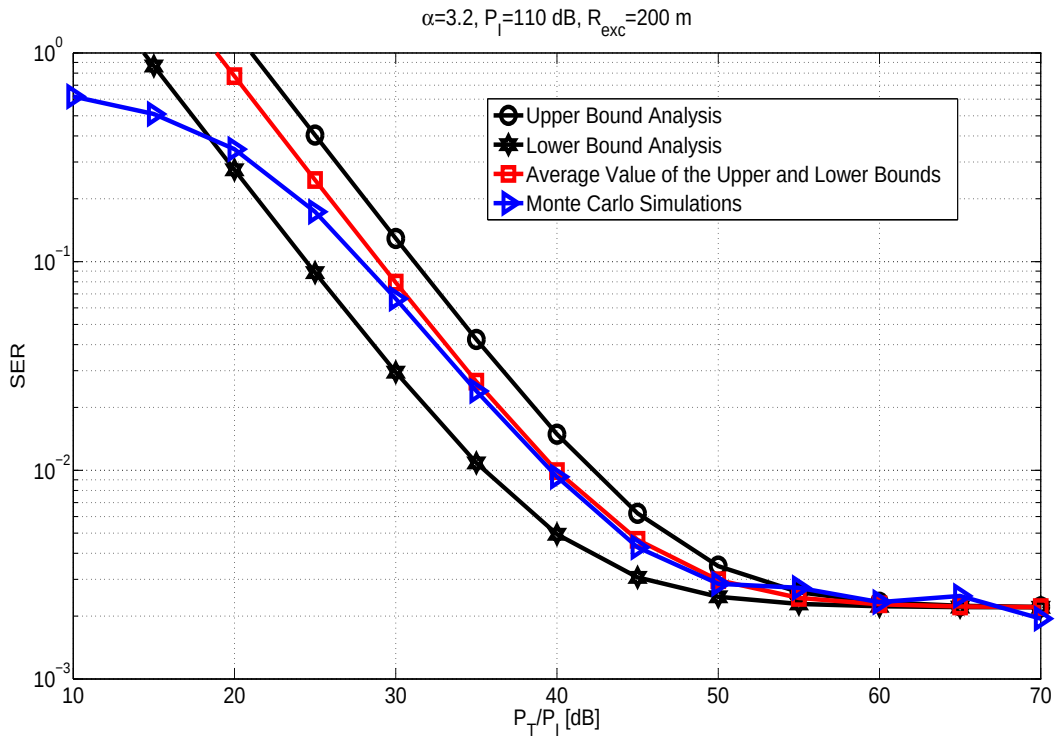

Figure 3.9: SER vs. P_T/P_I for $a = 3.2$, $P_I = 110$ dB, and $R_{exc} = 200$ m.

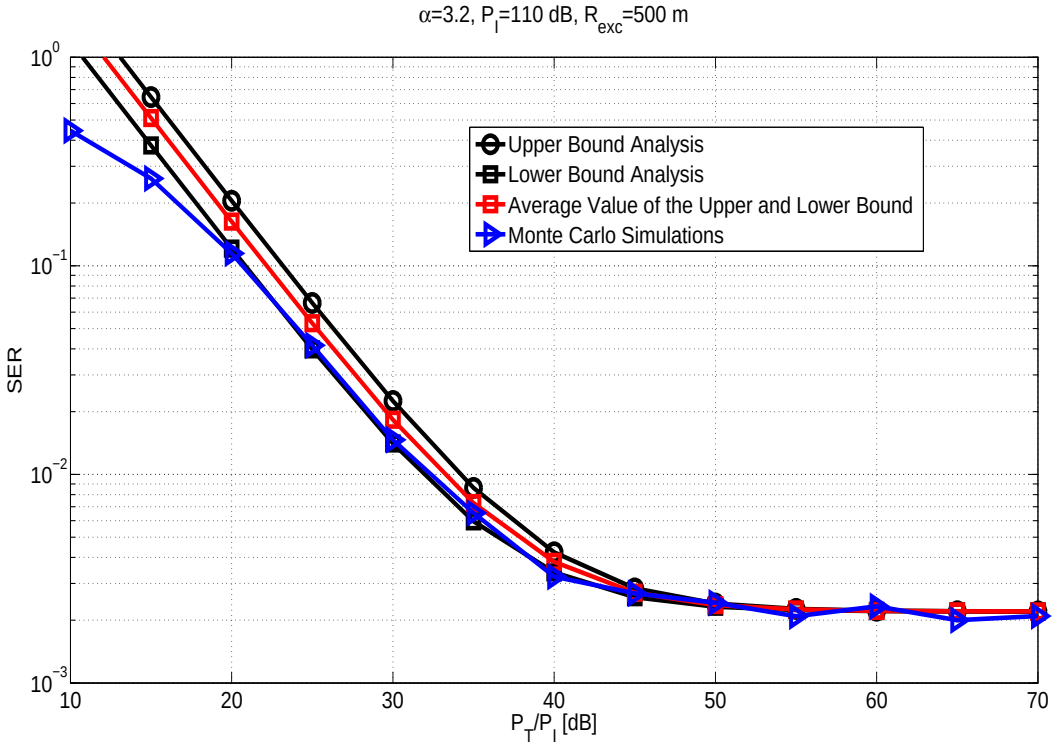

Figure 3.10: SER vs. P_T/P_I for $a = 3.2$, $P_I = 110$ dB, and $R_{exc} = 500$ m.

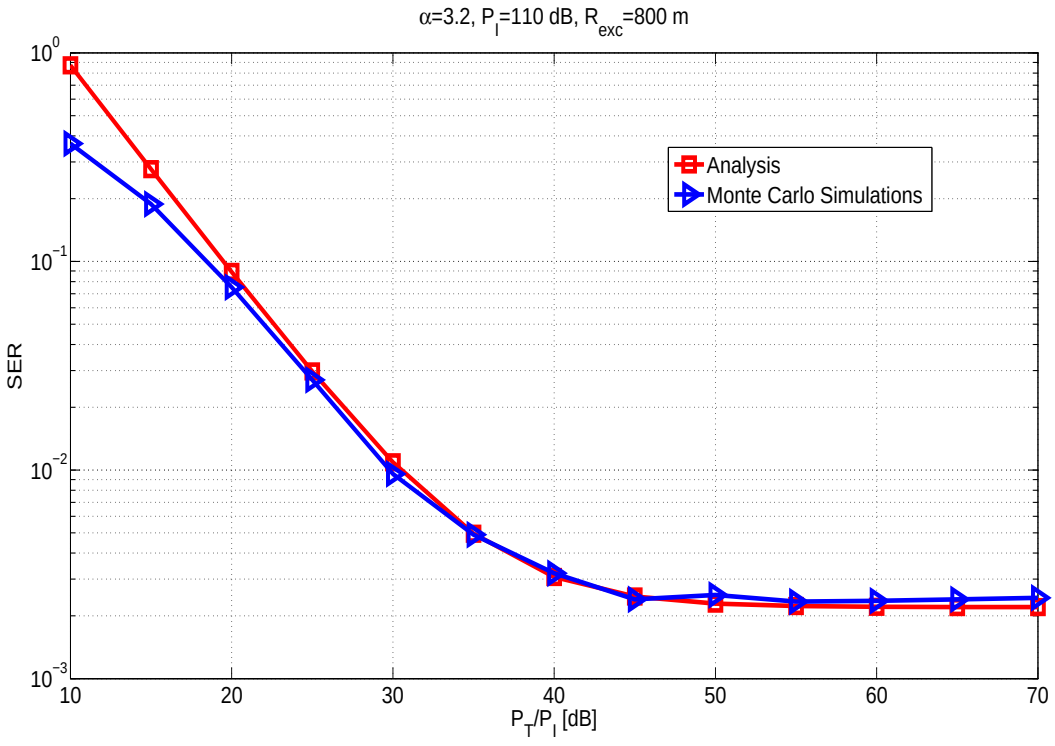

Figure 3.11: SER vs. P_T/P_I for $a = 3.2$, $P_I = 110$ dB, and $R_{exc} = 800$ m.

3.4 Conclusions

In this chapter, two scenarios where ANC can find implementation were presented. In particular,

1) Regarding ANC in the MARC:

i) Assuming the optimal ML detector at the destination, a closed-form mathematical expression of the SER in the high-SNR regime was derived, by considering fixed-gain relays. By comparing them with Monte Carlo simulations, this expression was shown to be sufficiently accurate in the SNR range of interest. Furthermore, based on this framework, an energy efficiency comparison with the TDMA approach was conducted and it is mathematically proved that as either the number of sources, or relays, or the modulation order increases, the possibility of ANC in the MARC being more energy efficient than TDMA increases as well. Numerical results validated these findings.

ii) To alleviate the high detection complexity of the optimal ML detector, analytical high-SNR SER frameworks were developed for the linear ZF and MMSE detectors at the destination. Based on the derived closed-form expressions of the SER, the coding gain and diversity order achieved by each of these linear detectors were computed. These metrics highlight how the number of sources and relays affect the SER. Furthermore, it was proved that the ratio of the coding gains of the ZF and MMSE detectors is monotonic as a function of the number of sources, relays, and modulation order.

iii) The optimal power allocation problem that minimizes the SER for a given total power budget shared among the sources and relays was formulated and it was proved to be convex for the three detectors under consideration (ML, ZF, and MMSE). In addition, a closed-form solution for the optimal power allocation was provided for the ZF and MMSE case. Numerical results showed that the optimal power allocation policy is particularly beneficial as the number of sources increases and when the quality of the source-relay links is better than the one of the relay-destination links.

2) Regarding ANC in the two-way relaying channel:

i) Analytical expressions for the SER of the two sources in the high Signal-to-Interference-plus-Noise (SINR) region were derived by considering the impact of network interference, which is a more realistic assumption for the interference that is likely to appear in heteroge-

neous networks. These expressions exhibit a close match with Monte Carlo simulations, as it was shown.

ii) Based on these SER expressions, the relative energy gain achieved regarding the transmission power level of the sources was numerically substantiated, as the radius of the exclusion region increases. Significant gains were observed.

3.5 APPENDIX A

A.1. *Proof of Proposition 1*: Based on (3.5), $PEP_{s_q,ij}$ is given by [48]

$$PEP_{s_q,ij} = E\left\{Q\left(\sqrt{\sum_{m=1}^{M}\frac{1}{2}\frac{P_S\sigma_{SR}^2 P_R\sigma_{RD}^2\left|\mathbf{h}_m\mathbf{\Delta s}_{i,j}\right|^2\left|f_m\right|^2}{P_R\sigma_{RD}^2\left|f_m\right|^2+KP_S\sigma_{SR}^2+1}}\right)\right\}, \tag{3.102}$$

where $\mathbf{h}_m = \left(h_{1m}h_{2m}h_{Km}\right)$ and $\mathbf{\Delta s}_{i,j} = \mathbf{s}_i - \mathbf{s}_j$. Due to the difficulty of analytically solving (3.102) in its exact form, the exponential approximation of the Q-function is considered [19, Eq. (31)]:

$$Q\left(x\right) \approx \frac{1}{12}e^{-\frac{x^2}{2}} + \frac{1}{6}e^{-\frac{2x^2}{3}}, \quad x \geqslant 0. \tag{3.103}$$

By plugging (3.103) into (3.102) and by taking into account that all the channel links are independent, we obtain

$$PEP_{s_q,ij} \approx \frac{1}{12}\prod_{m=1}^{M}\int_0^\infty e^{-u_m}f_m\left(u_m\right)du_m + \frac{1}{6}\prod_{m=1}^{M}\int_0^\infty e^{-\frac{4}{3}u_m}f_m\left(u_m\right)du_m, \tag{3.104}$$

where $u_m = \frac{1}{4}\frac{P_S\sigma_{SR}^2 P_R\sigma_{RD}^2\left|\mathbf{h}_m\mathbf{\Delta s}_{i,j}\right|^2\left|f_m\right|^2}{P_R\sigma_{RD}^2\left|_m\right|^2+KP_S\sigma_{SR}^2+1}$ and $f_m\left(u\right)$ is the probability density function of u_m. According to [5, Eq. (10)],

$$f_m\left(u\right) = \frac{2}{b}e^{-\frac{u}{b}}\left[\sqrt{\frac{cu}{ab}}K_1\left(2\sqrt{\frac{cu}{ab}}\right) + \frac{c}{a}K_0\left(2\sqrt{\frac{cu}{ab}}\right)\right]. \tag{3.105}$$

By plugging (3.105) into (3.104) and by using [13, 6.643.3] and [14, 13.1.33 and 13.2.5], we obtain (3.7).

A.2. *Proof of Proposition 2*: For $P_S, P_R \to \infty$ and by using the inequality $E_1\left(z\right) < e^{-z}\log\left(1+\frac{1}{z}\right)$ [14, 5.1.20] and the fact that $\log\left(\log\left(P_R\sigma_{RD}^2\right)\right) \ll \log\left(P_R\sigma_{RD}^2\right)$ for $P_R \to \infty$, (3.7) is upper bounded as

$$PEP_{s_q,ij} \lessapprox \frac{1}{\left(\sigma_{RD}^2\|\mathbf{\Delta s}_{i,j}\|_F^2\right)^M}\left[\frac{\left(4K\right)^M}{12} + \frac{\left(3K\right)^M}{6}\right]P_R^{-M}. \tag{3.106}$$

By considering that in the high-SNR regime the SER of an uncoded (or coded) system can be approximated as $SER \approx (G_c\bar{\gamma})^{-G_d}$ [46], where G_c, G_d, and $\bar{\gamma}$ denote the coding gain, diversity order, and average SNR, respectively, the proof of Proposition 2 is concluded.

A.3. *Proof of Proposition 3*: The proof consists of the following two steps: i) An approximate expression for the post-processing SNR of the k_{th} source is derived, which is denoted as γ_k^{ZF}. ii) Based on i), an approximate expression of the MGF of γ_k^{ZF} is obtained, which is denoted as $M_{\gamma,k}^{ZF}(s)$ from which the SER per source of the ZF detector can be obtained as [19, Eq. (33)]

$$SER_{ZF} \approx c_1 \left[\frac{1}{3}M_{\gamma,k}^{ZF}(c_2) + \frac{2}{3}M_{\gamma,k}^{ZF}(c_3)\right]. \tag{3.107}$$

i) γ_k^{ZF}: First find the expected value of the covariance matrix of $\tilde{\mathbf{n}}_{ZF}$ is calculated, conditioned on $\mathbf{H}$ and $\mathbf{F}$, which is denoted as $E\left\{\tilde{\mathbf{n}}_{ZF}\tilde{\mathbf{n}}_{ZF}^H|\mathbf{H},\mathbf{F}\right\}$. We have

$$E\left\{\tilde{\mathbf{n}}_{ZF}\tilde{\mathbf{n}}_{ZF}^H|\mathbf{H},\mathbf{F}\right\} = \mathbf{G}_{ZF}E\left\{\tilde{\mathbf{n}}_D\tilde{\mathbf{n}}_D^H\right\}\mathbf{G}_{ZF}^H. \tag{3.108}$$

Now, for the term $E\left\{\tilde{\mathbf{n}}_D\tilde{\mathbf{n}}_D^H\right\}$ of (3.108), we have

$$E\left\{\tilde{\mathbf{n}}_D\tilde{\mathbf{n}}_D^H\right\} = \left[\frac{P_R\sigma_{RD}^2}{KP_S\sigma_{SR}^2+1}\mathbf{F}\mathbf{F}^H + \mathbf{I}_M\right] \overset{(b)}{\approx} \left(\frac{P_R\sigma_{RD}^2}{KP_S\sigma_{RD}^2+1}+1\right)\mathbf{I}_M, \tag{3.109}$$

where the approximation in (b) comes as a result of considering $KP_S\sigma_{SR}^2+1 \gg P_R\sigma_{RD}^2$. This is due to the fact that by this assumption the variance of $\frac{P_R\sigma_{RD}^2}{KP_S\sigma_{SR}^2+1}|f_m|^2$, which the element of the m_{th} row and m_{th} column of the diagonal matrix $\frac{P_R\sigma_{RD}^2}{KP_S\sigma_{SR}^2+1}\mathbf{F}\mathbf{F}^H$, is much smaller than 1 (since $|f_m|^2$ has a unit variance). Hence, $\frac{P_R\sigma_{RD}^2}{KP_S\sigma_{SR}^2+1}|f_m|^2$ can be approximated by its mean value, which is $\frac{P_R\sigma_{RD}^2}{KP_S\sigma_{SR}^2+1}$. By plugging (3.109) into (3.108), we get

$$E\left\{\tilde{\mathbf{n}}_{ZF}\tilde{\mathbf{n}}_{ZF}^H|\mathbf{H},\mathbf{F}\right\} \approx \left(\frac{P_R\sigma_{RD}^2}{KP_S\sigma_{RD}^2+1}+1\right)\left(\mathbf{H}\mathbf{V}\mathbf{H}^H\right)^{-1}. \tag{3.110}$$

Consequently, the approximate post-processing SNR for the k_{th} source is given by

$$\gamma_k^{ZF} \approx \frac{\frac{P_S\sigma_{SR}^2P_R\sigma_{RD}^2}{KP_S\sigma_{SR}^2+1}}{\left(\frac{P_R\sigma_{RD}^2}{KP_S\sigma_{SR}^2+1}+1\right)\left[\left(\mathbf{H}^H\mathbf{V}\mathbf{H}\right)^{-1}\right]_{kk}} \overset{(c)}{=} \bar{\gamma}\mathbf{h}_k^H\left(\mathbf{V}-\mathbf{V}\mathbf{H}_{(-k)}\left(\mathbf{H}_{(-k)}^H\mathbf{V}\mathbf{H}_{(-k)}\right)^{-1}\mathbf{H}_{(-k)}^H\mathbf{V}\right)\mathbf{h}_k, \tag{3.111}$$

where in (c) we consider that the element of the k_{th} row and k_{th} column of the inverse of a square matrix $\mathbf{A}$, which is denoted as $[\mathbf{A}^{-1}]_{kk}$, can be written as [49, Eq. (8)]

$$\left[\mathbf{A}^{-1}\right]_{kk} = \left(\mathbf{A}_{kk} - \mathbf{a}_{k(-k)}^H\left(\mathbf{A}_{(-k,-k)}\right)^{-1}\mathbf{a}_{k(-k)}\right)^{-1}, \tag{3.112}$$

where $\mathbf{a}_{k(-k)}$ is the k_{th} column of $\mathbf{A}$ with the k_{th} entry removed and $\mathbf{A}_{(-k,-k)}$ is $\mathbf{A}$ with the k_{th} row and k_{th} column removed.

ii) $M_{\gamma,k}^{ZF}(s)$: For the derivation of a closed-form of $M_{\gamma,k}^{ZF}(s)$, we follow a two-step procedure: 1) We first derive the MGF of γ_k^{ZF} conditioned on $\mathbf{F}$, which we denote as $M_{\gamma,k}^{ZF}(s\,|\mathbf{F})$. 2) After deriving $M_{\gamma,k}^{ZF}(s\,|\mathbf{F})$, $M_{\gamma,k}^{ZF}(s)$ is obtained by marginalizing over $\mathbf{F}$ as $M_{\gamma,k}^{ZF}(s) = E_{\mathbf{F}}\left\{M_{\gamma,k}^{ZF}(s\,|\mathbf{F})\right\}$.

1) *Derivation of* $M_{\gamma,k}^{ZF}(s\,|\mathbf{F})$: By conditioning on $\mathbf{F}$, the channel matrix $\mathbf{FH}$ is equivalent to a Gaussian channel matrix $\mathbf{H}$ with correlation at the receive side. The receive correlation matrix is $\mathbf{V} = \mathbf{F}^H\mathbf{F} = \mathbf{F}\mathbf{F}^H$. By considering this, γ_k^{ZF} has the same form as [50, Eq. (5)] and, consequently, $M_{\gamma,k}^{ZF}(s\,|\mathbf{F})$ is given by

$$M_{\gamma,k}^{ZF}(s\,|\mathbf{F}) \overset{(d)}{\approx} \frac{1}{\det\left(s\bar{\gamma}\mathbf{V}+\mathbf{I}_M\right)} E_{\mathbf{H}_{(-k)}|\mathbf{F}}\left\{\frac{\det\left(\mathbf{H}_{(-k)}^H\mathbf{V}\mathbf{H}_{(-k)}\right)}{\det\left(\mathbf{H}_{(-k)}^H\mathbf{V}\left(s\bar{\gamma}\mathbf{V}+\mathbf{I}_M\right)^{-1}\mathbf{H}_{(-k)}\right)}\right\}$$
$$\overset{s\bar{\gamma}\gg 1}{\approx} \frac{\left(s\bar{\gamma}\right)^{K-1}}{\det\left(\mathbf{I}_M+s\bar{\gamma}\mathbf{V}\right)} E_{\mathbf{H}_{(-k)}|\mathbf{F}}\left\{\frac{\det\left(\mathbf{H}_{(-k)}^H\mathbf{V}\mathbf{H}_{(-k)}\right)}{\det\left(\mathbf{H}_{(-k)}^H\mathbf{I}_M\mathbf{H}_{(-k)}\right)}\right\}, \tag{3.113}$$

where in (d) [50, Eq. (15)] is used. Now, according to [50, Eq. (17)], we have

$$E_{\mathbf{H}_{(-k)}|\mathbf{F}}\left\{\frac{\det\left(\mathbf{H}_{(-k)}^H\mathbf{V}\mathbf{H}_{(-k)}\right)}{\det\left(\mathbf{H}_{(-k)}^H\mathbf{I}_M\mathbf{H}_{(-k)}\right)}\right\} = el_{K-1}(\mathbf{V})\,(K-1)\,B(K-1, M-K+2), \tag{3.114}$$

where $B(x,y) = \int_0^\infty \frac{t^{x-1}}{(1+t)^{x+y}}dt = \frac{(x-1)!(y-1)!}{(x+y-1)!}$ is the Beta function [14]. By plugging (3.114) into (3.113) and by using $\frac{|f_m|^2}{1+s\bar{\gamma}|f_m|^2} \approx \left(s\bar{\gamma}\right)^{-1}$, which holds in the high-SNR regime ($s\bar{\gamma} \gg 1$), we get

$$M_{\gamma,k}^{ZF}(s\,|\mathbf{F}) \approx \frac{el_{M-K+1}\left(\left(\mathbf{I}_M+s\bar{\gamma}\mathbf{V}\right)^{-1}\right)}{\binom{M}{K-1}}, \tag{3.115}$$

2) *Derivation of* $M_{\gamma,k}^{ZF}(s)$: We have

$$M_{\gamma,k}^{ZF}(s) = E_{\mathbf{F}}\left\{M_{\gamma,k}^{ZF}(s\,|\mathbf{F})\right\} \overset{(e)}{\approx} \frac{E_{\mathbf{F}}\left\{el_{M-K+1}\left(\left(\mathbf{I}_M+s\bar{\gamma}\mathbf{V}\right)^{-1}\right)\right\}}{\binom{M}{K-1}}, \tag{3.116}$$

where in (e) we use (3.115). Now, by considering that $f_1, ..., f_M$ are independent and identically distributed complex Gaussian random variables and by using [13, 3.352.4], we get

$$E_{\mathbf{F}}\left\{el_{M-K+1}\left(\left(\mathbf{I}_M+s\bar{\gamma}\mathbf{V}\right)^{-1}\right)\right\} = \binom{M}{M-K+1}\left[\frac{1}{s\bar{\gamma}}e^{\frac{1}{s\bar{\gamma}}}E_1\left(\frac{1}{s\bar{\gamma}}\right)\right]^{M-K+1}. \tag{3.117}$$

By plugging (3.117) into (3.116) and by using (3.107), the proof of Proposition 3 is concluded.

A.4. *Proof of Proposition 4*: For $\bar{\gamma} \to \infty$ and by using the inequality $E_1(z) < e^{-z} \log\left(1 + \frac{1}{z}\right)$ [14, 5.1.20] and the fact that $\log(c\bar{\gamma}) \simeq \log(\bar{\gamma})$ for $c > 0$ and $\log(\bar{\gamma}) \gg \log(\log(\bar{\gamma}))$, as $\bar{\gamma} \to \infty$, (3.17) becomes

$$SER_{ZF} \lessapprox \frac{c_1}{3}\left[c_2^{-(M-K+1)} + 2c_3^{-(M-K+1)}\right]\bar{\gamma}^{-(M-K+1)}, \tag{3.118}$$

which concludes the proof of Proposition 4.

A.5. *Proof of Proposition 5*: Again the following two steps are considered, as in the proof of Proposition 3 for the ZF detector: i) An approximate expression for the post-processing Signal-to-Interference plus Noise Ratio (SINR) per source, which is denoted as γ_k^{MMSE} is derived. ii) Based on i), an approximate expression of the MGF of the derived post-processing SINR is obtained, which is denoted as $M_{\gamma,k}^{MMSE}(s)$, from which the SER per source of the MMSE detector can be obtained as [19, Eq. (33)]

$$SER_{MMSE} \approx c_1\left[\frac{1}{3}M_{\gamma,k}^{MMSE}(c_2) + \frac{2}{3}M_{\gamma,k}^{MMSE}(c_3)\right]. \tag{3.119}$$

i) γ_k^{MMSE}: We first find the variance of $\tilde{n}_k^{MMSE}$, conditioned on $\mathbf{H}$ and $\mathbf{F}$, which is denoted as $\sigma^2_{MMSE,k|\mathbf{H},\mathbf{F}}$. We have

$$\sigma^2_{MMSE,k|\mathbf{H},\mathbf{F}} = E\left\{\left(\tilde{n}_k^{MMSE}\right)^2\right\} - \left[E\left\{\tilde{n}_k^{MMSE}\right\}\right]^2 \overset{(h)}{\approx} \frac{P_S\sigma^2_{SR}P_R\sigma^2_{RD}}{KP_S\sigma^2_{SR}+1} \times \left[\mathbf{g}^H_{MMSE,k}\mathbf{F}\mathbf{h}_k - \left(\mathbf{g}^H_{MMSE,k}\mathbf{F}\mathbf{h}_k\right)^2\right], \tag{3.120}$$

where in (h) we use (3.109). Consequently, based on (3.22) and after some algebraic manipulations, we have

$$\gamma_k^{MMSE} \approx \frac{\left(\mathbf{g}^H_{MMSE,k}\mathbf{F}\mathbf{h}_k\right)^2}{\left[\mathbf{g}^H_{MMSE,k}\mathbf{F}\mathbf{h}_k - \left(\mathbf{g}^H_{MMSE,k}\mathbf{F}\mathbf{h}_k\right)^2\right]} = \mathbf{h}_k^H\mathbf{F}^H\left(\mathbf{F}\mathbf{H}_{(-k)}\mathbf{H}^H_{(-k)}\mathbf{F}^H + \frac{1}{\bar{\gamma}}\mathbf{I}_M\right)^{-1}\mathbf{F}\mathbf{h}_k. \tag{3.121}$$

ii) $M_{\gamma,k}^{MMSE}(s)$: The approximate closed-form expression for $M_{\gamma,k}^{MMSE}(s)$ will be derived in a two-step procedure, as in the case of the ZF detector: 1) First, the MGF of γ_k^{MMSE} conditioned on $\mathbf{F}$ is derived, which is denoted as $M_{\gamma,k}^{MMSE}(s\,|\mathbf{F})$. 2) After deriving $M_{\gamma,k}^{MMSE}(s\,|\mathbf{F})$, $M_{\gamma,k}^{ZF}(s)$ is obtained by marginalizing over $\mathbf{F}$ as $M_{\gamma,k}^{MMSE}(s) = E_{\mathbf{F}}\left\{M_{\gamma,k}^{MMSE}(s\,|\mathbf{F})\right\}$.

1) *Derivation of* $M_{\gamma,k}^{MMSE}(s\,|\mathbf{F})$: Again it is noted that by conditioning on $\mathbf{F}$ the channel matrix $\mathbf{FH}$ is equivalent to a Gaussian channel matrix $\mathbf{H}$ with receive correlation, which is

represented by the matrix $\mathbf{V}$. By considering this, γ_k^{MMSE} has the same form as [50, Eq. (9)] and, consequently, $M_{\gamma,k}^{MMSE}(s\,|\mathbf{F})$ is given by

$$M_{\gamma,k}^{MMSE}(s\,|\mathbf{F}) \overset{(h)}{\approx} \frac{1}{\det(\mathbf{I}_M + s\bar{\gamma}\mathbf{V})} E_{\mathbf{H}_{(-k)}}\left\{\frac{\det\left(\mathbf{I}_{K-1} + \mathbf{H}_{(-k)}^H(\bar{\gamma}\mathbf{V})\mathbf{H}_{(-k)}\right)}{\det\left(\mathbf{I}_{K-1} + \mathbf{H}_{(-k)}^H\left(\frac{1}{\bar{\gamma}}\mathbf{V}^{-1} + s\mathbf{I}_M\right)^{-\mathbf{1}}\mathbf{H}_{(-k)}\right)}\right\}$$
$$\overset{s\bar{\gamma}\gg 1}{\approx} \frac{1}{\det(\mathbf{I}_M + s\bar{\gamma}\mathbf{V})} E_{\mathbf{H}_{(-k)}}\left\{\frac{\det\left(\mathbf{H}_{(-k)}^H(\bar{\gamma}\mathbf{V})\mathbf{H}_{(-k)}\right)}{\det\left(\mathbf{I}_{K-1} + \frac{1}{s}\mathbf{H}_{(-k)}^H\mathbf{H}_{(-k)}\right)}\right\}, \tag{3.122}$$

where in (h) [50, Eq. (24)] is used. Now, according to [50, Eq. (25)], we have

$$E_{\mathbf{H}_{(-k)}}\left\{\frac{\det\left(\mathbf{H}_{(-k)}^H(\bar{\gamma}\mathbf{V})\mathbf{H}_{(-k)}\right)}{\det\left(\mathbf{I}_{K-1} + \frac{1}{s}\mathbf{H}_{(-k)}^H\mathbf{H}_{(-k)}\right)}\right\} \overset{(i)}{=} (K-1)\,el_{K-1}(\bar{\gamma}\mathbf{V})\,s^{K-1}e^s\sum_{k=0}^{K-2}(-1)^k\binom{K-2}{k}$$
$$\times E_{M-K+3+k}(s), \tag{3.123}$$

where in (i) [51, Eq. (6.21)] is used. By plugging (3.123) into (3.122) and by considering that $\frac{|f_m|^2}{1+s\bar{\gamma}|f_m|^2} \approx (s\bar{\gamma})^{-1}$ $(s\bar{\gamma} \gg 1)$, we get

$$M_{\gamma,k}^{MMSE}(s\,|\mathbf{F}) \approx (K-1)\,el_{M-K+1}\left((\mathbf{I}_M + s\bar{\gamma}\mathbf{V})^{-1}\right)e^s\sum_{k=0}^{K-2}(-1)^k\binom{K-2}{k}$$
$$\times E_{M-K+3+k}(s). \tag{3.124}$$

2) *Derivation of* $M_{\gamma,k}^{MMSE}(s)$: We have

$$M_{\gamma,k}^{MMSE}(s) = E_{\mathbf{F}}\left\{M_{\gamma,k}^{MMSE}(s\,|\mathbf{F})\right\} \overset{(j)}{\approx} (K-1)\binom{M}{M-K+1}\left[\frac{1}{s\bar{\gamma}}e^{\frac{1}{s\bar{\gamma}}}E_1\left(\frac{1}{s\bar{\gamma}}\right)\right]^{M-K+1}$$
$$\times e^s\sum_{k=0}^{K-2}(-1)^k\binom{K-2}{k}E_{M-K+3+k}(s), \tag{3.125}$$

where in (j) (3.117) and (3.124) is used.

A.6. *Proof of Proposition 6*: For $\bar{\gamma} \to \infty$ and by using the inequality $E_1(z) < e^{-z}\log\left(1+\frac{1}{z}\right)$ [14, 5.1.20] and the fact that $\log(c\bar{\gamma}) \simeq \log(\bar{\gamma})$ for $c > 0$ and $\log(\bar{\gamma}) \gg \log(\log(\bar{\gamma}))$, as $\bar{\gamma} \to \infty$, (3.24) becomes

$$SER_{MMSE} \lessapprox \frac{c_1}{3}(K-1)\binom{M}{M-K+1}\left[C(c_2) + 2C(c_3)\right]\bar{\gamma}^{-(M-K+1)}. \tag{3.126}$$

Hence, the proof of Proposition 6 is concluded.

3.6 APPENDIX B

B.1. *Proof of Theorem 1*: *Preliminaries*: Considering the high-SNR region, then

$$r_{TDMA/ANC} \overset{P_{ANC}\to\infty,\ (3.9),\ (3.10),\ (3.12)}{\approx} \frac{1}{K}\left[\frac{2\left(M+1\right)}{\left(K+1\right)\left(K+M\right)}\right]^{M} \times \frac{\sum\limits_{\mathbf{\Delta s}} \frac{1}{\left(|\mathbf{\Delta s}_{i,j}|_F^2\right)_{TDMA}^{M}}}{\sum\limits_{\mathbf{\Delta s}} \frac{1}{\left(|\mathbf{\Delta s}_{i,j}|_F^2\right)_{ANC}^{M}}}. \tag{3.127}$$

To simplify things, only the the closest neighbors in the error vectors $\mathbf{\Delta s}_{i,j}$ of (3.127) are considered. Hence, due to the geometry of a square QAM constellation it holds that:

$$\sum_{\mathbf{\Delta s}} \frac{1}{\left(|\mathbf{\Delta s}_{i,j}|_F^2\right)_{ANC}^{M}} \approx 4\left(Q_{ANC}-\sqrt{Q_{ANC}}\right) \times \left[\frac{\left(Q_{ANC}-1\right)}{6}\right]^{M} Q_{ANC}^{K-1} \tag{3.128a}$$

$$\begin{aligned}\sum_{\mathbf{\Delta s}} \frac{1}{\left(|\mathbf{\Delta s}_{i,j}|_F^2\right)_{TDMA}^{M}} &\approx 4\left(Q_{TDMA}-\sqrt{Q_{TDMA}}\right) \times \left[\frac{\left(Q_{TDMA}-1\right)}{6}\right]^{M} \\ &= 4\left(Q_{ANC}^{K}-\sqrt{Q_{ANC}^{K}}\right) \times \left[\frac{\left(Q_{ANC}^{K}-1\right)}{6}\right]^{M}.\end{aligned} \tag{3.128b}$$

(3.128a) and (3.128b) hold because $\frac{6}{Q-1}$ is the minimum squared Euclidean Distance of a square QAM constelation of order Q and $4\left(Q-\sqrt{Q}\right)$ is the total number of minimum squared Euclidean distances of the same constellation. Hence, by plugging (3.128a) and (3.128b) into (3.127), we get

$$r_{TDMA/ANC} \approx \frac{1}{K}\left[\frac{2\left(M+1\right)\left(Q_{ANC}^{K}-1\right)}{\left(K+1\right)\left(K+M\right)\left(Q_{ANC}-1\right)}\right]^{M} \times \frac{\left(Q_{ANC}^{K}-\sqrt{Q_{ANC}^{K}}\right)\left(Q_{ANC}^{K}-1\right)}{\left(Q_{ANC}-\sqrt{Q_{ANC}}\right)Q_{ANC}^{K-1}}. \tag{3.129}$$

i) *Proving that* $r_{TDMA/ANC}$ *is a monotonically increasing function of* K:

$$\begin{aligned}\frac{d\left(r_{TDMA/ANC}\right)}{dK} > 0 \Rightarrow\ & K\left(K+1\right)\left(K+M\right) \\ & \times \log\left(Q_{ANC}\right)\left(M+1\right) > K\left(K+1\right)\left(2M+1\right) \\ & + KM^2+M \quad true.\end{aligned} \tag{3.130}$$

ii) *Proving that $r_{TDMA/ANC}$ is a monotonically increasing function of M*:

$$\begin{aligned}\frac{d\left(r_{TDMA/ANC}\right)}{dM} > 0 \Rightarrow & (K+1)(K+M) \\ & \times \log\left[\frac{2(M+1)\left(Q_{ANC}^{K}-1\right)}{(K+1)(K+M)(Q_{ANC}-1)}\right] \\ & + (K-1)M > 0 \quad true, \end{aligned} \tag{3.131}$$

since

$$\begin{aligned}\log\left[\frac{2(M+1)\left(Q_{ANC}^{K}-1\right)}{(K+1)(K+M)(Q_{ANC}-1)}\right] \geqslant 0 \Rightarrow & \frac{Q_{ANC}^{K}-1}{Q_{ANC}-1} \\ & \geqslant \frac{(K+1)(K+M)}{2(M+1)} \\ & true. \end{aligned} \tag{3.132}$$

iii) *Proving that $r_{TDMA/ANC}$ is a monotonically increasing function of Q_{ANC}*:

$$\begin{aligned}\frac{d\left(r_{TDMA/ANC}\right)}{dQ_{ANC}} > 0 \overset{Q_{ANC}\gg 1}{\Rightarrow} & M(K-1)+K > \frac{1}{2\sqrt{Q}_{ANC}} \\ & true. \end{aligned} \tag{3.133}$$

B.2. *Proof of Theorem 2*: For analytical simplicity and without loss of generality, the ratio $\frac{G_{MMSE}^{cod}}{G_{ZF}^{cod}}$ can be approximated by taking the first terms of enumerator and denominator of (3.28), i.e.

$$\frac{G_{MMSE}^{cod}}{G_{ZF}^{cod}} = \left[\frac{1}{(K-1)\binom{M}{M-K+1}e^{c_2}\sum\limits_{k=0}^{K-2}(-1)^k\binom{K-2}{k}E_{M-K+3+k}(c_2)}\right]^{\frac{1}{M-K+1}} \tag{3.134}$$

The approximation of (3.134) comes a result of considering the Chernoff bound in the approximation of the Q-function, instead of (3.103). Intuitively thinking, the value of $\frac{G_{MMSE}^{cod}}{G_{ZF}^{cod}}$ can only be slightly affected by this consideration since it is a ratio of coding gains, where each coding gain is obtained by the same approximation of the Q-function. This makes (3.134) a valid approximation. In addition,

$$e^{c_2}\sum_{k=0}^{K-2}(-1)^k\binom{K-2}{k}E_{M-K+3+k}(c_2) \overset{(k)}{>} c_2^{K-1}\frac{\Gamma(K-1)\Gamma(\mathrm{M}-K+3+c_2)}{\Gamma(\mathrm{M}+2+c_2)}, \tag{3.135}$$

where in (k) [14, 5.1.19] is used.

By plugging (3.135) into (3.134), we get an upper bound of $\frac{G_{MMSE}^{cod}}{G_{ZF}^{cod}}$, that is

$$\frac{G_{MMSE}^{cod}}{G_{ZF}^{cod}} < \left.\frac{G_{MMSE}^{cod}}{G_{ZF}^{cod}}\right|_{UB} = \left[\frac{(M-K+1)!\Gamma\left(M+2+c_2\right)}{M!\Gamma\left(M-K+3+c_2\right)}\right]^{\frac{1}{M-K+1}}. \tag{3.136}$$

A good approximation for the argument of the factorial or gamma function can be obtained from Stirling's approximation, that is [14]

$$n! \approx \sqrt{2\pi n}\left(\frac{n}{e}\right)^n, \quad \Gamma\left(1+t\right) \approx \sqrt{2\pi t}\left(\frac{t}{e}\right)^t. \tag{3.137}$$

By plugging (3.137) into (3.136), we get

$$\left.\frac{G_{MMSE}^{cod}}{G_{ZF}^{cod}}\right|_{UB} \approx \left[\frac{\left(M+1+c_2\right)^{M+c_2+\frac{3}{2}}\left(M-K+1\right)^{M-K+\frac{3}{2}}}{M^{M+\frac{1}{2}}\left(M-K+2+c_2\right)^{M-K+c_2+\frac{5}{2}}}\right]^{\frac{1}{M-K+1}} = m\left(K,M,c_2\right)^{b(K,M)}, \tag{3.138}$$

where

$$m\left(K,M,c_2\right) = \frac{\left(M+1+c_2\right)^{M+c_2+\frac{3}{2}}\left(M-K+1\right)^{M-K+\frac{3}{2}}}{M^{M+\frac{1}{2}}\left(M-K+2+c_2\right)^{M-K+c_2+\frac{5}{2}}} \quad and \quad b\left(K,M\right) = \frac{1}{M-K+1}. \tag{3.139}$$

Now, since the gap between the coding gain (and, consequently, the corresponding SER) of the MMSE and ZF detectors is non-vanishing and does not depend on the SNR in the high-SNR regime, as it can be observed from (3.134), and as it was also proved in [1] for non-relay channels, then we have

$$\frac{G_{MMSE}^{cod}}{G_{ZF}^{cod}} > 1 \Rightarrow \log\left(\frac{G_{MMSE}^{cod}}{G_{ZF}^{cod}}\right) > 0 \Rightarrow \log\left(\left.\frac{G_{MMSE}^{cod}}{G_{ZF}^{cod}}\right|_{UB}\right) > 0 \Rightarrow \log\left[m\left(K,M,c_2\right)\right] > 0. \tag{3.140}$$

Finally, we assume that $Q \gg 1$, which means that $c_2 \approx \frac{3}{2Q}$.

i) *Proving that* $\left.\frac{G_{MMSE}^{cod}}{G_{ZF}^{cod}}\right|_{UB}$ *is a monotonically increasing function of* K: We have

$$\frac{d\left(\left.\frac{G_{MMSE}^{cod}}{G_{ZF}^{cod}}\right|_{UB}\right)}{dK} = \left.\frac{G_{MMSE}^{cod}}{G_{ZF}^{cod}}\right|_{UB}\left[\frac{1}{\left(M-K+1\right)^2}\log\left[m\left(K,M,c_2\right]\right) + \frac{1}{M-K+1}\frac{\frac{d(m(K,M,c_2))}{dK}}{m\left(K,M,c_2\right)}\right]. \tag{3.141}$$

Hence, considering (3.140), to prove that (3.141) is a positive quantity it is adequate to prove that $\frac{d(m(K,M,c_2))}{dK}$ is positive. We have:

$$\frac{d\left(m\left(K,M,c_2\right)\right)}{dK} > 0 \overset{(l)}{\Rightarrow} \left(1+c_2\right)\left(M-K+\frac{1}{2}\right) > 0 \quad true, \tag{3.142}$$

where in (l) the inequality $\log(x) \leqslant x-1$ [20] is used. Consequently, i) is proved.

ii) *Proving that* $\left.\frac{G_{MMSE}^{cod}}{G_{ZF}^{cod}}\right|_{UB}$ *is a monotonically decreasing function of* M: We have

$$\frac{d\left(\left.\frac{G_{MMSE}^{cod}}{G_{ZF}^{cod}}\right|_{UB}\right)}{dM} = \left.\frac{G_{MMSE}^{cod}}{G_{ZF}^{cod}}\right|_{UB}\left[-\frac{1}{(M-K+1)^2}\log\left[m\left(K,M,c_2\right)\right]+\frac{1}{M-K+1}\frac{\frac{d(m(K,M,c_2))}{dM}}{m\left(K,M,c_2\right)}\right]. \tag{3.143}$$

Hence, by again considering (3.140), to prove that (3.143) is a negative quantity it is adequate to prove that $\frac{d(m(K,M,c_2))}{dM}$ is negative. We have:

$$\begin{aligned}&\frac{d\left(m\left(K,M,c_2\right)\right)}{dM} < 0\\ &\overset{(m)}{\Rightarrow} 2+\frac{M-K+2.5+c_2}{M-K+2+c_2}+\frac{0.5}{M}-\frac{M+1.5+c_2}{M+1+c_2}-\frac{M-K+1.5}{M-K+1}-\frac{\left(M+1+c_2\right)\left(M-K+1\right)}{\left(M-K+2+c_2\right)M}\\ &> 0 \quad true,\end{aligned} \tag{3.144}$$

where in (m) we use the inequality $\log(x) \leqslant x-1$ [20][3]. Consequently, ii) is proved.

iii) *Proving that* $\left.\frac{G_{MMSE}^{cod}}{G_{ZF}^{cod}}\right|_{UB}$ *is a monotonically decreasing function of* Q: We have

$$\frac{d\left(\left.\frac{G_{MMSE}^{cod}}{G_{ZF}^{cod}}\right|_{UB}\right)}{dQ} = b\left(K,M\right)m(K,M,c_2)^{b(K,M)-1}\frac{d\left[m\left(K,M,c_2\right)\right]}{dQ}. \tag{3.145}$$

Hence, to prove that (3.145) is a negative quantity it is adequate to prove that $\frac{d[m(K,M,c_2)]}{dQ}$ is negative. We have:

$$\frac{d\left[m\left(K,M,c_2\right)\right]}{dQ} < 0 \overset{(n)}{\Rightarrow} \left(M+1\right)\left(2M-2K+3\right) > \frac{3}{2Q} \quad true, \tag{3.146}$$

where in (n) we use the inequality $1-\frac{1}{x} \leqslant \log(x)$ [20]. Consequently, iii) is proved, which concludes the proof of Theorem 2.

B.3. *Proof of Theorem 3*: From (3.32), we see that $D_{ML}\left(P_R\right) = D_1\left(P_R\right) + D_2\left(P_R\right)$, where

$$D_1\left(P_R\right) = \frac{1}{\sigma_{SR}^2\left(P_{budget}-MP_R\right)} \quad and \quad D_2\left(P_R\right) = \frac{\log\left(1+\sigma_{RD}^2P_R\right)}{\sigma_{RD}^2P_R}. \tag{3.147}$$

Hence, to prove that $D_{ML}\left(P_R\right)$ is convex, it is sufficient to prove that both $D_1\left(P_R\right)$ and $D_2\left(P_R\right)$ are convex since the sum of two convex functions in the same domain is also a convex

[3]We note that we have verified that the term $2+\frac{M-K+2.5+c_2}{M-K+2+c_2}+\frac{0.5}{M}-\frac{M+1.5+c_2}{M+1+c_2}-\frac{M-K+1.5}{M-K+1}-\frac{(M+1+c_2)(M-K+1)}{(M-K+2+c_2)M}$ of (3.144) is positive by seeing that it has no real root (by means of MATLAB). Hence, it maintains its positive sign for any value of K, M, and Q.

function. This is because $D_{ML}^{''}(P_R) = D_1''(P_R) + D_2''(P_R)$, where $D_{ML}^{''}(P_R)$, $D_1''(P_R)$, and $D_2''(P_R)$ denote the second derivatives with respect to P_R of $D_{ML}(P_R)$, $D_1(P_R)$, and $D_2(P_R)$, respectively. We have

$$D_1''(P_R) = \frac{2M^2(P_{budget} - MP_R)}{\sigma_{SR}^2(P_{budget} - MP_R)^4} > 0, \quad \text{since} \quad P_R \in \left(0, \frac{P_{budget}}{M}\right). \tag{3.148}$$

and

$$D_2''(P_R) = \frac{2(1+\sigma_{RD}^2 P_R)^2 \log(1+\sigma_{RD}^2 P_R) - \sigma_{RD}^2 P_R(3\sigma_{RD}^2 P_R + 2)}{\sigma_{RD}^2 P_R^3 (1+\sigma_{RD}^2 P_R)^2} \overset{(o)}{\geqslant} \frac{(\sigma_{RD}^2)^2}{(2+\sigma_{RD}^2 P_R)(1+\sigma_{RD}^2 P_R)^2} > 0 \tag{3.149}$$

where in (o) the inequality $\log(1+x) \geqslant \frac{2x}{2+x}$ is used [20]. Consequently, it is proved that $D_{ML}(P_R)$ is a convex function.

B.4. *Proof of Theorem 4*: The proof of Theorem 4 consists of two steps: i) It is proved that $S(P_R)$ is a concave function by taking its second derivative and showing that it is negative in $P_R \in \left(0, \frac{P_{budget}}{M}\right)$. ii) Having proven in the first step that $S(P_R)$ is concave in $P_R \in \left(0, \frac{P_{budget}}{M}\right)$, the second step consists of proving that $R(P_R) = \frac{\log(1+S(P_R))}{S(P_R)}$ is a convex function in $P_R \in \left(0, \frac{P_{budget}}{M}\right)$.

i) *Proving that $S(P_R)$ is a concave function in $P_R \in \left(0, \frac{P_{budget}}{M}\right)$*: The second derivative of $S(P_R)$ is given by

$$S''(P_R) = -\frac{2(\sigma_{SR}^2 P_{budget} + 1)(\sigma_{RD}^2 P_{budget} + M)}{[\sigma_{SR}^2 P_{budget} - P_R(M\sigma_{SR}^2 - \sigma_{RD}^2) + 1]^3} < 0. \tag{3.150}$$

ii) *Proving that $R(P_R) = \frac{\log(1+S(P_R))}{S(P_R)}$ is a convex function in $P_R \in \left(0, \frac{P_{budget}}{M}\right)$*: By recalling (3.149), which proves that the function $\frac{\log(1+x)}{x}$, $x > 0$, is a convex function and by considering Lemma 1 and that $S(P_R)$ is a concave function in $P_R \in \left(0, \frac{P_{budget}}{M}\right)$, it follows that $R(P_R) = \frac{\log(1+S(P_R))}{S(P_R)}$ is a convex function in $P_R \in \left(0, \frac{P_{budget}}{M}\right)$. The value of P_R, $P_{R_{sol}}$, that minimizes $R(P_R)$ can be found by taking the first derivative of $S(P_R)$ and setting it equal to 0 to find the root that falls in $P_R \in \left(0, \frac{P_{budget}}{M}\right)$. This leads to (3.37), which concludes the proof of Theorem 4.

Bibliography

[1] Yi Jiang; Varanasi, M.K.; Jian Li, "Performance Analysis of ZF and MMSE Equalizers for MIMO Systems: An In-Depth Study of the High SNR Regime," Information Theory, IEEE Transactions on , vol.57, no.4, pp.2008,2026, April 2011.

[2] M. Haenggi, *Stochastic Geometry for Wireless Networks*. Cambridge University Press, 2012.

[3] Yang Yang; Honglin Hu; Jing Xu; Guoqiang Mao, "Relay technologies for WiMax and LTE-advanced mobile systems," Communications Magazine, IEEE , vol.47, no.10, pp.100,105, October 2009.

[4] S. Catti, S. Gollacota, and D. Katabi, "Embracing wireless interference: Analog network coding", *ACM SIGCOMM*, 2007.

[5] Hasna, M.O.; Alouini, M.-S., "A performance study of dual-hop transmissions with fixed gain relays," Wireless Communications, IEEE Transactions on , vol.3, no.6, pp.1963,1968, Nov. 2004.

[6] Xu Zhu; Murch, R.D., "Performance analysis of maximum likelihood detection in a MIMO antenna system," Communications, IEEE Transactions on , vol.50, no.2, pp.187,191, Feb 2002.

[7] Deqiang Chen; Azarian, K.; Laneman, J.N., "A Case for Amplify−Forward Relaying in the Block−Fading Multiple−Access Channel," Information Theory, IEEE Transactions on , vol.54, no.8, pp.3728,3733, Aug. 2008.

[8] Badr, M.; Belfiore, J.-C., "Distributed space time codes for the Amplify−and−Forward Multiple−Access Relay channel," Information Theory, 2008. ISIT 2008. IEEE International Symposium on , vol., no., pp.2543,2547, 6-11 July 2008.

[9] Yindi Jing; Hassibi, B., "Distributed Space-Time Coding in Wireless Relay Networks," Wireless Communications, IEEE Transactions on , vol.5, no.12, pp.3524,3536, December 2006.

[10] Jafar, S.A.; Krishna Srikanth Gomadam; Chiachi Huang, "Duality and Rate Optimization for Multiple Access and Broadcast Channels With Amplify-and-Forward Relays," Information Theory, IEEE Transactions on , vol.53, no.10, pp.3350,3370, Oct. 2007.

[11] Zhiguo Ding; Ratnarajah, T.; Leung, K.K., "On the study of network coded AF transmission protocol for wireless multiple access channels," Wireless Communications, IEEE Transactions on , vol.8, no.1, pp.118,123, Jan. 2009.

[12] W. Guan and K. J. R. Liu, "Diversity Analysis of Analog Network Coding with Multi-User Interferences", *IEEE Trans. Wireless Commun.*, vol. 12, no. 2, pp. 668−679, Feb. 2013.

[13] I. S. Gradshteyn and I. M. Ryzhik, *Table of Integrals, Series, and Products*, 7th edition. Academic, 2007.

[14] M. Abramowitz and I. A. Stegun, *Handbook of Mathematical Functions with Formulas, Graphs, and Mathematical Tables*, 9th edition. Dover, 1972.

[15] Raghothaman, B.; Sternberg, G.; Kaur, S.; Pragada, R.; Tao Deng; Vanganuru, K., "System Architecture for a Cellular Network with Cooperative Mobile Relay," Vehicular Technology Conference (VTC Fall), 2011 IEEE , vol., no., pp.1,5, 5-8 Sept. 2011.

[16] Elkourdi, T.; Simeone, O., "Femtocell as a Relay: An Outage Analysis," Wireless Communications, IEEE Transactions on , vol.10, no.12, pp.4204,4213, December 2011.

[17] Jacob, P.; Madhukumar, A.S., "Femto-relays: A power efficient coverage extension mechanism for femtocells," Personal Indoor and Mobile Radio Communications (PIMRC), 2011 IEEE 22nd International Symposium on , vol., no., pp.975,979, 11-14 Sept. 2011.

[18] Caijun Zhong; Ratnarajah, T.; Zhaoyang Zhang; Kai-Kit Wong; Sellathurai, M., "Performance of Rayleigh-Product MIMO Channels with Linear Receivers," Wireless Communications, IEEE Transactions on , vol.13, no.4, pp.2270,2281, April 2014.

[19] Kim, Namshik; Yusung Lee; Hyuncheol Park, "Performance Analysis of MIMO System with Linear MMSE Receiver," Wireless Communications, IEEE Transactions on , vol.7, no.11, pp.4474,4478, November 2008.

[20] F. Topsoe, *Some bounds for the logarithmic function*, RGMIA Research Report Collection, vol. 7(2), no. 6, 2004.

[21] S. Boyd and L. Vandenberghe, *Convex Optimization*. Cambridge University Press, 2004.

[22] Vaze, R.; Heath, R.W., "On the Capacity and Diversity-Multiplexing Tradeoff of the Two-Way Relay Channel," Information Theory, IEEE Transactions on , vol.57, no.7, pp.4219,4234, July 2011.

[23] Xilin Cheng; Bo Yu; Xiang Cheng; Liuqing Yang, "Two-Way Full-Duplex Amplify-and-Forward Relaying," Military Communications Conference, MILCOM 2013 - 2013 IEEE , vol., no., pp.1,6, 18-20 Nov. 2013.

[24] Rui Wang; Meixia Tao, "Joint Source and Relay Precoding Designs for MIMO Two-Way Relaying Based on MSE Criterion," Signal Processing, IEEE Transactions on , vol.60, no.3, pp.1352,1365, March 2012

[25] Meixia Tao; Rui Wang, "Linear Precoding for Multi-Pair Two-Way MIMO Relay Systems With Max-Min Fairness," Signal Processing, IEEE Transactions on , vol.60, no.10, pp.5361,5370, Oct. 2012.

[26] Min Zhou; Qimei Cui; Jantti, R.; Xiaofeng Tao, "Energy-Efficient Relay Selection and Power Allocation for Two-Way Relay Channel with Analog Network Coding," Communications Letters, IEEE , vol.16, no.6, pp.816,819, June 2012.

[27] Xiaodong Ji; Baoyu Zheng; Yueming Cai; Li Zou, "On the Study of Half-Duplex Asymmetric Two-Way Relay Transmission Using an Amplify-and-Forward Relay," Vehicular Technology, IEEE Transactions on , vol.61, no.4, pp.1649,1664, May 2012.

[28] Chenyuan Wang; Liu, T.C.-K.; Xiaodai Dong, "Impact of Channel Estimation Error on the Performance of Amplify-and-Forward Two-Way Relaying," Vehicular Technology, IEEE Transactions on , vol.61, no.3, pp.1197,1207, March 2012.

[29] A. Goldsmith, *Wireless Communications*, Cambridge University Press, Aug. 2005.

[30] Xuesong Liang; Shi Jin; Wenjin Wang; Xiqi Gao; Kai-Kit Wong, "Outage Probability of Amplify-and-Forward Two-Way Relay Interference-Limited Systems," Vehicular Technology, IEEE Transactions on , vol.61, no.7, pp.3038,3049, Sept. 2012.

[31] Junchao Shen; Nan Sha; Yuemin Cai; Chunxiao Cai; Weiwei Yang, "Outage probability of two-way amplify-and-forward relaying system with interference-limited relay," Wireless Communications and Signal Processing (WCSP), 2011 International Conference on , vol., no., pp.1,5, 9-11 Nov. 2011.

[32] Ikki, S.S.; Aissa, S., "Performance Analysis of Two-Way Amplify-and-Forward Relaying in the Presence of Co-Channel Interferences," Communications, IEEE Transactions on , vol.60, no.4, pp.933,939, April 2012.

[33] Liang Yang; Qaraqe, K.; Serpedin, E.; Alouini, M.-S., "Performance Analysis of Amplify-and-Forward Two-Way Relaying with Co-Channel Interference and Channel Estimation Error," Communications, IEEE Transactions on , vol.61, no.6, pp.2221,2231, June 2013.

[34] Ghosh, A.; Mangalvedhe, N.; Ratasuk, R.; Mondal, B.; Cudak, M.; Visotsky, E.; Thomas, T.A.; Andrews, J.G.; Xia, P.; Jo, H.S.; Dhillon, H.S.; Novlan, T.D., "Heterogeneous cellular networks: From theory to practice," Communications Magazine, IEEE , vol.50, no.6, pp.54,64, June 2012.

[35] Andrews, J.G., "Seven ways that HetNets are a cellular paradigm shift," Communications Magazine, IEEE , vol.51, no.3, pp.136,144, March 2013.

[36] Win, M.Z.; Pinto, P.C.; Shepp, L.A., "A Mathematical Theory of Network Interference and Its Applications," Proceedings of the IEEE , vol.97, no.2, pp.205,230, Feb. 2009.

[37] Pinto, P.C.; Win, M.Z., "Communication in a Poisson Field of Interferers–Part I: Interference Distribution and Error Probability," Wireless Communications, IEEE Transactions on , vol.9, no.7, pp.2176,2186, July 2010.

[38] Heath, R.W.; Kountouris, M.; Tianyang Bai, "Modeling Heterogeneous Network Interference Using Poisson Point Processes," Signal Processing, IEEE Transactions on , vol.61, no.16, pp.4114,4126, Aug.15, 2013.

[39] Kountouris, M.; Pappas, N., "Approximating the interference distribution in large wireless networks," Wireless Communications Systems (ISWCS), 2014 11th International Symposium on , vol., no., pp.80,84, 26-29 Aug. 2014.

[40] Mohammadi, M.; Suraweera, H.A.; Xiangyun Zhou, "Outage probability of wireless ad hoc networks with cooperative relaying," Global Communications Conference (GLOBECOM), 2012 IEEE , vol., no., pp.4410,4416, 3-7 Dec. 2012.

[41] Guidotti, A.; Buccigrossi, V.; Di Renzo, M.; Corazza, G.E.; Santucci, F., "Outage and symbol error probabilities of dual-hop AF relaying in a Poisson field of interferers," Wireless Communications and Networking Conference (WCNC), 2013 IEEE , vol., no., pp.3704,3709, 7-10 April 2013.

[42] Tanbourgi, R.; Jakel, H.; Jondral, F.K., "Cooperative relaying in a poisson field of interferers: A diversity order analysis," Information Theory Proceedings (ISIT), 2013 IEEE International Symposium on , vol., no., pp.3100,3104, 7-12 July 2013.

[43] Aalo, V.A.; Peppas, K.P.; Efthymoglou, G.P.; Alwakeel, M.M.; Alwakeel, S.S., "Serial Amplify-and-Forward Relay Transmission Systems in Nakagami- m Fading Channels With a Poisson Interference Field," Vehicular Technology, IEEE Transactions on , vol.63, no.5, pp.2183,2196, Jun 2014.

[44] Di Renzo, M.; Wei Lu, "End-to-End Error Probability and Diversity Analysis of AF-Based Dual-Hop Cooperative Relaying in a Poisson Field of Interferers at the Destination," Wireless Communications, IEEE Transactions on , vol.14, no.1, pp.15,32, Jan. 2015.

[45] Di Renzo, M.; Wei Lu, "On the Diversity Order of Selection Combining Dual-Branch Dual-Hop AF Relaying in a Poisson Field of Interferers at the Destination," Vehicular Technology, IEEE Transactions on , vol.64, no.4, pp.1620,1628, April 2015.

[46] Zhengdao Wang; Giannakis, G.B., "A simple and general parameterization quantifying performance in fading channels," Communications, IEEE Transactions on , vol.51, no.8, pp.1389,1398, Aug. 2003.

[47] Lichte, H.S.; Valentin, S.; Karl, H., "Expected interference in wireless networks with geometric path loss: a closed-form approximation," Communications Letters, IEEE , vol.14, no.2, pp.130,132, February 2010.

[48] Taricco, Giorgio; Biglieri, Ezio, "Exact pairwise error probability of space-time codes," Information Theory, IEEE Transactions on , vol.48, no.2, pp.510,513, Feb 2002.

[49] Li, P.; Paul, D.; Narasimhan, R.; Cioffi, J., "On the distribution of SINR for the MMSE MIMO receiver and performance analysis," Information Theory, IEEE Transactions on , vol.52, no.1, pp.271,286, Jan. 2006.

[50] Kiessling, M.; Speidel, J., ”Unifying performance analysis of linear MIMO receivers in correlated Rayleigh fading environments,” Spread Spectrum Techniques and Applications, 2004 IEEE Eighth International Symposium on , vol., no., pp.634,638, 30 Aug.-2 Sept. 2004.

[51] M. Kiessling, “Statistical Analysis and Transmit Prefiltering for MIMO Wireless Systems in Correlated Fading Environments”, Ph. D. Thesis Dissertation, 2004.

Chapter 4

Conclusions and Future Work

4.1 Conclusions

This thesis focused on two promising approaches for the design of future low-complexity and energy-efficient wireless communications, namely SM and ANC. Thir choice stems from the fact that both methods offer multiplexing gains, which is an essential feature when there is scarcity of available resources, such as bandwidth. In particular,

• Firstly, we examined the SM MIMO transmission method in point-to-point systems, which is based on the innovative feature of exploiting the presence of multiple antennas at the transmitter to convey data with a smaller number of RF chains. However, the disadvantage of the conventional open-loop SM approach is unable to provide neither transmit-diversity gains nor a linear increase in the rate with the number of transmit antennas, compared to a SIMO system, as in the case of conventional spatial multiplexing MIMO, which can greatly inhibit its energy-efficiency potentials. Motivated by this, two closed-loop methods were proposed that provide transmit-diversity gains and one that combines the SM principle with the one of spatial multiplexing for increasing the achievable rates. More specifically:

i) Regarding transmit-diversity, the 1st closed-loop scheme proposed is based on the GSSK principle, which is a special category of GSM, as aforementioned. By assuming that the channel phases are available at the transmitter and by using the principle of time-orthogonal signal design, the proposed-scheme which is called AGSSK-TOSD achieves a transmit diversity that is greater than the number of active transmit antennas and, furthermore, it can be more energy efficient, in terms of energy needed at the transmitted to achieve a target SER, than several

SOTA closed-loop competitive technologies, such as the closed-loop Alamouti code and the closed-loop EGT.

The 2nd closed-loop scheme that was proposed is based on the assumption that only a single-RF is available at the transmitter and instead of using all the antennas to employ the SM principle, the subset of antennas that results in the minimum SER is selected at the the transmitter based on CSI at the receiver. This way, a competitive technology to the single-RF TAS-MRC is proposed, which had been the most-well know scheme when a single-RF chain is available at the transmitter. In fact, results showed that the proposed method can significantly outperform the latter in terms of energy efficiency at the transmitter as the number of receive antennas increases. As a trade-off, in terms of complex operations needed the proposed method exhibits a higher complexity for selecting the subset at the receiver than the TAS-MRC method.

ii) Regarding higher offered rates than the ones offered by the conventional SM/GSM approaches, this thesis proposed an open-loop GSM-based method which combines GSM with conventional spatial multiplexing. In other words, multistream transmission is allowed for GSM. This way, for the same number of RF chains (active transmit antennas) and the same modulation order used the achievable rate is higher than the one of conventional spatial multiplexing. Results showed that the proposed method is able to outperform in terms of energy efficiency, SOTA methods, such as the Alamouti scheme conventional spatial multiplexing, and conventional open-loop SM, especially for an adequate number of receive antennas.

• Secondly, we focused our attention on ANC due to the fact that it is the least complex ANC scheme as far as the operations needed at the relays are concerned (the relays only perform amplification-and-forwarding). More specifically, we considered the implementation of ANC into two well-known relaying channels, the MARC and the two-way relaying channel. In particular,

i) Regarding the MARC, where multiple sources want to convey their data to a common destination through the use of multiple relays, firstly an analytical framework for the error rate per source was derived for the optimal ML detector. Based on this framework, the energy efifciency comparison with TDMA was conducted and the results sows that for the same end-to-end rate ANC can be significantly more energy efficient than TDMA, as the number of sources, or relays, or the modulation order increases.

In addition, due to the exponential increase in the detection complexity with the number

for sources or relays, suboptimal detectors, such as the ZF and MMSE were also examined and for which an analytical SER framework was derived.

Finally, the OPA problem for was formulated and its convexity was proved for the 3 examined receivers. Also, its analytical solution was presented for the ZF and MMSE receivers.

The numerical results verify the energy efficiency advantage of ANC over TDMA for various scenarios and also show that for all the examined 3 detectors significant energy savings for the sources can be achieved with the OPA.

ii) Regarding the two-way relaying channel with ANC, where two sources want to exchange their data through a relay that employs ANC, the effect of network interference at the sources was considered and an analytical SER framework was derived. This was something important due to the fact that previous works considered unrealistic distributions for the interference, such as the Gaussian model, whereas the intuition says that the interferers should follow a PPP distribution and, hence, the distribution of the summed interference at the two sources should deviate from that of a Gaussian. Considering that there is an exclusion region around the two sources where no interferer can be located, based on the derived SER expression the energy gains for the two sources were numerically substantiated as the radius of the exclusion region increases.

All in all, the above studies prove the energy efficiency potentials of SM and ANC-based transmission methods. This, together with the fact that they consist low-complexity alternatives to known conventional approaches, verify the need for their implementation in future wireless networks.

4.2 Future Work

There are several research directions in both SM and ANC areas. In particular,

• Regarding SM, the following issues can be addressed:

i) The vast majority of works on SM do not consider the energy consumption required at the receiver to estimate the channel coefficients from the transmit to the receive antennas. This can pose serious problems to the energy efficiency of the whole system (both the transmitter and receiver) considering that single stream SM-based systems use a higher number of antenna elements at the transmitter to achieve the same rate with a spatial multiplexing MIMO system,

for instance. Consequently, the energy consumption for channel estimation at the receiver becomes more pronounced in SM systems than conventional MIMO ones. Due to this, it is of interest to take into account the energy consumption of channel estimation for the comparison of the proposed SM-based schemes with the competitive SOTA technologies.

ii) Another interesting topic is the performance analysis of the proposed subset antenna selection scheme for SM of Section 2.2.2.2. This way, the coding and diversity gain can be extracted and so the scenarios where the proposed scheme outperforms TAS-MRC can be analytically found. Furthermore, the consideration of channel estimation errors in this comparison are of practical importance.

iii) Finally, the diversity-multiplexing trade-off of SM systems is also another research line.

• As far as ANC is concerned, some research lines are the following:

i) In reality, there is no perfect synchronization at the relays of the incoming signals from the sources. Hence, there are synchronization errors, which can lead to performance degradation if not treated. Based on this, it is interesting to examine how synchronization errors affect the energy efficiency comparison of ANC with TDMA. Intuitively, the larger the errors are, the highest the performance degradation of ANC is.

ii) A SER analysis can be conducted for the MARC considering the effect of network interference. In addition, more advanced suboptimal receiver types can be considered in the analysis, such as ZF and MMSE with successive interference cancellation.

iii) Lastly, the multihop relay case can be considered for the MARC in which multiple amplitude-and-forward relays exist between the sources and the destination.